Doctoral Dissertation

Machine Learning-Aided Structure Determination for Ziegler-Natta Catalysts Primary Particles and their Performance Elucidation

Gentoku Takasao

Supervisor: Prof. Toshiaki Taniike

Graduate School of Advanced Science and Technology

Japan Advanced Institute of Science and Technology

[Materials Science]

2022 March

Referee-in-chief: Professor Toshiaki Taniike

Japan Advanced Institute of Science and Technology

Referees: Professor Yoshifumi Oshima

Japan Advanced Institute of Science and Technology

Professor Shinya Maenosono

Japan Advanced Institute of Science and Technology

Associate Professor Kenta Hongo

Japan Advanced Institute of Science and Technology

Professor Takeshi Shiono

Hiroshima University

Preface

The present thesis is submitted for the Degree of Doctor of Philosophy at Japan Advanced Institute of Science and Technology, Japan. The thesis is consolidation of results of the research work on the topic “Machine Learning-Aided Structure Determination for Ziegler-Natta Catalysts Primary Particles and their Performance Elucidation” under the supervision of Prof. Toshiaki Taniike.

Chapter 1 describes a general introduction and the purpose of this thesis. **Chapter 2** focuses on the development of non-empirical structure determination for $TiCl_4$-capped $MgCl_2$ nanoplates of heterogeneous Ziegler-Natta catalysts. **Chapter 3** pursues the structure determination for $TiCl_4$-capped $MgCl_2$ nanoplates with various sizes and chemical compositions. The obtained results are subsequently analyzed to estimate structural and electronic distributions as an intrinsic nature of the $TiCl_4$-capped $MgCl_2$ nanoplates. **Chapter 4** addresses the impact of the structural and electronic distribution on the propylene polymerization performance of a Ziegler-Natta catalyst, which relates to the origin of the stereospecificity of the donor-free Ziegler-Natta catalysts. **Chapter 5** describes implementation of a distributed genetic algorithm based on the migration from a structure database for solving the premature convergence problem and realizing the structure determination for $TiCl_4$-capped $MgCl_2$ nanoplates with a size comparable to that of real Ziegler-Natta catalysts. **Chapter 6** delivers the general conclusion of the thesis.

Gentoku Takasao
Graduate School of Advanced Science and Technology
Japan Advanced Institute of Science and Technology
March 2022

Table of Contents

Chapter 1:
General Introduction

1.1. First-principles calculations

"First-principles calculation" is a method of calculating physical properties of molecules such as energies, structures, electronic states, spectroscopic characteristics, etc. on the basis of the principles of quantum mechanics. In other words, the calculation derives electronic states by solving the Schrödinger equation for a given atomic configuration without using empirical parameters such as experimental parameters. From the calculation of the electronic state, one can predict the stability of a model structure with a certain atomic configuration, optimize the structure toward a minimum in the potential energy surface, evaluate the feasibility of a reaction by calculating a transition state, and simulate various spectroscopic characteristics of the structure such as IR, Raman, UV, and NMR spectra of the structure. With significant advances in computational methods and resources, the first-principles calculation has been an indispensable method for understanding the properties of known materials as well as predicting the properties of hypothetical materials.

The calculation of electronic states of atoms or molecules except hydrogen-like atoms, i.e., multi-electron systems, is a many-body problem, and it is impossible in principle to obtain an exact solution of the Schrödinger equation in an analytical form, and even using a numerical method due to the unaffordable computational cost. For those reasons, in first-principles calculations, various approximations are made to simplify the calculations and obtain an approximate solution in a feasible cost. Various approximation and calculation methods for many-electron systems have been developed, staring from the Hartree-Fock (HF) method [1], which does not consider electron correlation. From the viewpoint of balancing chemical accuracy and computational cost, recent studies mainly use the calculation based on the density functional theory (DFT).

1.2. Density functional theory (DFT)

Density functional theory (DFT) is a theory that the energy of a system can be calculated as a functional of the electron density. According to the Hohenberg-Kohn theorem [2], there is a one-to-one correspondence between the wave function and the electron density, and physical quantities such as energies can be derived from the electron density instead of the wave function. The wave function of an N-electron system in 3D space is a function that depends on 3 coordinate variables for each electron, i.e., 3N coordinate variables, but the electron density depends only on the xyz coordinates in 3D space, i.e., 3 coordinate variables, regardless of the number of electrons, N. In other words, DFT offers a potential advantage of requiring far fewer dimensions in the numerical calculation than the wave function-based methods. In the practical DFT calculations, the electron density is obtained by solving the Kohn-Sham equation [3] just as the wave function is obtained by solving the Schrödinger equation. The exchange-correlation functional describes the interelectronic interaction excluding the classical Coulomb interaction, in particular the electronic correlation and exchange interaction. A variety of functional forms have been developed, such as PBE [4] used in this thesis, B3LYP, TS1, etc, which are selected according to the system and accuracy needed. The general DFT calculation scales on the order of the third power of the number of electrons similar to the HF method, while it can capture electronic correlation, which is not in the HF method.

1.3. Non-empirical structure determination

Geometry optimization in quantum mechanical calculations is generally a calculation to obtain a stable structure by successively adjusting the input structure toward a minimum on the potential energy surface. It is an operation to search for a minimum point belonging to the same valley of the

potential energy surface. The stable structure obtained by geometry optimization is a minimum located in the neighborhood of the input initial structure, but since potential energy space is a multidimensional and multimodal space consisting of many combinations of atomic coordinates, the minimum in the neighborhood is not necessarily the global minimum i.e., the most stable structure in the system. In other words, geometry optimization only seeks local solutions in the neighborhood of a given structure, and does not perform a search that jumps from valley to valley. Hence, in order to obtain an accurate structure, it is necessary to give a sufficiently plausible structure at the time of initial structure construction. In general, the initial structure is constructed based on empirical information, such as physicochemical guesses and experimental findings, but it is difficult to uniquely determine the structure for a complicated system such as solid catalysts that often lack experimental information at a molecular/atomic precision.

In order to cope with the problem of guessing accurate initial structures, it has been attempted to obtain the most stable structure in a non-empirical fashion by repeatedly optimizing the structures while changing the initial structures from valley to valley in the potential energy surface using a search algorithm such as simulated annealing [5], basin hopping [6], and genetic algorithms. In particular, the genetic algorithm is highly compatible with chemical structure search because it can perform optimization without depending on the starting point, it is easy to express the atomic coordinates in the algorithm, and it can acquire various metastable structures in the search process in addition to determining the most stable structure. Optimization using the genetic algorithm has been studied since 1990s. This thesis also employs the structure determination by the genetic algorithm.

1.4. Genetic algorithm

The genetic algorithm is a global search algorithm proposed based on the analogy to natural selection and genetics in evolutionary theory [7]. The genetic algorithm searches for optimal solutions to complex problems by mimicking the processes of evolution in nature, especially the principle of survival of the fittest proposed by Charles Darwin. In other words, it is a method of evolving a solution to an optimal solution by identifying the solution that produced better results as an individual that has adapted to the environment and is superior, and passing on the characteristics, or genes, of that solution to the next generation of solutions.

In the genetic algorithm, the numerical representation of the solution to be searched corresponds to the genes, chromosomes, and individuals. Genetic algorithms are meta-heuristic algorithms that can be used universally for any problem, not just for a specific problem, so the actual coding is arbitrarily determined for the target problem. In the structure determination problem, as pursued in this thesis, the structure itself corresponds to the individual, the atomic coordinates that make up the structure correspond to the genes, and the combinations of the genes correspond to the chromosomes. The inheritance of genes in nature is done by male and female individuals leaving offspring, and the accumulation of genetic diversity is caused by mutation. In the genetic algorithm, two individuals with a high degree of adaptation, which is an indicator of the excellence of the solution, are preferentially selected, and a new solution is generated by crossover operation multiplying the characteristics of the solutions and mutation operations randomly recombining parts of the solution.

In principle, the genetic algorithm is a search algorithm that does not guarantee an optimal solution. However, they are effective in reaching a reasonable solution at a practical computational cost for

unknown solution spaces where no solution method has been established or for problems where the optimal solution is unrealistic. It is also possible to search for solutions in a multi-modal solution space, i.e., when there are local solutions in addition to the global optimal solution, and it is robust against noise.

In the early days, research on the genetic algorithm was conducted on problems such as the traveling salesman problem and the eight queens problem. In recent years, various improvements have been made and applied to a wide variety of fields. One of the most famous examples is the nose shape of the N700 series bullet train, which was designed by the genetic algorithm. According to Wolpert et al.'s no-free lunch theorem [8], "any algorithm, any elevated performance over one class of problems is offset by performance over another class". This means that there is no universal algorithm that can solve all problems efficiently, and if we want to perform an efficient search, we need to specialize our algorithm using knowledge about the problem domain. For this reason, it is common to add constraints in the solution space based on domain-specific knowledge. In case of structure determination, this corresponds to the elimination of physicochemically unrealistic structures from the configuration space. In this thesis, I implemented a structure determination program based on knowledge of the target system, $MgCl_2/TiCl_4$, and the details are shown in Chapter 2.

1.5. $MgCl_2$

$MgCl_2$ is a common support for heterogeneous Ziegler-Natta catalysts and has been used since the 1970's [9]. $MgCl_2$ has three crystal polymorphs: α, β, and δ. Among these, the α crystal is the most stable form of $MgCl_2$, which has a cadmium chloride type crystal structure with Mg^{2+} cations in

octahedral voids and with Cl^- anions arranged in a face-centered cubic configuration. As shown in Figure 1.1, in the α form, the $MgCl_2$ layers are stacked by electrostatic attraction in order to arrange the Cl^- anions in a face-centered cubic arrangement. The main difference between the α and β crystals is due to the stacking of the $MgCl_2$ layers. Since the electrostatic force acting between the layers is small compared to the interactions within the layers, the structure within the $MgCl_2$ layer is almost identical in both crystal structures.

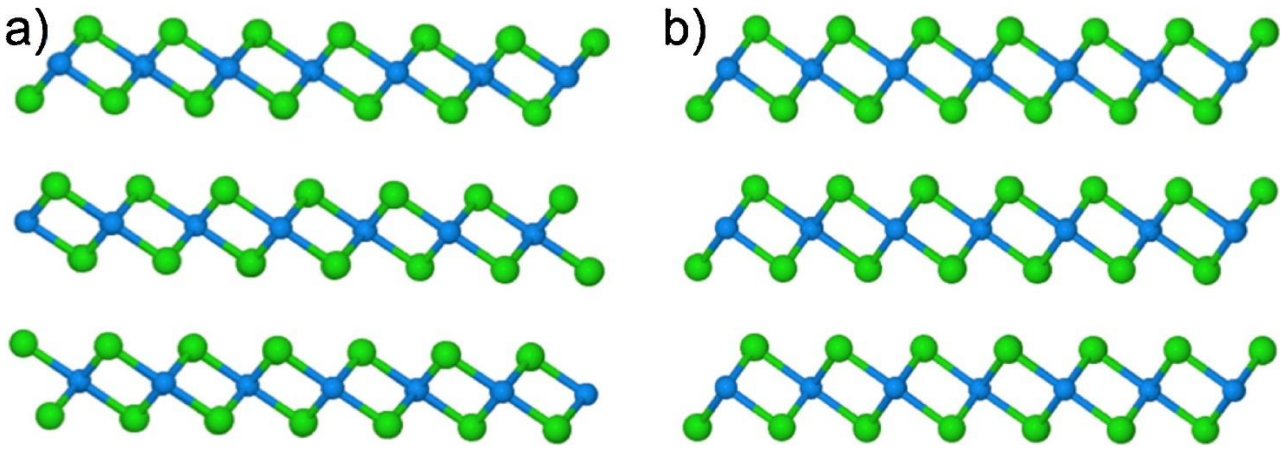

Figure 1.1. (a) α-$MgCl_2$ and (b) β-$MgCl_2$ structures. Adapted from Ref. [10].

In Ziegler-Natta catalysts, to obtain a highly active catalyst, physically or chemically activated $MgCl_2$ is used as a catalyst support. The activated $MgCl_2$ that acts as a catalyst support is called δ-$MgCl_2$, whose identity has been the subject of historical discussion in the field. Broad XRD patterns obtained from δ-$MgCl_2$ indicate that the periodicity of the crystal is highly disordered [11], but there are various structures that can be inferred from such XRD patterns, and the detailed morphology of δ-$MgCl_2$ is still insufficiently understood. To date, the most widely accepted structure is nanosized

$MgCl_2$ with an irregular stacking of $MgCl_2$ monolayers and exposing mainly three planes, (110) and (104) planes terminating the horizontal or lateral sides and the (001) plane terminating the vertical or basal direction, which is shown in Figure 1.2.

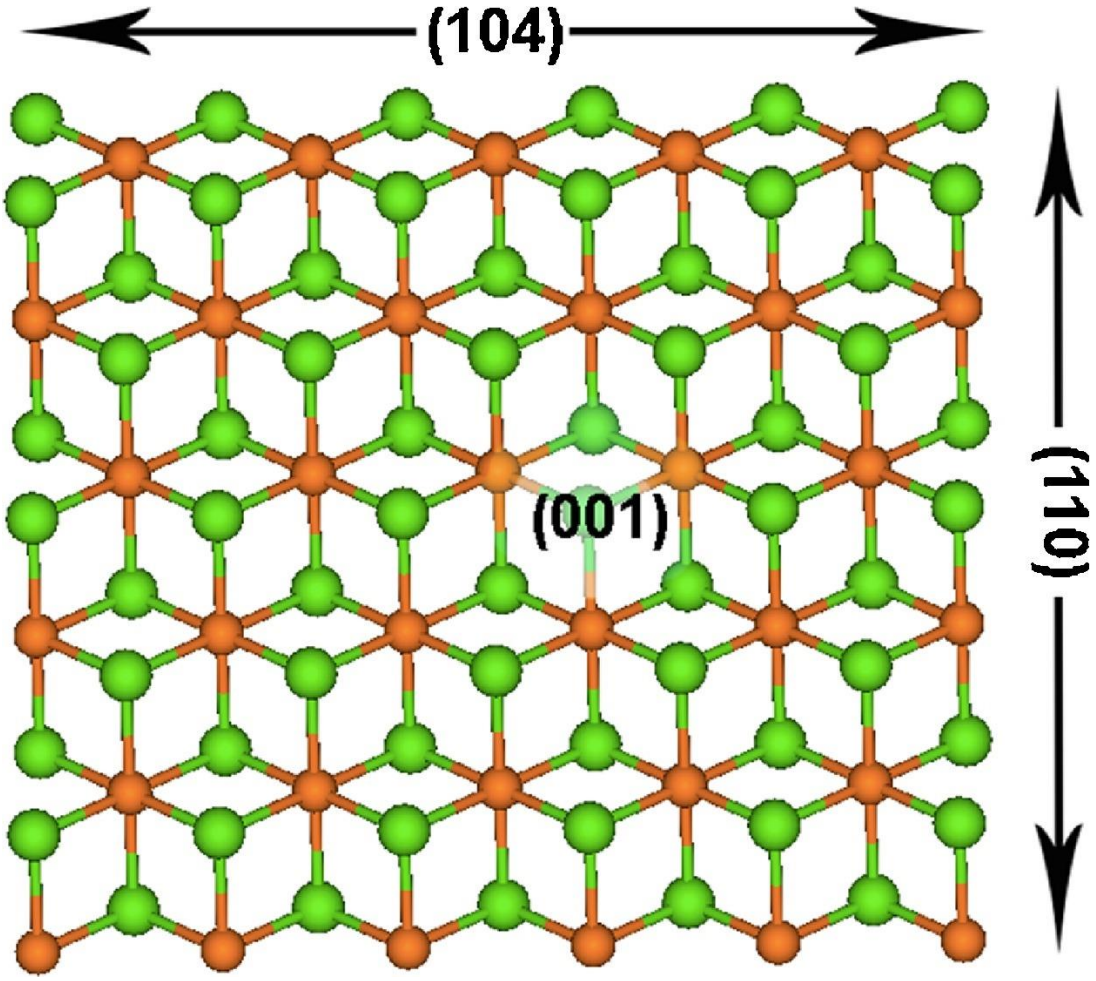

Figure 1.2. Model of a $MgCl_2$ monolayer together with indication of the basal (001) plane, and two lateral cuts: (110) and (104). Adapted from Ref. [10].

1.6. Ziegler-Natta catalysts

Heterogeneous Ziegler-Natta catalysts are the industrial catalysts responsible for the majority of polyolefin (polypropylene, polyethylene, etc.) production, and after about 60 years of research and

development, $TiCl_4/MgCl_2$-based catalysts is currently used in industry. Solid catalysts typically consist of $MgCl_2$ as a support, $TiCl_4$ as an active species precursor, and Lewis base as a modifier. The Lewis base, called donor, exerts steric and electronic effects on the active site, alkylated Ti^{3+}, leading to improvements in important properties such as stereospecificity [9], [12]. For kinetic and morphological reasons, macro-scale Ziegler-Natta catalyst particles form a multigrain structure formed by the hierarchical aggregation of smaller catalyst particles, resulting in micro- to macro-sized pores [13], [14]. The smallest constituent unit in this aggregation is called the primary particle. The structure of the primary particles of the catalyst has been represented as $MgCl_2$ nanoplates with stacking disorder in the c-axis direction [11], [15] and their lateral surfaces terminated by the adsorption of $TiCl_4$ and donor molecules. However, this is based on the interpretation of the broad XRD patterns obtained from activated $MgCl_2$, and experimental knowledge on its detailed morphology including surface exposure is still scarce, even though it is the important basis for the adsorption of catalytic components and the catalysis.

Apart from the uncertainty of the primary particle structure, a number of DFT calculations have been performed on Ziegler-Natta catalysts. Most of them concern the (co-)adsorption of $TiCl_4$ and donor molecules on ideal single-crystal surfaces of $MgCl_2$, such as the (110) or (104) plane [16], [17], [26]–[33], [18]–[25]. The consistent conclusions of these calculations are that $TiCl_4$ energetically prefers unimolecular adsorption onto the (110) surface, and that its interaction with donor molecules co-adsorbed nearby improves the properties of stereospecificity, regiospecificity, and molecular weight control. In recent years, the non-ideal nature of the catalyst primary particles has been taken into account in the calculations. Typical examples are the evaluation of step defect

stabilization by donor adsorption by introducing step defects into the slab model [34], [35], and the derivation of structure-performance relationships for polypropylene polymerization against external donors in the alkoxysilane system by introducing active point models on edge defects. The nano-size of Ziegler-Natta catalyst primary particles has been represented in the form of $MgCl_2$ nanoplates exposing (110) or (100) planes whose lateral ends are terminated by Cl-Ti-Cl trilayers [36]–[38]. Thus, computational studies on the primary particles of Ziegler-Natta catalysts are progressing from understanding the surface chemistry using simplified surface models to establishing accurate surface models. In this regard, one of the important insights into $MgCl_2$ that is still unclear is the dynamic response of $MgCl_2$ to a given environment. Recent experimental results have revealed the fact that $MgCl_2$ flexibly changes its structure depending on the presence of coordination molecules; Andoni et al. observed the effect of different donors on the crystal morphology of $MgCl_2$ by electron microscopy [39]. D'Amore et al. reported that the presence of alcohols significantly affects the morphology of activated $MgCl_2$ and that methanol stabilizes certain surfaces such as (012), (015), and (110) surfaces using CO adsorption IR and other techniques. As shown in Figure 1.3, the coexistence of (110) and (104) surfaces in activated $MgCl_2$ was observed by high-resolution TEM [40].

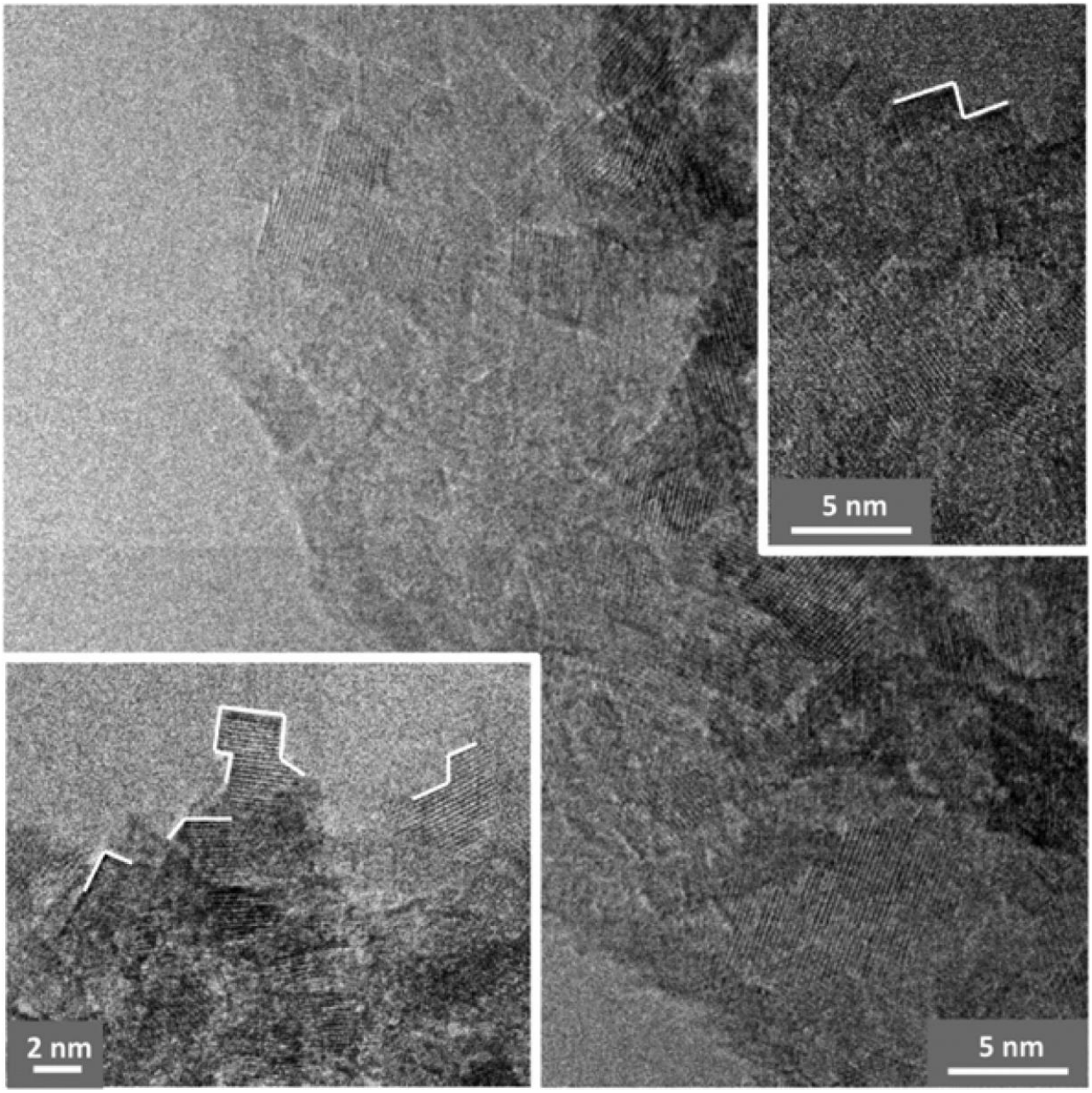

Figure 1.3. Representative HR-TEM pictures of activated $MgCl_2$. White segments are a guide to highlight the edges of the nanocrystals. Both 90°and 120° edge angles can be found. Adapted from Ref. [40].

Taniike et al. demonstrated the surface reconstruction due to the presence of adsorbates in $MgCl_2$ thin films terminated by (001) surfaces by low-energy electron scattering in ultra-high vacuum [62].

These previous studies show that surface reconstruction is an important factor in the simulation of Ziegler-Natta catalytic primary particles and that it is not sufficient to use slab and cluster models that represent only certain predefined surfaces, such as (100) and (110) surfaces and defects on them. Therefore, in order to simulate the primary particles of the Ziegler-Natta catalysts, it is necessary to explore the vast configuration space consisting of $MgCl_2$ and adsorbates, but there is no precedent for such calculations. Thus, this thesis challenges this problem by combining the genetic algorithm and DFT calculation.

1.7. Objective

The heterogeneous Ziegler-Natta catalyst is a major catalyst for the industrial production of polyolefins. The detailed morphology and surface exposure of its primary particles are fundamental to the adsorption of catalytic components and catalysis; however, they have not yet been experimentally accessed. The computational studies on this catalyst mostly assumed pre-defined surfaces, despite of the importance of the reconstruction of the support surfaces upon adsorption.

This thesis aims to determine the structure of $TiCl_4$-capped $MgCl_2$ nanoparticles for the primary particle of Ziegler-Natta catalyst and to elucidate the origin of its catalysis by derived structure models.

For this purpose, in Chapter 2, I developed the non-empirical structure determination program by a combination of the genetic algorithm and the DFT calculation, where reconstruction of $MgCl_2$ by the chemisorption of $TiCl_4$ was explicitly handled.

In Chapter 3, I performed a series of machine learning-aided structure determination for $TiCl_4$-capped $MgCl_2$ nanoplates of different sizes and chemical compositions. The morphology and surface

structure of the catalyst nanoparticles, as well as the structure and distribution of the active species, were determined by analyzing the structure determination process and the resulting structures, thus I propose a new hypothesis for the multisite nature of the Ziegler-Natta catalyst.

In Chapter 4, propylene insertion simulation was performed for the active sites on $TiCl_4$-capped $MgCl_2$ structures derived by non-empirical structure determination and the origin of stereospecificity in donor-free catalyst was clarified.

In Chapter 5, I improved an efficiency of the structure determination program and demonstrated determination for the systems with sizes comparable to real catalysts.

I believe that the research works important advances not only in understanding the catalysis of the Ziegler-Natta catalyst but also in establishing a realistic model of complicated supported catalysts.

REFERENCES

[1] J. C. Slater, "A Simplification of the Hartree-Fock Method," *Phys. Rev.*, vol. 81, no. 3, p. 385, Feb. 1951, doi: 10.1103/PhysRev.81.385.

[2] P. Hohenberg and W. Kohn, "Inhomogeneous electron gas," *Phys. Rev.*, vol. 136, no. 3B, p. B864, Nov. 1964, doi: 10.1103/PHYSREV.136.B864/FIGURE/1/THUMB.

[3] W. Kohn and L. J. Sham, "Self-consistent equations including exchange and correlation effects," *Phys. Rev.*, vol. 140, no. 4A, p. A1133, Nov. 1965, doi: 10.1103/PHYSREV.140.A1133/FIGURE/1/THUMB.

[4] J. P. Perdew, K. Burke, and M. Ernzerhof, "Generalized Gradient Approximation Made

Simple," *Phys. Rev. Lett.*, vol. 77, no. 18, pp. 3865–3868, Oct. 1996, doi: 10.1103/PhysRevLett.77.3865.

[5] S. Kirkpatrick, C. D. Gelatt, and M. P. Vecchi, "Optimization by simulated annealing," *Science (80-.).*, vol. 220, no. 4598, pp. 671–680, May 1983, doi: 10.1126/science.220.4598.671.

[6] D. J. Wales and J. P. K. Doye, "Global optimization by basin-hopping and the lowest energy structures of Lennard-Jones clusters containing up to 110 atoms," *J. Phys. Chem. A*, vol. 101, no. 28, pp. 5111–5116, 1997, doi: 10.1021/jp970984n.

[7] D. Whitley, "A genetic algorithm tutorial," *Stat. Comput.*, vol. 4, no. 2, pp. 65–85, Jun. 1994, doi: 10.1007/BF00175354.

[8] D. H. Wolpert and W. G. Macready, "No free lunch theorems for optimization," *IEEE Trans. Evol. Comput.*, vol. 1, no. 1, pp. 67–82, Apr. 1997, doi: 10.1109/4235.585893.

[9] N. Pasquini and A. Addeo, "Catalysts for Polymerization," in *Polypropylene Handbook*, 2nd ed., Boca Raton: Hanser Gardner Publications, 2005, pp. 11–112.

[10] N. Bahri-Laleh *et al.*, "Computational modeling of heterogeneous Ziegler-Natta catalysts for olefins polymerization," *Prog. Polym. Sci.*, vol. 84, pp. 89–114, Sep. 2018, doi: 10.1016/j.progpolymsci.2018.06.005.

[11] R. Zannetti, C. Marega, A. Marigo, and A. Martorana, "Layer-lattices in Ziegler–Natta catalysts," *J. Polym. Sci. Part B Polym. Phys.*, vol. 26, no. 12, pp. 2399–2412, Nov. 1988,

doi: 10.1002/polb.1988.090261202.

[12] T. Taniike and M. Terano, “The use of donors to increase the isotacticity of polypropylene,” *Adv. Polym. Sci.*, vol. 257, pp. 81–97, 2013, doi: 10.1007/12_2013_224.

[13] T. Taniike, T. Funako, and M. Terano, “Multilateral characterization for industrial Ziegler-Natta catalysts toward elucidation of structure-performance relationship,” *J. Catal.*, vol. 311, pp. 33–40, Mar. 2014, doi: 10.1016/j.jcat.2013.10.023.

[14] T. Taniike, P. Chammingkwan, V. Q. Thang, T. Funako, and M. Terano, “Validation of BET specific surface area for heterogeneous Ziegler-Natta catalysts based on α_s-plot,” *Appl. Catal. A Gen.*, vol. 437–438, pp. 24–27, Sep. 2012, doi: 10.1016/j.apcata.2012.06.006.

[15] U. Giannini, “Polymerization of Olefins with High Activity Catalysts,” *Makromol. Chem., Suppl*, vol. 5, no. S19811, pp. 216–229, 1981, doi: 10.1002/macp.1981.020051981113.

[16] M. Boero, M. Parrinello, and K. Terakura, “First Principles Molecular Dynamics Study of Ziegler- Natta Heterogeneous Catalysis,” *J. Am. Chem. Soc*, vol. 120, no. 12, pp. 2746–2752, 1998, doi: 10.1021/ja972367i.

[17] M. Boero, M. Parrinello, and K. Terakura, “Ziegler-Natta heterogeneous catalysis by first principles computer experiments,” *Surf. Sci.*, vol. 438, no. 1–3, pp. 1–8, Sep. 1999, doi: 10.1016/S0039-6028(99)00537-3.

[18] M. Boero, M. Parrinello, S. Hüffer, and H. Weiss, “First principles study of propene polymerization in Ziegler-Natta heterogeneous catalysis,” *J. Am. Chem. Soc.*, vol. 122, no.

3, pp. 501–509, 2000, doi: 10.1021/ja990913x.

[19] M. Boero, M. Parrinello, H. Weiss, and S. Hüffer, “A first principles exploration of a variety of active surfaces and catalytic sites in Ziegler-Natta heterogeneous catalysis,” *J. Phys. Chem. A*, vol. 105, no. 21, pp. 5096–5105, 2001, doi: 10.1021/jp010780d.

[20] M. Boero, M. Parrinello, K. Terakura, and H. Weiss, “Car-Parrinello study of Ziegler-Natta heterogeneous catalysis: Stability and destabilization problems of the active site models,” *Mol. Phys.*, vol. 100, no. 18, pp. 2935–2940, Sep. 2002, doi: 10.1080/00268970110109899.

[21] T. Taniike and M. Terano, “Coadsorption and support-mediated interaction of Ti species with ethyl benzoate in $MgCl_2$-supported heterogeneous ziegler-natta catalysts studied by density functional calculations,” *Macromol. Rapid Commun.*, vol. 28, no. 18–19, pp. 1918–1922, Sep. 2007, doi: 10.1002/marc.200700363.

[22] T. Taniike and M. Terano, “Reductive formation of isospecific Ti dinuclear species on a $MgCl_2$ (110) surface in heterogeneous ziegler-natta catalysts,” *Macromol. Rapid Commun.*, vol. 29, no. 17, pp. 1472–1476, Sep. 2008, doi: 10.1002/marc.200800310.

[23] T. Taniike and M. Terano, “A Density Functional Study on the Influence of the Molecular Flexibility of Donors on the Insertion Barrier and Stereoselectivity of Ziegler-Natta Propylene Polymerization,” *Macromol. Chem. Phys.*, vol. 210, no. 24, pp. 2188–2193, Dec. 2009, doi: 10.1002/macp.200900465.

[24] T. Taniike and M. Terano, “Coadsorption model for first-principle description of roles of

donors in heterogeneous Ziegler-Natta propylene polymerization," *J. Catal.*, vol. 293, pp. 39–50, Sep. 2012, doi: 10.1016/j.jcat.2012.06.001.

[25] A. Matta, P. Chammingkwan, B. K. Singh, M. Terano, T. Kaneko, and T. Taniike, "Truxillic and truxinic acid-based, bio-derived diesters as potent internal donor in Ziegler-Natta catalyst for propylene polymerization," *Appl. Catal. A Gen.*, vol. 554, pp. 80–87, Mar. 2018, doi: 10.1016/J.APCATA.2018.01.030.

[26] T. Taniike and M. Terano, "High-precision Molecular Modelling for Ziegler-Natta Catalysts," *J. Japan Pet. Inst.*, vol. 61, no. 3, pp. 182–190, 2018.

[27] V. Busico *et al.*, "Periodic DFT and High-Resolution Magic-Angle-Spinning (HR-MAS) ^{1}H NMR Investigation of the Active Surfaces of $MgCl_2$-Supported Ziegler−Natta Catalysts. The $MgCl_2$ Matrix," *J. Phys. Chem. C*, vol. 112, no. 4, pp. 1081–1089, Jan. 2008, doi: 10.1021/jp076679b.

[28] M. D'Amore, R. Credendino, P. H. M. Budzelaar, M. Causá, and V. Busico, "A periodic hybrid DFT approach (including dispersion) to $MgCl_2$-supported Ziegler-Natta catalysts - 1: $TiCl_4$ adsorption on $MgCl_2$ crystal surfaces," *J. Catal.*, vol. 286, pp. 103–110, Feb. 2012, doi: 10.1016/j.jcat.2011.10.018.

[29] R. Credendino, J. T. M. Pater, A. Correa, G. Morini, and L. Cavallo, "Thermodynamics of formation of uncovered and dimethyl ether-covered $MgCl_2$ crystallites. consequences in the structure of Ziegler-Natta heterogeneous catalysts," *J. Phys. Chem. C*, vol. 115, no. 27, pp.

13322–13328, Jul. 2011, doi: 10.1021/jp201410n.

[30] R. Credendino, D. Liguori, G. Morini, and L. Cavallo, “Investigating phthalate and 1,3-diether coverage and dynamics on the (104) and (110) surfaces of $MgCl_2$-supported Ziegler-Natta catalysts,” *J. Phys. Chem. C*, vol. 118, no. 15, pp. 8050–8058, Apr. 2014, doi: 10.1021/jp501390e.

[31] D. V. Stukalov, I. L. Zilberberg, and V. A. Zakharov, “Surface species of titanium(IV) and titanium(III) in $MgCl_2$-Supported Ziegler-Natta catalysts. A periodic density functional theory study,” *Macromolecules*, vol. 42, no. 21, pp. 8165–8171, Nov. 2009, doi: 10.1021/ma901413b.

[32] D. V. Stukalov and V. A. Zakharov, “Active site formation in $MgCl_2$-supported ziegler - Natta catalysts. A density functional theory study,” *J. Phys. Chem. C*, vol. 113, no. 51, pp. 21376–21382, Dec. 2009, doi: 10.1021/jp907812k.

[33] D. V. Stukalov, V. A. Zakharov, and I. L. Zilberberg, “Adsorption species of ethyl benzoate in $MgCl_2$-supported ziegler-natta catalysts. A density functional theory study,” *J. Phys. Chem. C*, vol. 114, no. 1, pp. 429–435, Jan. 2010, doi: 10.1021/jp908551k.

[34] A. Bazhenov, M. Linnolahti, T. A. Pakkanen, P. Denifl, and T. Leinonen, “Modeling the stabilization of surface defects by donors in ziegler-natta catalyst support,” *J. Phys. Chem. C*, vol. 118, no. 9, pp. 4791–4796, Mar. 2014, doi: 10.1021/jp412386u.

[35] M. S. Kuklin, A. S. Bazhenov, P. Denifl, T. Leinonen, M. Linnolahti, and T. A. Pakkanen,

"Stabilization of magnesium dichloride surface defects by mono- And bidentate donors," *Surf. Sci.*, vol. 635, pp. 5–10, May 2015, doi: 10.1016/j.susc.2014.11.026.

[36] M. Toto, G. Morini, G. Guerra, P. Corradini, and L. Cavallo, "Influence of 1,3-diethers on the stereospecificity of propene polymerization by supported Ziegler-Natta catalysts. A theoretical their adsorption on (110) and (100) lateral cuts of $MgCl_2$ platelets," *Macromolecules*, vol. 33, no. 4, pp. 1134–1140, 2000, doi: 10.1021/ma990959a.

[37] E. Breuza, G. Antinucci, P. H. M. Budzelaar, V. Busico, A. Correa, and C. Ehm, "$MgCl_2$-supported Ziegler-Natta catalysts: A DFT-D 'flexible-cluster' approach. $TiCl_4$ and probe donor adducts," *Int. J. Quantum Chem.*, vol. 118, p. e25721, Sep. 2018, doi: 10.1002/qua.25721.

[38] E. Breuza, G. Antinucci, P. H. M. Budzelaar, V. Busico, A. Correa, and C. Ehm, "$MgCl_2$-Supported Ziegler-Natta Catalysts: A DFT-D 'flexible-Cluster' Approach to Internal Donor Adducts," *J. Phys. Chem. C*, vol. 122, no. 16, pp. 9046–9053, Apr. 2018, doi: 10.1021/acs.jpcc.8b01500.

[39] A. Andoni, J. C. Chadwick, H. J. W. Niemantsverdriet, and P. C. Thüne, "The role of electron donors on lateral surfaces of $MgCl_2$-supported Ziegler-Natta catalysts: Observation by AFM and SEM," *J. Catal.*, vol. 257, no. 1, pp. 81–86, Jul. 2008, doi: 10.1016/j.jcat.2008.04.020.

[40] M. D'Amore, K. S. Thushara, A. Piovano, M. Causà, S. Bordiga, and E. Groppo, "Surface

Investigation and Morphological Analysis of Structurally Disordered $MgCl_2$ and $MgCl_2/TiCl_4$ Ziegler-Natta Catalysts," *ACS Catal.*, vol. 6, no. 9, pp. 5786–5796, Sep. 2016, doi: 10.1021/acscatal.6b00871.

Chapter2:
Non-empirical Structure Determination for $TiCl_4$–Capped $MgCl_2$ Nanoplate of Heterogeneous Ziegler–Natta Catalyst

Abstract

Dynamic reconstruction under a physicochemical environment is an intrinsic nature of solid surfaces, in particular associated with catalysis on nano-sized or nano-structured materials. This chapter reports non-empirical structure determination of $TiCl_4$-capped $MgCl_2$ nanoplates based on combination of a genetic algorithm and density functional calculations. The methodology for the non-empirical structure determination was developed, and its application was demonstrated for $7MgCl_2$, $15MgCl_2$, and $15MgCl_2/4TiCl_4$ in relation to the hidden identity of primary particles of the Ziegler-Natta catalyst. Bare $MgCl_2$ nanoplates dominantly exposed {100} surfaces at their lateral cuts, but the chemisorption of $TiCl_4$ induced reconstruction by stabilizing {110} surfaces. The most important finding of this chapter is that $TiCl_4$ exhibited distributed adsorption states as consequences of chemisorption on nonideal finite surfaces and the diversity of thermodynamically accessible structures. The assessment of the Ti distribution is essential for the distribution of primary structures of produced polymer and this chapter realized it.

Keywords: Ziegler-Natta catalyst, genetic algorithm, structure determination, density functional theory, surface reconstruction

2.1. Introduction

Recent developments in computers and first-principle calculations have enabled realistic simulation of complicated systems. The role of computational chemistry in materials science is shifting from one of characterization tools toward the mechanistic elucidation at a molecular level [1]–[3], and even the prediction of unknown materials [4]–[7]. All computational chemistry requires a molecular model of materials as an initial structure, while it is still hard to experimentally acquire molecular-scale knowledge of complex materials like solid catalysts. In many cases, the construction of molecular models relies on physicochemical inference or limited experimental clues, and inaccurate molecular models fall in wrong local minima as a result of usual geometry optimization. Accordingly, a method for non-empirical structure determination is desired.

Combination patterns of atomic and molecular arrangements explode exponentially with their numbers; hence it is impossible to search structure candidates by brute force. To efficiently explore this huge configuration space, non-empirical structure determination methods typified by simulated annealing method [8], basin hopping method [9], and an evolutionary algorithm have been devised. Structure optimization using the genetic algorithm has been studied since 1990s. It starts from randomly generated structures, and evolves them for a predefined index (mostly energy) through operators that mimic the evolution of creatures, such as crossover, mutation, and natural selection. Compared to other contemporary methods, the genetic algorithm method is not often as efficient, but robust in exploring a vast configuration space without pre-knowledge. Moreover, a large number of meta-stable structures are obtained in the course of the evolution, which are of thermodynamic and catalytic interests.

Table 2.1 summarizes selected efforts on the development and applications of non-empirical structure determination [9]–[33]. A majority of previous efforts were devoted to the methodological development and demonstration for molecular clusters or crystals using empirically built potentials. Since 2005, the focus of the non-empirical structure determination has shifted to practical applications as exemplified by noble metal clusters as well as the utilization of DFT calculations for "local" geometry optimization and energy assessment. To be more relevant, structure determination of noble metal clusters on solid surfaces has started to emerge in 2010s, where the structure of the metal clusters was optimized on the assumption of a non-reconstructable or even non-relaxable single-crystal surface [11], [19]. So far, dynamic reconstruction of the support surfaces upon adsorption has been scarcely accounted at the best of our knowledge [33].

Table 2.1. Selected efforts on non-empirical structure determination.

Ref.	Year	Method	Potential	System
[10]	1995	Genetic algorithm (GA)	Born	Li_3RuO_4 crystals
[9]	1997	Basin hopping (BH)	Lennard-Jones (LJ)	$(LJ\ cluster)_{2–110}$
[21]	1997	GA	LJ, TIP3P	$(LJ\ cluster)_{13,19}$, $(H_2O)_{2–13}$
[27]	1999	GA	Born	Crystals of binary and ternary oxides (e.g. TiO_2, $MgAl_2O_4$)
[28]	1999	BH	Born-Mayer-Huggins	$(NaCl)_{35}Cl^–$
[29]	2000	GA	LJ	$Si_{9–23}$
[30]	2003	Parallel tempering	LJ, Murthy	$(CO_2)_{6–19}$

[31]	2005	GA	DFT (B3LYP)	$Li_{5-7}^{0/+1/-1}$
[32]	2007	GA	LJ, Williams and Starr	$(LJ\ cluster)_{10-561}$, $(C_6H_6)_{30}$
[33]	2010	GA	DFT (PBE)	$Ag_7(SR)_4^-$
[11]	2014	GA	DFT (PBE)	$Pd_nAg_{(4-n)}$, $Pd_nPt_{(4-n)}$ on MgO (100) ($0 \le n \le 4$)
[12]	2014	GA	LJ, Coulomb	$(CO_2)_{2-13}$
[13]	2014	BH	DFT (BLYP)	$(H_2O)_{4-10}$, $NO_3^-(H_2O)_{1-7}$, $C_2O_4^{2-}(H_2O)_{1-6}$
[14]	2014	GA	DFT (PBE)	Li_5Ge_2 crystals
[15]	2014	GA, SA	Coulomb-Backingham (CB)	$(TiO_2)_{1-12}$
[16]	2014	GA, simulated annealing (SA)	Born-Meyer, Coulomb	$(MgO)_{2-15}$
[17]	2015	GA, SA	CB	$(MgF_2)_{2-10}$
[18]	2015	GA	DFT (PBE)	Ir_{10-20}
[19]	2016	GA	DFT (PBE)	Pd_n, Au_m, Au_mPd_n (n+m = 4–10) on MgO (100)
[20]	2017	GA	DFT (PBE)	Ru_{3-12}, Pt_{3-10}, Ru_mPt_n ($3 \le m + n \le 8$)
[22]	2017	GA	DFT (PBE)	g–C_3N_4 crystals
[23]	2017	GA	DFT (PBE)	Au_mRh_n ($6 \le m + n \le 10$)
[24]	2017	BH	DFT (PBE)	Au_{21-25}^-
[25]	2017	GA	DFT (PBE, TPSS)	Au_{27-30}
[26]	2017	Particle swarm optimization	LJ	$(LJ\ cluster)_{2-60}$

The heterogeneous Ziegler-Natta (ZN) catalyst is a main catalyst for the industrial production of polyolefins. The constituents of its solid procatalyst are $MgCl_2$ as a support, $TiCl_4$ as an active site precursor, and an organic Lewis base as a modifier. The Lewis base, called donor, exerts steric and electronic influences on active sites (alkylated Ti^{3+}) so as to improve their stereospecificity and

modify other important properties [34], [35]. For kinetic and morphological reasons, catalyst macroparticles are composed by hierarchical agglomeration of smaller particles, resulting in the formation of pores whose sizes range from micro to macro [36], [37]. The smallest building unit of this agglomeration, hence that of the catalyst, is termed primary particle. For the identity of the primary particles, a certain consensus exists in the community: $MgCl_2$ nanocrystals are featured with stacking discontinuity and/or fault along the *c*-axis [38], [39] and its lateral surfaces are capped by $TiCl_4$ and donor molecules. However, this consensus has been reached mainly based on the interpretation of broad XRD patterns of activated $MgCl_2$. The detailed morphology and surface exposure of the primary particles are still experimentally unaccessed, even though they offer a basis for the adsorption of the catalytic constituents and catalysis.

Apart from the uncertainty of the primary particles, a number of DFT studies have been reported on this system. Assuming ideal single-crystal surfaces of $MgCl_2$ such as (110), (104) or (100), the adsorption of $TiCl_4$ and donor molecules and their interaction upon coadsorption were studied [5], [40]–[56]. Consistent conclusions from these calculations are that $TiCl_4$ prefers unimolecular adsorption on the (110) surface, and its interaction with a donor molecule explains experimentally known consequences of the addition of donors. Recently, non-ideal aspects of the catalyst primary particles have been taken into account. For instance, step defects were expressed in a slab model in order to examine potential stabilization of the defects by the adsorption of donors [57], [58] and an active site model at an edge defect was employed to describe the structure-performance relationship of alkoxysilane external donors in propylene polymerization [5], [59]. The finite size of the primary particles was expressed by employing $MgCl_2$ nanoplates consisting of a single Cl-Ti-Cl trilayer that

exposes either the (110) or (100) surface on their lateral terminations [60]–[62]. Likewise, computational studies on the ZN catalyst has advanced from understanding the surface chemistry on simplified models to establishing accurate surface models. In this light, yet an unaccounted important aspect of $MgCl_2$ is its dynamic response to a given environment. Recent experimental results have uncovered the fact that $MgCl_2$ flexibly adjusts its structure in the presence of coordinating molecules. Andoni et al. observed a structure directing role of different donors in the formation of $MgCl_2$ crystal morphology [63]. D'Amore et al. reported that the presence of alcohol significantly affects the morphology of activated $MgCl_2$ by means of high-resolution TEM and CO-probed IR [64]. Taniike et al. demonstrated the reconstruction of (001)-terminated $MgCl_2$ films in the presence of donors based on ultrahigh vacuum low-energy electron diffraction [65]. For incorporating the said reconstruction as a factor of the simulation, calculations on predefined surfaces of slabs and clusters are not sufficient. A vast configuration space spanned by combining $MgCl_2$ and adsorbates needs to be explored, and such simulation has never been reported.

In this chapter, a methodology of non-empirical structure determination for $MgCl_2/TiCl_4$ primary particles was developed based on the combination of the genetic algorithm and DFT calculations, where reconstruction of $MgCl_2$ by the chemisorption of $TiCl_4$ was explicitly handled for the first time. The structure determination was implemented for $7MgCl_2$, $15MgCl_2$, and $15MgCl_2/4TiCl_4$ not only to confirm proper operation of the method, but also to investigate potential reconstruction of $MgCl_2$ and other effects caused by the chemisorption of $TiCl_4$.

2.2. Numerical methods

For the primary particles of the ZN catalyst, a structure determination program was developed by combining the genetic algorithm for global structure exploration and DFT for local geometry optimization. The program targets $MgCl_2/TiCl_4$, where a $MgCl_2$ monolayer capped with $TiCl_4$ molecules was presumed. The program flow is illustrated in Figure 2.1. First, initial structures are generated based on random numbers under restrictions that are later defined. Then, generated structures are subjected to geometry optimization by DFT. To the optimized structures, the "fitness score" is individually assigned according to their energy. A structure having a larger fitness score has a higher opportunity to be selected for crossover, mutation, and elitism operations, thus inheriting its feature to the next generation. The repetition of this cycle evolves the structures in a way to lower the energy. In principle, the genetic algorithm does not guarantee the optimal solution in finite generations. For this reason, the solution was regarded as the optimal one (*i.e.* the most stable structure), when the solution satisfied the requirement that multiple runs independently converged to the same physicochemically reasonable structure after a sufficient number of generations. The details of the program and other numerical information are described hereafter.

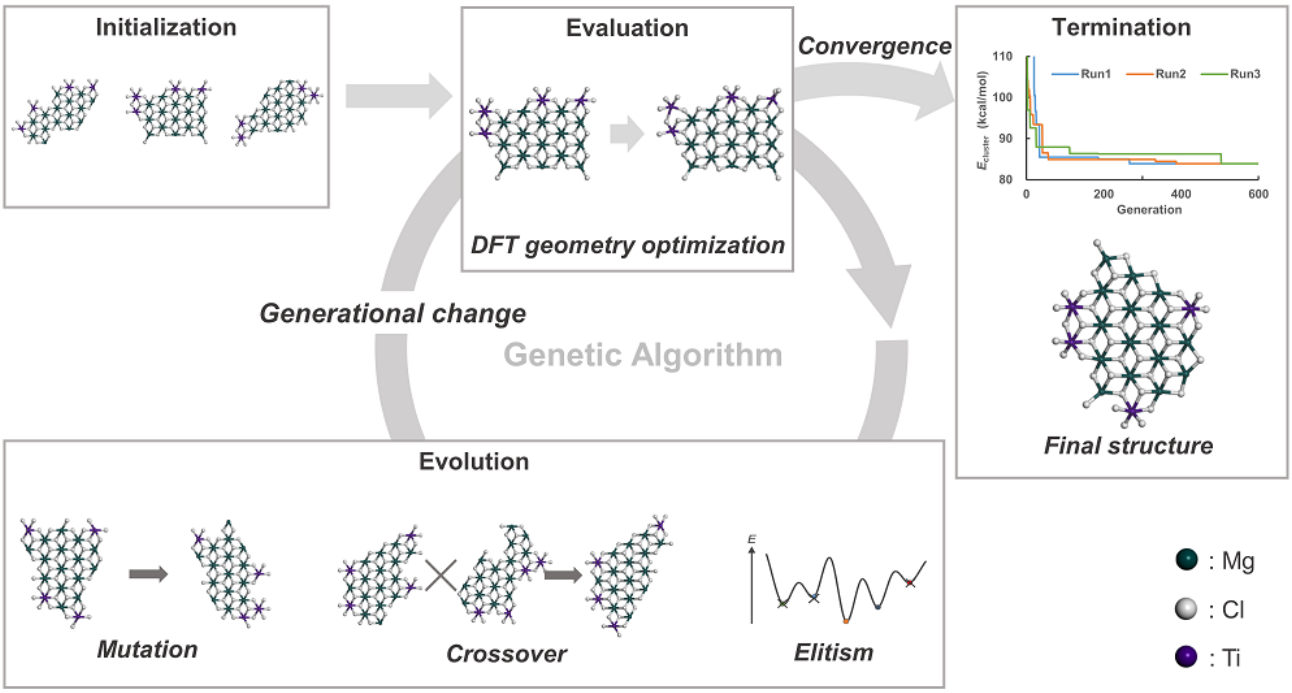

Figure 2.1. Structure determination program developed in this work.

2.2.1 Initialization

The first step of the program is initialization. A pre-defined number of initial structures (the population in one generation) are generated based on random numbers according to the procedure of Figure 2.2. The skeleton of a $MgCl_2$ monolayer is expressed by mutually connected hexagons that represent the ionic lattice of $MgCl_2$. When projected to a two-dimensional space, Mg^{2+} cations are placed at the center of the hexagons while Cl^- anions are placed at their apexes.

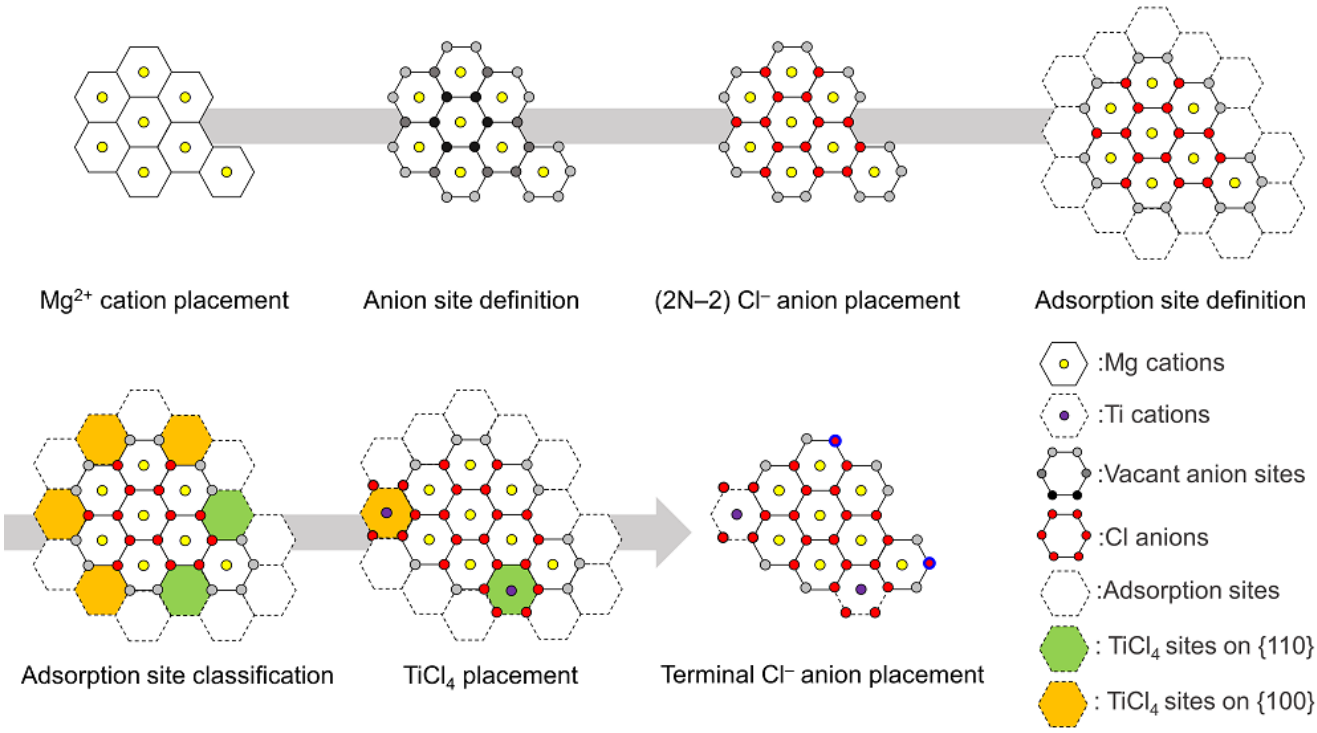

Figure 2.2. Schematic representation of initial structure generation (*e.g.* $8MgCl_2/2TiCl_4$). The skeleton of $MgCl_2$ is projected onto a two-dimensional space, where the mutually connected hexagons represent the ionic lattice of $MgCl_2$. Mg^{2+} cations (yellow) are located at the center of the hexagons and anion sites are defined at their apexes. The coordination numbers of the anion sites are classified by the depth of the color (black: 3-fold, dark gray: 2-fold, light gray: 1-fold). The 3-fold and 2-fold coordinated anion sites are unequivocally occupied by (2N–2) Cl^- anions (red). Adsorption sites are defined at the periphery of the skeleton. $TiCl_4$ and the remaining two terminal Cl^- anions (red with a blue circle) are placed at randomly selected appropriate sites in this order.

First, N Mg^{2+} cations are placed according to self-avoiding random walk, which spans connected N hexagons (non-convex morphologies were excluded for an energetic reason). To the potential anion sites, (2N−2) Cl^- anions are placed in the descending order of the coordination number to the Mg^{2+} cations for keeping the local electronic neutrality. Note that the self-avoiding random walk

results in skeletons having (2N−2) anion sites of the coordination number of 2 or 3, so that these anion sites are unequivocally occupied by (2N−2) Cl^- anions. Adsorption sites are defined as additional hexagons at the lateral periphery of the Mg skeleton. The adsorption sites are classified according to the occupation pattern of anion sites. For example, the adsorption of $TiCl_4$ molecules occurs in a way that a Ti^{4+} cation is centered at the hexagon of an adsorption site that possesses 3–4 Cl^- anions from $MgCl_2$, resulting in the coordination number of Ti^{4+} cation of 5–6. Finally, $TiCl_4$ molecules and the remaining two terminal Cl^- anions are placed at randomly selected appropriate sites, where the terminal Cl^- anions are placed in the end to avoid the lack of available sites, especially at a high surface coverage.

2.2.2. Evaluation

Each structure is evaluated based on the energy after geometry optimization. The DFT geometry optimization was performed at the level of GGA PBE[66] using the basis set of DNP[67] with effective core potentials [68], [69] in $DMol^3$ [67]. All the atoms were allowed to relax from their original positions. The convergence criteria for geometry optimization were set to 0.01255 kcal/mol in energy, 2.510 kcal/(mol Å) in force, and 0.005 Å in displacement. These computational methods were chosen for a balance between the computational cost and accuracy [56], while the program is readily applicable for a higher level of methods [43], [62]. The energies obtained after the geometry optimization are used to derive the fitness of the corresponding structures according to

$$\rho_i = \frac{E_i - E_{min}}{E_{max} - E_{min}} \quad (2.1)$$

$$f_i = exp(-3\rho_i) \quad (2.2)$$

where E_i, E_{min}, E_{max}, and f_i are the energy of the i^{th} structure in a generation, the energies of the most and least stable structures in the same generation, and the fitness of the i^{th} structure, respectively.

2.2.3. Evolution

The evolution is performed by creating new structures from the structures of the last generation through genetic operators: Crossover, mutation and elitism. The elitism carries over a predefined number of lower-energy structures from the last generation. The other operators work as follows and as exemplified in Figure 2.3.

Crossover: Succeeding features of selected two structures by extracting a shared part of Mg^{2+} cations while randomly inheriting unshared Mg^{2+} cations from the two structures. After defining a new skeleton, (2N–2) Cl^- anions are similarly relocated, adsorption sites are similarly redefined, and the adsorbates are inherited from the parent structures as long as the adsorption sites are still available. If unavailable, un-inherited adsorbates are randomly relocated on available sites.

Mutation (skeleton): Randomly relocating a part of Mg^{2+} cations of selected one structure. The Cl^- anions and adsorbates are similarly treated.

Mutation (adsorbate): Randomly relocating a part of $TiCl_4$ molecules and terminal Cl^- anions of selected one structure. The skeleton is kept unchanged.

Structures used in these operators are selected based on fitness proportionate selection, which is also called roulette wheel selection. The newly generated structures are subjected to the above-mentioned evaluation, and this cycle stepwise updates the generation.

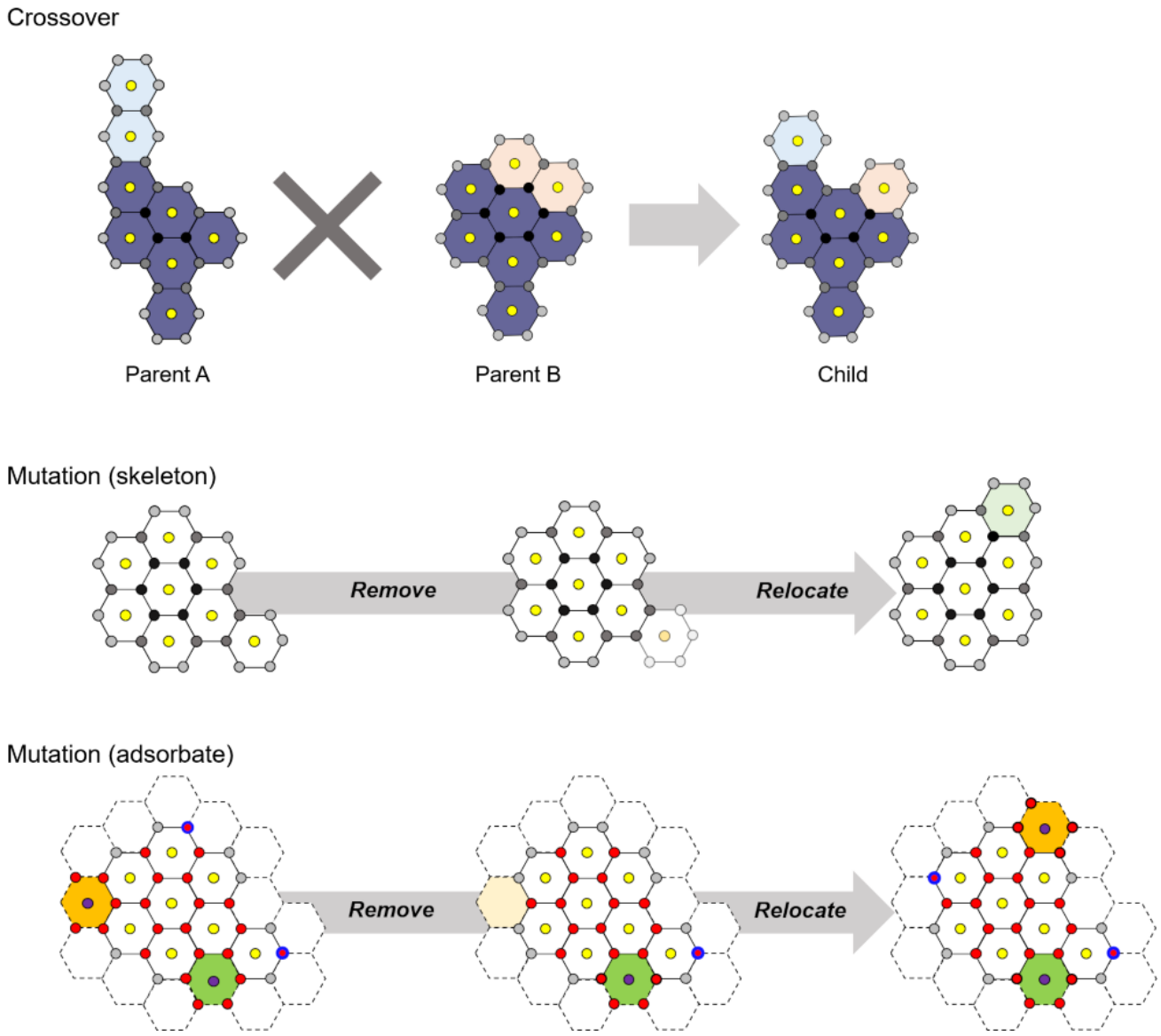

Figure 2.3. Schematic representation of crossover and mutation operations. In the crossover, a shared part of the skeletons for the parents is colored as dark blue. The unshared part is randomly inherited from either of the parents. In the mutation, a specified portion of the hexagons (*i.e.* Mg^{2+} cations) or adsorbates are randomly relocated.

2.2.4. Demonstration

The developed program was demonstrated by implementing structure determination on $7MgCl_2$, $15MgCl_2$ and $15MgCl_2/4TiCl_4$. The structure of the lowest energy was already reported for $7MgCl_2$

by Luhtanen et al. at the MP2/6-311G* level (based on manual exploration) [70], so it was used for the initial validation. Dynamic reconstruction of $MgCl_2$ in the presence of $TiCl_4$ was investigated by comparing the structures between $15MgCl_2$ and $15MgCl_2/4TiCl_4$. The size of $15MgCl_2$ was computationally facilely tractable, but believed to be not too small compared to the reported primary particle size [39], [71], [72] (*ca.* 1.1–2.0 nm *vs.* 2.4–4.0 nm). Parameters used in the genetic algorithm are summarized in Table 2.2.

Table 2.2. Parameters of the genetic algorithm[a]

	$7MgCl_2$	$15MgCl_2$	$15MgCl_2/4TiCl_4$
Population	16	26	36
Crossover [%]	57.1	38.5	27.8
Mutation (skeleton)[b] [%]	14.3	15.4	16.7
Mutation (adsorbate)[b] [%]	14.3	15.4	11.1
Elitism [%]	14.3	30.7	44.4

[a]The population represents the number of structures in one generation. Except the 1st generation, the structures are produced based on crossover, mutation, and elitism operations, whose proportions in a generation are described by percentages. [b]In the mutation, the maximum percentage of relocated ions (skeleton) or molecules (adsorbate) was set to 20%. The number of relocated ions and molecules is stochastically chosen from integers excluding zero in the range of 0–20%.

2.3. Results and Discussion

Figures 2.4 and 2.5 show evolutionary progress plots of the genetic algorithm for the structure determination of $7MgCl_2$ and $15MgCl_2$, respectively. The progress was monitored by the energy of

the best-of-generation individual (*i.e.* the most stable structure in a generation). The energy was expressed as the cluster energy (E_{cluster}) according to

$$E_{\text{cluster}} = E - N_{\text{MgCl}_2} \times E_{\text{MgCl}_2} - N_{\text{TiCl}_4} \times E_{\text{TiCl}_4} \quad (2.3)$$

where E is the energy of a structure after the geometry optimization, N_{MgCl_2} is the number of $MgCl_2$ units, E_{MgCl_2} is the energy of a $MgCl_2$ unit in the α form (bulk), N_{TiCl_4} is the number of $TiCl_4$ molecules, E_{TiCl_4} is the energy of an isolated $TiCl_4$ molecule in vacuum. E_{cluster} corresponds to the sum of the surface energy of a bare cluster and the adsorption energy of $TiCl_4$ on it, and evaluates the competition between the penalty to expose a coordinatively unsaturated surface and its stabilization by the adsorption. The declining tendencies along the generation were confirmed for the energy of the best-of-generation individual, encompassing proper learning. Moreover, independently implemented runs converged into the same reasonable structure as a result of the evolution over sufficient generations (40 for $7MgCl_2$ and 80 for $15MgCl_2$). The final structure of $7MgCl_2$ possessed a isosceles trapezoid morphology, which was identical to the most stable structure reported by Luhtanen et al. [70]. The structure of $15MgCl_2$ has not been determined in literature, but the obtained parallelogram structure equipped similar features with that of $7MgCl_2$: The lateral termination was fully done by the most stable {100} surface (except {001} for the basal plane), and two terminal Cl^- anions were symmetrically placed for minimizing overall polarization. Though $7MgCl_2$ and $15MgCl_2$ were much smaller than the experimentally reported primary particle size around 3 nm [39], [71], [72] (corresponding to $100MgCl_2$), stable structures of larger $MgCl_2$ clusters are expected to have similar features. The E_{cluster} value of $15MgCl_2$ was 34.3 kcal/mol larger than

that of $7MgCl_2$ as the former exposed more unsaturated Mg^{2+} cations. When normalized by the number of the $MgCl_2$ units, the penalty of the exposure was smaller for $15MgCl_2$.

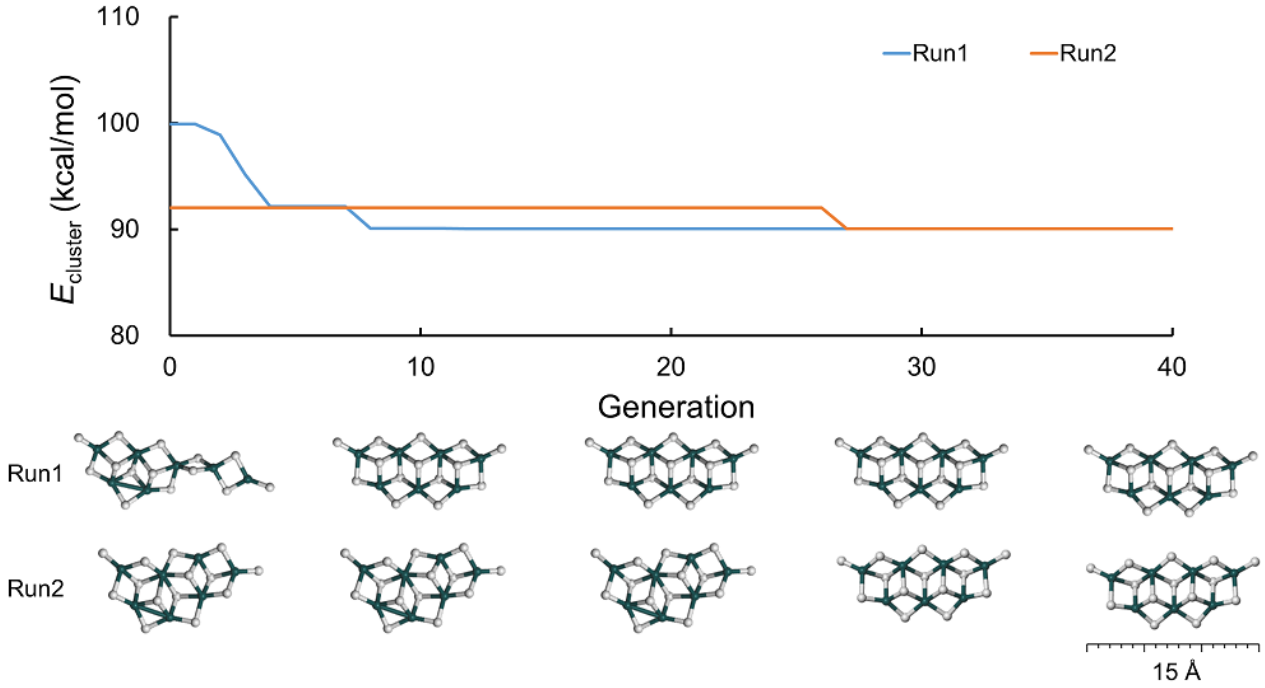

Figure 2.4. Evolutionary progress plot for the structure determination of $7MgCl_2$. The energy of the best-of-generation individual (*i.e.* the most stable structure in a generation) is plotted against the generation. The structure of the most stable individual is also shown for each of 10 generations.

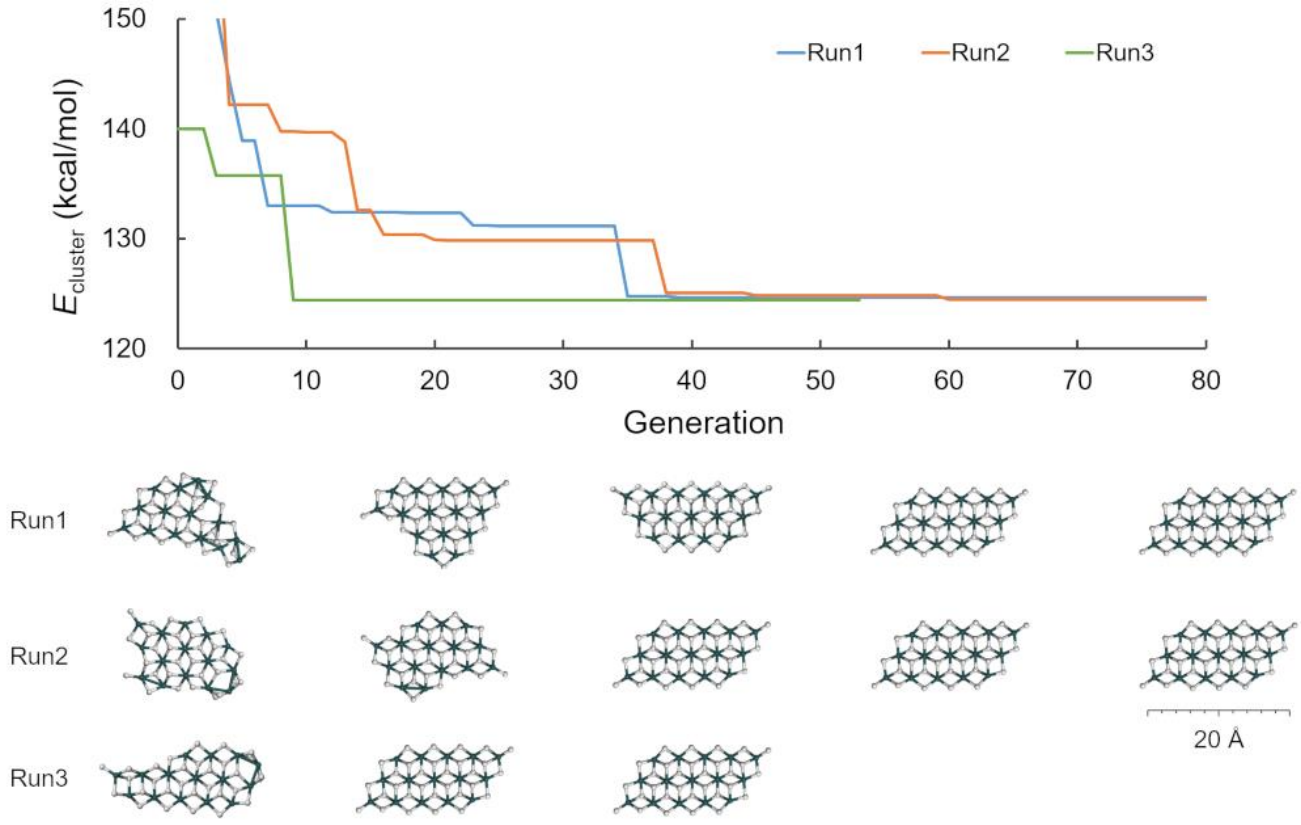

Figure 2.5. Evolutionary progress plot for the structure determination of $15MgCl_2$.

The above results for bare $MgCl_2$ clusters validated the proper operation of the developed program. Accordingly, the program was applied to the structure determination of $15MgCl_2/4TiCl_4$. From the evolutionary progress plot in Figure 2.6, the feasibility of non-empirical structure determination in the presence of adsorbates was proven by the monotonic decrement of the energy as well as by the convergence of multiple runs into the same structure. To be interesting, the number of generations required for the convergence was dramatically increased from 80 to 600 by the addition of $4TiCl_4$ molecules, while it was not the case when $4MgCl_2$ units were added to $15MgCl_2$ ($19MgCl_2$, not shown). This is because the number of isomeric structures having similar energies was significantly diversified in the presence of $TiCl_4$. This observation is later addressed in detail. The $MgCl_2$ skeleton

of the final structure was at glance different from that of bare $15MgCl_2$, *i.e.* the reconstruction of the $MgCl_2$ nanoplate in the presence of $TiCl_4$ was non-empirically confirmed for the first time. To elaborate on this reconstruction, three structures and their energies are compared in Figure 2.7. As mentioned above, the most stable structure of bare $15MgCl_2$ was fully terminated by {100} surfaces with 60°/120° edges at the intersection of two lateral surfaces, thus forming a parallelogram morphology (Figure 2.7a). When the placement of $4TiCl_4$ molecules was optimized assuming this morphology (*i.e.* no reconstruction), two dinuclear species were formed on the longer-side surfaces (Figure 2.7b). Its energy was 36.7 kcal/mol lower than that of the bare cluster, corresponding to the adsorption energy of 9.2 kcal/mol per $TiCl_4$ molecule. When the reconstruction of the skeleton was allowed using the developed program, the skeleton of the final structure exposed both of the {110} and {100} surfaces, and the {110} surfaces were necessarily capped by $TiCl_4$ (Figure c). In detail, one $MgCl_2$ unit was removed from a 120° edge of the parallelogram and instead put it on a longer-side {100} surface, which afforded three small {110} terraces, and these were capped by $TiCl_4$ mononuclear species. The remaining $TiCl_4$ molecule was placed on a shorter-side {100} surface. The energy of the most stable $15MgCl_2/4TiCl_4$ was about 4 kcal/mol lower than that of the non-reconstructed structure (Figure 2.7b), indicating that the penalty of exposing coordinatively more unsaturated {110} surfaces was overcome by stronger adsorption on the same surfaces and this was the driving force of the reconstruction.

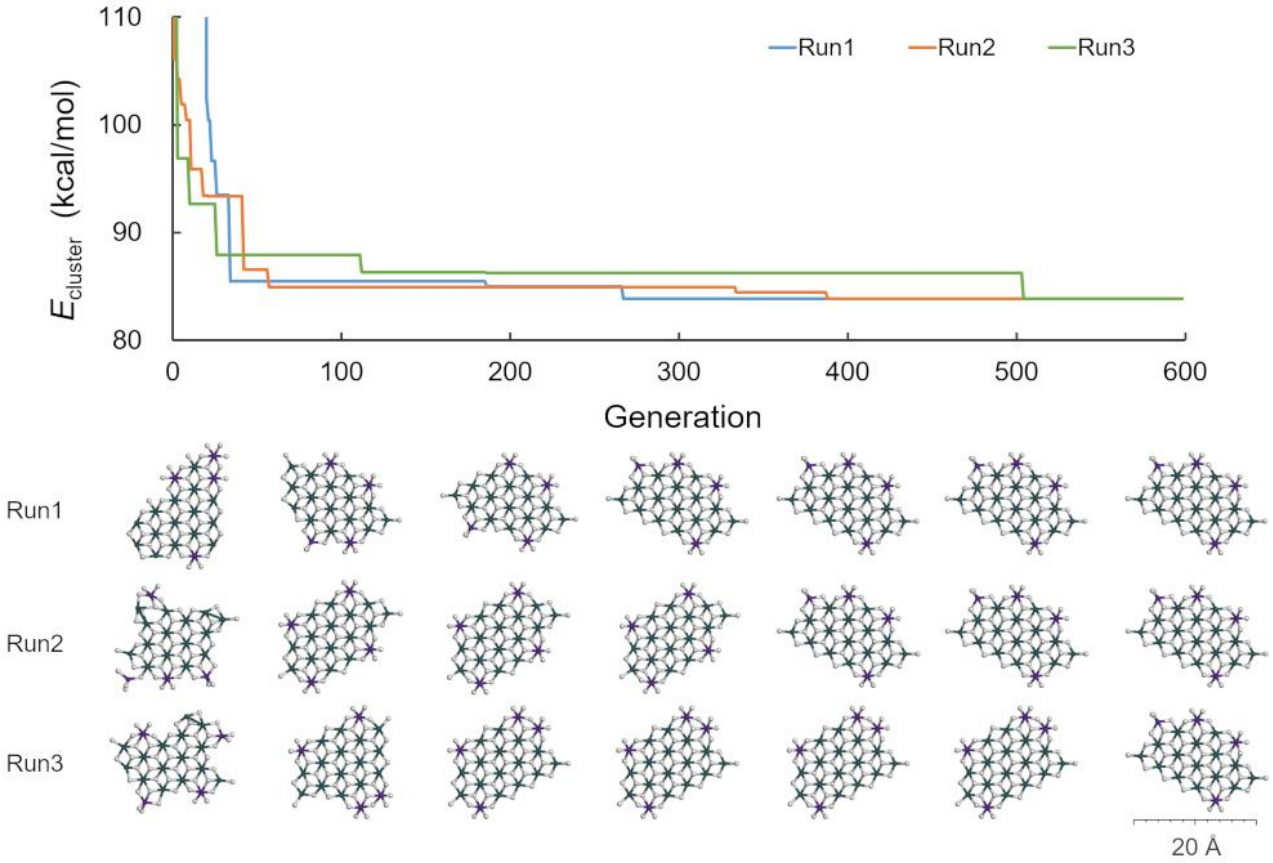

Figure 2.6. Evolutionary progress plot for the structure determination of $15MgCl_2/4TiCl_4$.

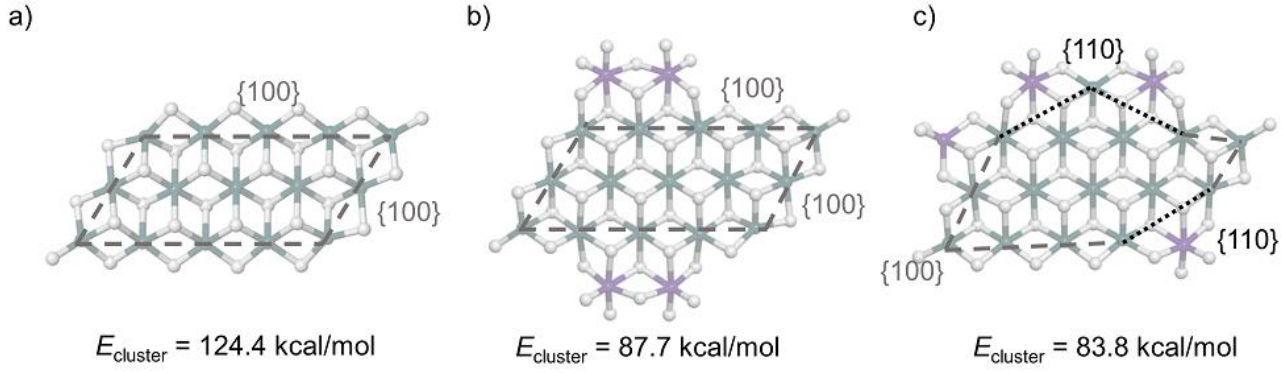

Figure 2.7. Comparison of the morphology and energy of $15MgCl_2$. a) The most stable structure of bare $15MgCl_2$. b) The placement of $4TiCl_4$ was optimized assuming the structure of a). c) The most stable structure of $15MgCl_2/4TiCl_4$.

To show the convergence of the genetic algorithm, the progress of the savings, the repetition of the structures, the appearance of energetically accessible structures are summarized in Figure 2.8.

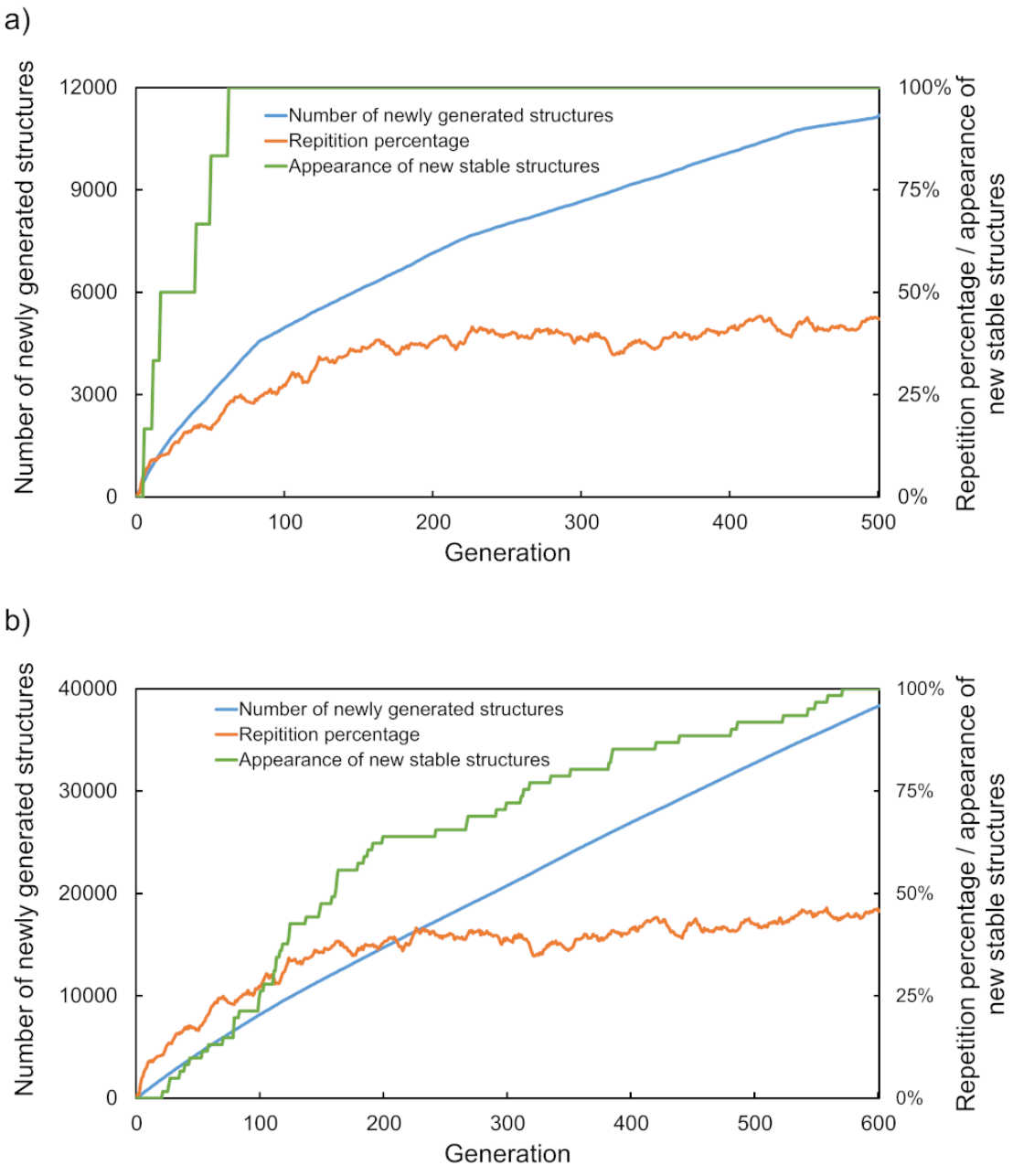

Figure 2.8. Progress of savings, repetition of structures, and appearance of energetically accessible structures along the generation: a) $15MgCl_2$ and b) $15MgCl_2/4TiCl_4$. The progress of savings corresponds to the cumulative number of structures along the generation, which excludes repeated structures. The repetition of structures describes the percentage that generated structures are already saved. The appearance of energetically accessible structures shows when metastable structures whose energies were not greater than 6 kcal/mol with respect to the energy of the corresponding most stable structure are generated in the cumulative percentage. It can be seen that the number of newly generated structures continuously increases along the generation, while the appearance of energetically accessible structures more or less converged in the later stage. This corresponds to preferential sampling of energetically advantageous structures in the genetic algorithm.

The implementation of the structure determination derived not only the most stable but also a huge number of metastable structures of $15MgCl_2$ and $15MgCl_2/4TiCl_4$. The analysis of these structures and energies were expected to confer important aspects of the $MgCl_2/TiCl_4$ system in relation to the ZN catalyst. Figure 2.9 lists up isomeric structures of $15MgCl_2$ and $15MgCl_2/4TiCl_4$, whose energies were not greater than 6 kcal/mol with respect to the energy of the corresponding most stable structure. In this energy range, bare $MgCl_2$ afforded only 6 isomeric structures. This is because the exposure of the bare {110} surface is energetically demanding, and only these 6 structures can dominantly expose the {100} surfaces. Contrary, over 50 isomeric structures were listed for $15MgCl_2/4TiCl_4$. This diversification by the adsorption of $TiCl_4$ arose from the following two reasons. First, the energetic penalty of $TiCl_4$ adsorption on a non-reconstructed {100} surface is not extremely large in

comparison with the reconstruction and subsequent $TiCl_4$ adsorption on a newly created {110} surface. Second, there are many ways of reconstruction that can create small {110} terraces on {100} surfaces. The diversification necessarily meant an expansion of the relevant configuration space, which explains why the number of generations till the convergence was significantly increased for $15MgCl_2/4TiCl_4$.

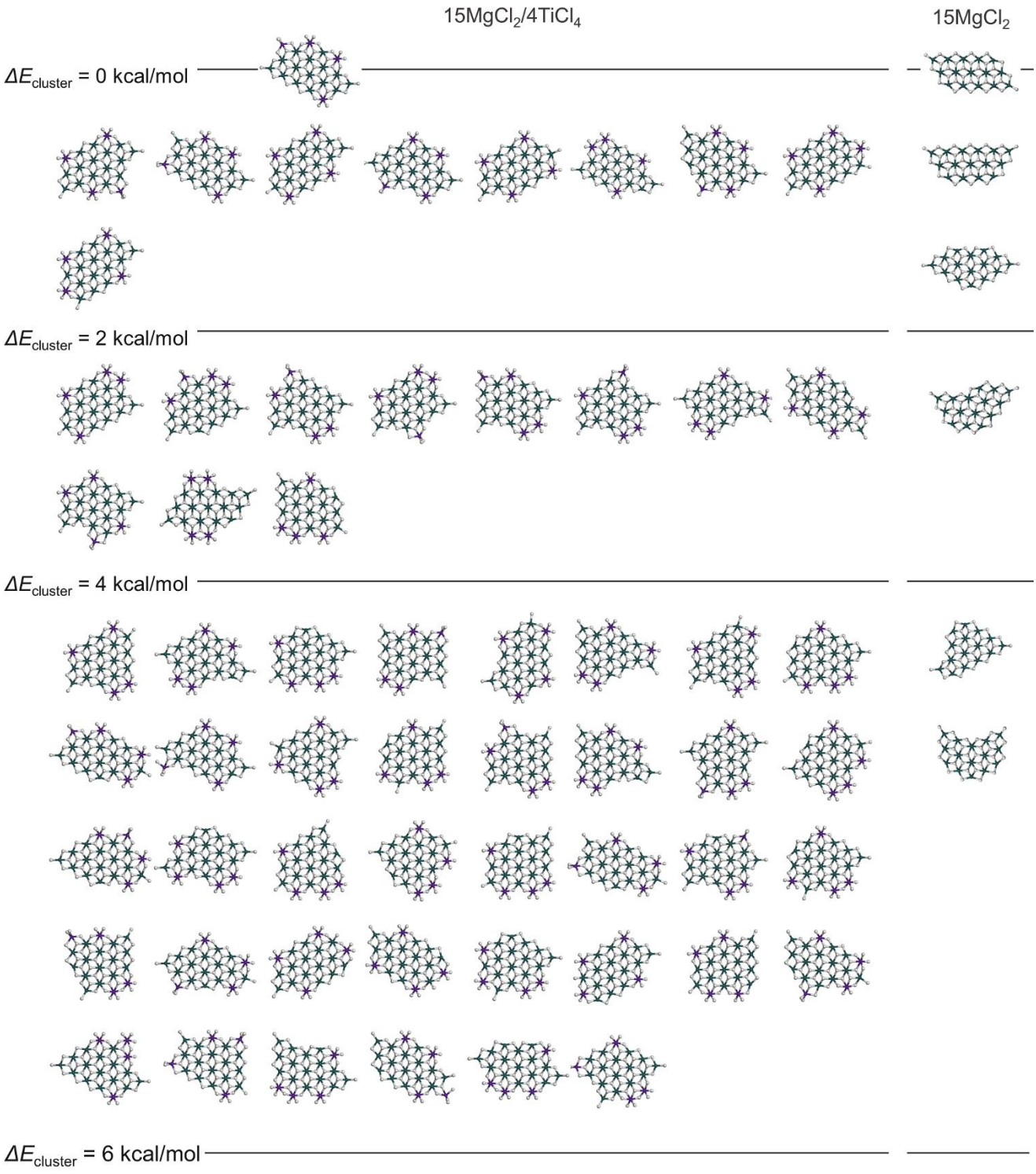

Figure 2.9. List of thermodynamically accessible structures for $15MgCl_2/4TiCl_4$ and bare $15MgCl_2$. The energy is denoted with respect to the energy of the corresponding most stable structure. Note that the number of accessible structures significantly increased in the presence of $TiCl_4$.

The presence of many isomeric structures suggested that the structure of the $MgCl_2/TiCl_4$ system is largely distributed and interconvertible as its intrinsic thermodynamic nature (at least true for $15MgCl_2/4TiCl_4$). This suggestion may also explain why the polymer produced by the ZN catalyst is always distributed in the stereoregularity, molecular weight, and chemical composition. In order to understand the distribution produced by the adsorption of $TiCl_4$, the equilibrium distribution of individual structures was estimated based on the Boltzmann factor

$$p = e^{-\frac{\Delta E_{\text{cluster}}}{RT}} \tag{2.4}$$

where p is the relative population of a structure with respective to the most stable one, and $\Delta E_{\text{cluster}}$ is its relative energy to that of the most stable one. Note that the estimation of the distribution based on (2.4) accompanied the following assumptions: The entropic difference among structures was ignored since structures of the same composition possess similar vibrations. Structures are purely under thermodynamic control, not kinetic control. Hiraoka et al. reported that the catalyst preparation protocol does not affect the stereospecificity of individual active sites as long as the same internal donor is employed, while the proportion of these active sites was affected by the preparation method [73]. Hence, it is believed that the presence of the distribution itself is not eliminated by a kinetic reason, but the kinetic factor modulates the distribution from the thermodynamic one; the heterogeneity of the chemical composition of primary particles was neglected as it has never been experimentally reported.

In spite of these assumptions, this is the first *ab-initio* estimation of the distribution in the ZN catalyst, which is important to understand the intrinsic nature of this catalyst and is never realized when predetermined $MgCl_2$ surfaces and clusters are employed. After calculating the equilibrium

population of individual structures for $15MgCl_2/4TiCl_4$, the population of three different $TiCl_4$ species was derived, that is, mononuclear species on {110}, mononuclear species on {100}, and dinuclear species on {100}. The structure of these species and the corresponding population are shown in Figure 10. The mononuclear species on the {110} surface was found to be dominant (76.1%), consistent with the prior conclusion obtained using ideal infinite surfaces [43], [56]. However, the presence of the other two species was not negligible: They were formed as a result of the fact that a $MgCl_2$ nanoplate could not offer a sole ideal surface due to the finite size. Even in the most stable structure, one mononuclear species was observed on {100} (*cf.* Figure 2.7c). Based on this result, it was postulated that $TiCl_4$ exhibits distributed adsorption states as combined consequences of the adsorption on nonideal finite surfaces and the diversity of thermodynamically accessible structures.

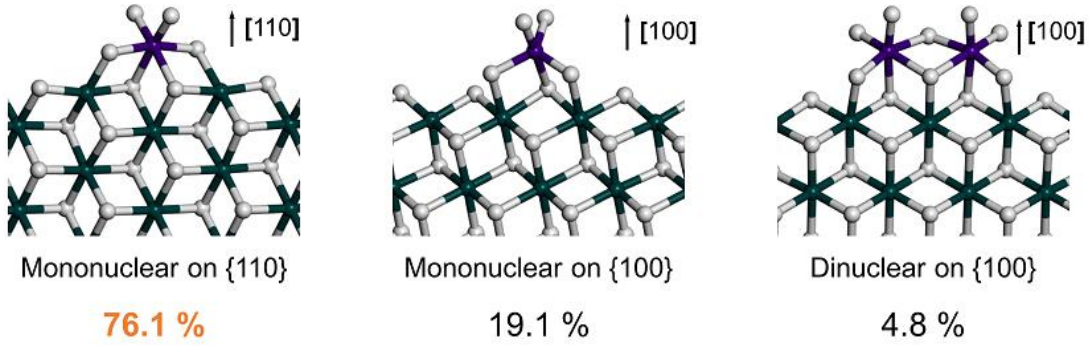

Figure 2.10. Equilibrium distribution of $TiCl_4$ species (T = 350 K).

In the same way, the coordination number distribution of Mg^{2+} cations was estimated for $15MgCl_2$ and $15MgCl_2/4TiCl_4$. The results are shown in Table . 4- and 5-fold coordinated Mg^{2+} cations are mainly attributed to the {110} and {100} surfaces, respectively. 3- and 6-coordinated Mg^{2+} cations correspond to the edge and bulk parts. In the absence of $TiCl_4$, the majority of the undercoordinated

Mg^{2+} cations was 5-fold coordinated, in agreement with the dominant exposure of the {100} termination. The addition of $4TiCl_4$ significantly decreased the proportion of 5-fold coordinated Mg^{2+} cations and instead increased the proportion of 4- and 6- coordinated ones. The increased population of the 4-fold coordinated Mg^{2+} cations corresponded to the exposure of the {110} surface by the adsorption of $TiCl_4$, and this resulted in a rounder morphology of the skeletons surrounded by small {110} and {100} terraces, which in turn increased the population of the 6-fold coordinated Mg^{2+} cations. Hence, the energetic penalty to expose the {110} terraces was compensated in one part by the adsorption of $TiCl_4$ and in the other part by a smaller number of undercoordinated Mg^{2+} cations. The reconstruction of $MgCl_2$ skeletons by the adsorption of $TiCl_4$ was again clarified in terms of the thermodynamic equilibrium.

Table 2.3. Equilibrium distribution of Mg^{2+} cations having different coordination numbers[a,b]

System	Equilibrium distribution of Mg^{2+} cations (%)				
	2-fold	3-fold	4-fold	5-fold	6-fold
$15MgCl_2$	0.0	13.3	13.7	52.7	20.3
$15MgCl_2/4TiCl_4$	0.1	17.3	26.8	20.4	35.4
Difference	+0.1	+4.0	+13.1	–32.3	+15.1

[a] At 350 K.

[b] The coordination numbers were counted after removing terminal Cl^- anions and $TiCl_4$.

2.4. Conclusion

In this chapter, a methodology was presented for the non-empirical structure determination of $TiCl_4$capped $MgCl_2$ nanoplates in relation to the primary particles of the ZN catalyst. The methodology was based on the combination of the genetic algorithm for the global exploration of a configuration space and DFT calculations for local geometry optimization. The presence of adsorbates was explicitly handled to simulate potential reconstruction of $MgCl_2$ upon the chemisorption of $TiCl_4$. The developed program successfully derived the most stable structures of $7MgCl_2$, $15MgCl_2$, and $15MgCl_2/4TiCl_4$ as model primary particles of the ZN catalyst without requiring any pre-knowledge. Stable structures of bare $MgCl_2$ were predominantly terminated by the least undercoordinated {100} surfaces, and this limits the variety of thermodynamically accessible structures. The adsorption of $TiCl_4$ induced the reconstruction of $MgCl_2$ in a way to expose small {110} terraces, and the energetic penalty of the exposure was overcome by the strong adsorption. Moreover, the adsorption of $TiCl_4$ significantly expanded the variety of thermodynamically accessible structures. This diversification and non-ideal finite surfaces led to the distribution of adsorption states of $TiCl_4$ as an intrinsic nature of the $MgCl_2/TiCl_4$ system. This chapter brings important advances not only in understanding the hidden identity of primary particles of the ZN catalyst but also in establishing a realistic model of complicated supported catalysts.

REFERENCES

[1] T. Taniike, M. Tada, Y. Morikawa, T. Sasaki, and Y. Iwasawa, “Density functional theoretical calculations for a Co_2/γ- Al_2O_3 model catalyst: Structures of the γ-Al_2O_3 bulk and surface and attachment sites for Co^{2+} ions,” *J. Phys. Chem. B*, vol. 110, no. 10, pp. 4929–4936, 2006, doi: 10.1021/jp057341p.

[2] M. Stamatakis and D. G. Vlachos, “Unraveling the complexity of catalytic reactions via kinetic monte carlo simulation: Current status and frontiers,” *ACS Catal.*, vol. 2, no. 12, pp. 2648–2663, Dec. 2012, doi: 10.1021/cs3005709.

[3] N. Bahri-Laleh *et al.*, “Computational modeling of heterogeneous Ziegler-Natta catalysts for olefins polymerization,” *Prog. Polym. Sci.*, vol. 84, pp. 89–114, Sep. 2018, doi: 10.1016/j.progpolymsci.2018.06.005.

[4] J. K. Nørskov *et al.*, “Origin of the Overpotential for Oxygen Reduction at a Fuel-Cell Cathode,” *J. Phys. Chem. B*, vol. 108, no. 46, pp. 17886–17892, Nov. 2004, doi: 10.1021/jp047349j.

[5] T. Taniike and M. Terano, “High-precision Molecular Modelling for Ziegler-Natta Catalysts,” *J. Japan Pet. Inst.*, vol. 61, no. 3, pp. 182–190, 2018.

[6] A. J. Medford, M. R. Kunz, S. M. Ewing, T. Borders, and R. Fushimi, “Extracting Knowledge from Data through Catalysis Informatics,” *ACS Catal.*, vol. 8, no. 8, pp. 7403–7429, Aug. 2018, doi: 10.1021/acscatal.8b01708.

[7] D. J. Audus and J. J. De Pablo, “Polymer Informatics: Opportunities and Challenges,” *ACS Macro Lett.*, vol. 6, no. 10, pp. 1078–1082, 2017, doi: 10.1021/acsmacrolett.7b00228.

[8] S. Kirkpatrick, C. D. Gelatt, and M. P. Vecchi, “Optimization by simulated annealing,” *Science (80-.).*, vol. 220, no. 4598, pp. 671–680, May 1983, doi: 10.1126/science.220.4598.671.

[9] D. J. Wales and J. P. K. Doye, “Global optimization by basin-hopping and the lowest energy structures of Lennard-Jones clusters containing up to 110 atoms,” *J. Phys. Chem. A*, vol. 101, no. 28, pp. 5111–5116, 1997, doi: 10.1021/jp970984n.

[10] T. S. Bush, C. R. A. Catlow, and P. D. Battle, “Evolutionary programming techniques for predicting inorganic crystal structures,” *J. Mater. Chem.*, vol. 5, no. 8, pp. 1269–1272, Jan. 1995, doi: 10.1039/jm9950501269.

[11] C. J. Heard, S. Heiles, S. Vajda, and R. L. Johnston, “$Pd_nAg_{(4-n)}$ and $Pd_nPt_{(4-n)}$ clusters on MgO (100): A density functional surface genetic algorithm investigation,” *Nanoscale*, vol. 6, no. 20, pp. 11777–11788, 2014, doi: 10.1039/c4nr03363a.

[12] S. G. Neogi, S. Talukder, and P. Chaudhury, “Structural and spectroscopic studies of carbon dioxide clusters: A combined genetic algorithm and DFT based study,” *Struct. Chem.*, vol. 25, no. 3, pp. 909–918, Jun. 2014, doi: 10.1007/s11224-013-0360-8.

[13] Y.-R. Liu *et al.*, “Structural Exploration of Water, Nitrate/Water, and Oxalate/Water Clusters with Basin-Hopping Method Using a Compressed Sampling Technique,” *J. Phys.*

Chem. A, vol. 118, no. 2, pp. 508–516, Jan. 2014, doi: 10.1021/jp4109128.

[14] W. W. Tipton, C. A. Matulis, and R. G. Hennig, "Ab initio prediction of the Li_5Ge_2 Zintl compound," *Comput. Mater. Sci.*, vol. 93, pp. 133–136, Oct. 2014, doi: 10.1016/j.commatsci.2014.06.014.

[15] S. G. Neogi and P. Chaudhury, "Structural, spectroscopic aspects, and electronic properties of $(TiO_2)_n$ clusters: A study based on the use of natural algorithms in association with quantum chemical methods," *J. Comput. Chem.*, vol. 35, no. 1, pp. 51–61, Jan. 2014, doi: 10.1002/jcc.23465.

[16] S. G. Neogi and P. Chaudhury, "Structure, spectroscopy and electronic properties of neutral lattice-like $(MgO)_n$ clusters: A study based on a blending of DFT with stochastic algorithms inspired by natural processes," *Struct. Chem.*, vol. 25, no. 4, pp. 1229–1244, Aug. 2014, doi: 10.1007/s11224-014-0394-6.

[17] S. G. Neogi and P. Chaudhury, "Structure, electronic properties and vibrational spectra of $(MgF_2)_n$ clusters through a combination of genetic algorithm and DFT-based approach," *Mol. Phys.*, vol. 113, no. 23, pp. 3729–3739, Dec. 2015, doi: 10.1080/00268976.2015.1059508.

[18] J. B. A. Davis, A. Shayeghi, S. L. Horswell, and R. L. Johnston, "The Birmingham parallel genetic algorithm and its application to the direct DFT global optimisation of Ir_N (N = 10-20) clusters," *Nanoscale*, vol. 7, no. 33, pp. 14032–14038, Aug. 2015, doi:

10.1039/c5nr03774c.

[19] H. A. Hussein, J. B. A. Davis, and R. L. Johnston, “DFT global optimisation of gas-phase and MgO-supported sub-nanometre AuPd clusters,” *Phys. Chem. Chem. Phys.*, vol. 18, no. 37, pp. 26133–26143, 2016, doi: 10.1039/c6cp03958h.

[20] I. Demiroglu, K. Yao, H. A. Hussein, and R. L. Johnston, “DFT Global Optimization of Gas-Phase Subnanometer Ru–Pt Clusters,” *J. Phys. Chem. C*, vol. 121, no. 20, pp. 10773–10780, May 2017, doi: 10.1021/acs.jpcc.6b11329.

[21] J. A. Niesse and H. R. Mayne, “Global optimization of atomic and molecular clusters using the space-fixed modified genetic algorithm method,” *J. Comput. Chem.*, vol. 18, no. 9, pp. 1233–1244, Jul. 1997, doi: 10.1002/(SICI)1096-987X(19970715)18:9<1233::AID-JCC11>3.0.CO;2-6.

[22] J. Wang, D. Hao, J. Ye, and N. Umezawa, “Determination of Crystal Structure of Graphitic Carbon Nitride: Ab Initio Evolutionary Search and Experimental Validation,” *Chem. Mater.*, vol. 29, no. 7, pp. 2694–2707, Apr. 2017, doi: 10.1021/acs.chemmater.6b02969.

[23] F. Buendía, J. A. Vargas, R. L. Johnston, and M. R. Beltrán, “Study of the stability of small AuRh clusters found by a Genetic Algorithm methodology,” *Comput. Theor. Chem.*, vol. 1119, pp. 51–58, Nov. 2017, doi: 10.1016/j.comptc.2017.09.008.

[24] N. S. Khetrapal, S. S. Bulusu, and X. C. Zeng, “Structural Evolution of Gold Clusters Au_n^- (n = 21–25) Revisited,” *J. Phys. Chem. A*, vol. 121, no. 12, pp. 2466–2474, Mar. 2017, doi:

10.1021/acs.jpca.7b00367.

[25] J. A. Vargas, F. Buendía, and M. R. Beltrán, "New Au_N (N = 27-30) Lowest Energy Clusters Obtained by Means of an Improved DFT-Genetic Algorithm Methodology," *J. Phys. Chem. C*, vol. 121, no. 20, pp. 10982–10991, May 2017, doi: 10.1021/acs.jpcc.6b12848.

[26] B. Yan *et al.*, "A particle swarm optimization algorithm with random learning mechanism and Levy flight for optimization of atomic clusters," *Comput. Phys. Commun.*, vol. 219, pp. 79–86, Oct. 2017, doi: 10.1016/j.cpc.2017.05.009.

[27] S. M. Woodley, P. D. Battle, J. D. Gale, and C. Richard A. Catlow, "The prediction of inorganic crystal structures using a genetic algorithm and energy minimisation," *Phys. Chem. Chem. Phys.*, vol. 1, no. 10, pp. 2535–2542, Jan. 1999, doi: 10.1039/a901227c.

[28] J. P. K. Doye and D. J. Wales, "Structural transitions and global minima of sodium chloride clusters," *Phys. Rev. B - Condens. Matter Mater. Phys.*, vol. 59, no. 3, pp. 2292–2300, Jan. 1999, doi: 10.1103/PhysRevB.59.2292.

[29] I. Rata, A. A. Shvartsburg, M. Horoi, T. Frauenheim, K. W. M. Siu, and K. A. Jackson, "Single-parent evolution algorithm and the optimization of Si clusters," *Phys. Rev. Lett.*, vol. 85, no. 3, pp. 546–549, Jul. 2000, doi: 10.1103/PhysRevLett.85.546.

[30] H. Liu and K. D. Jordan, "Finite temperature properties of $(CO_2)_n$ clusters," *J. Phys. Chem. A*, vol. 107, no. 30, pp. 5703–5709, 2003, doi: 10.1021/jp0345295.

[31] A. N. Alexandrova and A. I. Boldyrev, “Search for the $Li_n^{0/+1/-1}$ (n= 5-7) lowest-energy structures using the ab initio Gradient Embedded Genetic Algorithm (gega). Elucidation of the chemical bonding in the lithium clusters,” *J. Chem. Theory Comput.*, vol. 1, no. 4, pp. 566–580, 2005, doi: 10.1021/ct050093g.

[32] H. Takeuchi, “Novel method for geometry optimization of molecular clusters: Application to benzene clusters,” *J. Chem. Inf. Model.*, vol. 47, no. 1, pp. 104–109, Aug. 2007, doi: 10.1021/ci600336p.

[33] H. Xiang, S.-H. Wei, and X. Gong, “Structures of $[Ag_7(SR)_4]^-$ and $[Ag_7(DMSA)_4]^-$,” *J. Am. Chem. Soc.*, vol. 132, no. 21, pp. 7355–7360, Jun. 2010, doi: 10.1021/ja9108374.

[34] T. Taniike and M. Terano, “The use of donors to increase the isotacticity of polypropylene,” *Adv. Polym. Sci.*, vol. 257, pp. 81–97, 2013, doi: 10.1007/12_2013_224.

[35] N. Pasquini and A. Addeo, “Catalysts for Polymerization,” in *Polypropylene Handbook*, 2nd ed., Boca Raton: Hanser Gardner Publications, 2005, pp. 11–112.

[36] T. Taniike, T. Funako, and M. Terano, “Multilateral characterization for industrial Ziegler-Natta catalysts toward elucidation of structure-performance relationship,” *J. Catal.*, vol. 311, pp. 33–40, Mar. 2014, doi: 10.1016/j.jcat.2013.10.023.

[37] T. Taniike, P. Chammingkwan, V. Q. Thang, T. Funako, and M. Terano, “Validation of BET specific surface area for heterogeneous Ziegler-Natta catalysts based on α_s-plot,” *Appl. Catal. A Gen.*, vol. 437–438, pp. 24–27, Sep. 2012, doi: 10.1016/j.apcata.2012.06.006.

[38] U. Giannini, “Polymerization of Olefins with High Activity Catalysts,” *Makromol. Chem., Suppl*, vol. 5, no. S19811, pp. 216–229, 1981, doi: 10.1002/macp.1981.020051981113.

[39] R. Zannetti, C. Marega, A. Marigo, and A. Martorana, “Layer-lattices in Ziegler–Natta catalysts,” *J. Polym. Sci. Part B Polym. Phys.*, vol. 26, no. 12, pp. 2399–2412, Nov. 1988, doi: 10.1002/polb.1988.090261202.

[40] M. Boero, M. Parrinello, and K. Terakura, “First Principles Molecular Dynamics Study of Ziegler- Natta Heterogeneous Catalysis,” *J. Am. Chem. Soc*, vol. 120, no. 12, pp. 2746–2752, 1998, doi: 10.1021/ja972367i.

[41] A. Matta, P. Chammingkwan, B. K. Singh, M. Terano, T. Kaneko, and T. Taniike, “Truxillic and truxinic acid-based, bio-derived diesters as potent internal donor in Ziegler-Natta catalyst for propylene polymerization,” *Appl. Catal. A Gen.*, vol. 554, pp. 80–87, Mar. 2018, doi: 10.1016/J.APCATA.2018.01.030.

[42] V. Busico *et al.*, “Periodic DFT and High-Resolution Magic-Angle-Spinning (HR-MAS) ^{1}H NMR Investigation of the Active Surfaces of $MgCl_2$-Supported Ziegler−Natta Catalysts. The $MgCl_2$ Matrix,” *J. Phys. Chem. C*, vol. 112, no. 4, pp. 1081–1089, Jan. 2008, doi: 10.1021/jp076679b.

[43] M. D’Amore, R. Credendino, P. H. M. Budzelaar, M. Causá, and V. Busico, “A periodic hybrid DFT approach (including dispersion) to $MgCl_2$-supported Ziegler-Natta catalysts - 1: $TiCl_4$ adsorption on $MgCl_2$ crystal surfaces,” *J. Catal.*, vol. 286, pp. 103–110, Feb. 2012,

doi: 10.1016/j.jcat.2011.10.018.

[44] R. Credendino, J. T. M. Pater, A. Correa, G. Morini, and L. Cavallo, “Thermodynamics of formation of uncovered and dimethyl ether-covered $MgCl_2$ crystallites. consequences in the structure of Ziegler-Natta heterogeneous catalysts,” *J. Phys. Chem. C*, vol. 115, no. 27, pp. 13322–13328, Jul. 2011, doi: 10.1021/jp201410n.

[45] R. Credendino, D. Liguori, G. Morini, and L. Cavallo, “Investigating phthalate and 1,3-diether coverage and dynamics on the (104) and (110) surfaces of $MgCl_2$-supported Ziegler-Natta catalysts,” *J. Phys. Chem. C*, vol. 118, no. 15, pp. 8050–8058, Apr. 2014, doi: 10.1021/jp501390e.

[46] D. V. Stukalov, I. L. Zilberberg, and V. A. Zakharov, “Surface species of titanium(IV) and titanium(III) in $MgCl_2$-Supported Ziegler-Natta catalysts. A periodic density functional theory study,” *Macromolecules*, vol. 42, no. 21, pp. 8165–8171, Nov. 2009, doi: 10.1021/ma901413b.

[47] D. V. Stukalov and V. A. Zakharov, “Active site formation in $MgCl_2$-supported ziegler - Natta catalysts. A density functional theory study,” *J. Phys. Chem. C*, vol. 113, no. 51, pp. 21376–21382, Dec. 2009, doi: 10.1021/jp907812k.

[48] D. V. Stukalov, V. A. Zakharov, and I. L. Zilberberg, “Adsorption species of ethyl benzoate in $MgCl_2$-supported ziegler-natta catalysts. A density functional theory study,” *J. Phys. Chem. C*, vol. 114, no. 1, pp. 429–435, Jan. 2010, doi: 10.1021/jp908551k.

[49] M. Boero, M. Parrinello, and K. Terakura, “Ziegler-Natta heterogeneous catalysis by first principles computer experiments,” *Surf. Sci.*, vol. 438, no. 1–3, pp. 1–8, Sep. 1999, doi: 10.1016/S0039-6028(99)00537-3.

[50] M. Boero, M. Parrinello, S. Hüffer, and H. Weiss, “First principles study of propene polymerization in Ziegler-Natta heterogeneous catalysis,” *J. Am. Chem. Soc.*, vol. 122, no. 3, pp. 501–509, 2000, doi: 10.1021/ja990913x.

[51] M. Boero, M. Parrinello, H. Weiss, and S. Hüffer, “A first principles exploration of a variety of active surfaces and catalytic sites in Ziegler-Natta heterogeneous catalysis,” *J. Phys. Chem. A*, vol. 105, no. 21, pp. 5096–5105, 2001, doi: 10.1021/jp010780d.

[52] M. Boero, M. Parrinello, K. Terakura, and H. Weiss, “Car-Parrinello study of Ziegler-Natta heterogeneous catalysis: Stability and destabilization problems of the active site models,” *Mol. Phys.*, vol. 100, no. 18, pp. 2935–2940, Sep. 2002, doi: 10.1080/00268970110109899.

[53] T. Taniike and M. Terano, “Coadsorption and support-mediated interaction of Ti species with ethyl benzoate in $MgCl_2$-supported heterogeneous ziegler-natta catalysts studied by density functional calculations,” *Macromol. Rapid Commun.*, vol. 28, no. 18–19, pp. 1918–1922, Sep. 2007, doi: 10.1002/marc.200700363.

[54] T. Taniike and M. Terano, “Reductive formation of isospecific Ti dinuclear species on a $MgCl_2$ (110) surface in heterogeneous ziegler-natta catalysts,” *Macromol. Rapid Commun.*, vol. 29, no. 17, pp. 1472–1476, Sep. 2008, doi: 10.1002/marc.200800310.

[55] T. Taniike and M. Terano, “A Density Functional Study on the Influence of the Molecular Flexibility of Donors on the Insertion Barrier and Stereoselectivity of Ziegler-Natta Propylene Polymerization,” *Macromol. Chem. Phys.*, vol. 210, no. 24, pp. 2188–2193, Dec. 2009, doi: 10.1002/macp.200900465.

[56] T. Taniike and M. Terano, “Coadsorption model for first-principle description of roles of donors in heterogeneous Ziegler-Natta propylene polymerization,” *J. Catal.*, vol. 293, pp. 39–50, Sep. 2012, doi: 10.1016/j.jcat.2012.06.001.

[57] A. Bazhenov, M. Linnolahti, T. A. Pakkanen, P. Denifl, and T. Leinonen, “Modeling the stabilization of surface defects by donors in ziegler-natta catalyst support,” *J. Phys. Chem. C*, vol. 118, no. 9, pp. 4791–4796, Mar. 2014, doi: 10.1021/jp412386u.

[58] M. S. Kuklin, A. S. Bazhenov, P. Denifl, T. Leinonen, M. Linnolahti, and T. A. Pakkanen, “Stabilization of magnesium dichloride surface defects by mono- And bidentate donors,” *Surf. Sci.*, vol. 635, pp. 5–10, May 2015, doi: 10.1016/j.susc.2014.11.026.

[59] S. Poonpong, S. Dwivedi, T. Taniike, and M. Terano, “Structure-Performance Relationship for Dialkyldimethoxysilane as an External Donor in Stopped-Flow Propylene Polymerization Using a Ziegler-Natta Catalyst,” *Macromol. Chem. Phys.*, vol. 215, no. 18, pp. 1721–1727, Sep. 2014, doi: 10.1002/macp.201400157.

[60] M. Toto, G. Morini, G. Guerra, P. Corradini, and L. Cavallo, “Influence of 1,3-diethers on the stereospecificity of propene polymerization by supported Ziegler-Natta catalysts. A

theoretical their adsorption on (110) and (100) lateral cuts of $MgCl_2$ platelets," *Macromolecules*, vol. 33, no. 4, pp. 1134–1140, 2000, doi: 10.1021/ma990959a.

[61] E. Breuza, G. Antinucci, P. H. M. Budzelaar, V. Busico, A. Correa, and C. Ehm, "$MgCl_2$-supported Ziegler-Natta catalysts: A DFT-D 'flexible-cluster' approach. $TiCl_4$ and probe donor adducts," *Int. J. Quantum Chem.*, vol. 118, p. e25721, Sep. 2018, doi: 10.1002/qua.25721.

[62] E. Breuza, G. Antinucci, P. H. M. Budzelaar, V. Busico, A. Correa, and C. Ehm, "$MgCl_2$-Supported Ziegler-Natta Catalysts: A DFT-D 'flexible-Cluster' Approach to Internal Donor Adducts," *J. Phys. Chem. C*, vol. 122, no. 16, pp. 9046–9053, Apr. 2018, doi: 10.1021/acs.jpcc.8b01500.

[63] A. Andoni, J. C. Chadwick, H. J. W. Niemantsverdriet, and P. C. Thüne, "The role of electron donors on lateral surfaces of $MgCl_2$-supported Ziegler-Natta catalysts: Observation by AFM and SEM," *J. Catal.*, vol. 257, no. 1, pp. 81–86, Jul. 2008, doi: 10.1016/j.jcat.2008.04.020.

[64] M. D'Amore, K. S. Thushara, A. Piovano, M. Causà, S. Bordiga, and E. Groppo, "Surface Investigation and Morphological Analysis of Structurally Disordered $MgCl_2$ and $MgCl_2/TiCl_4$ Ziegler-Natta Catalysts," *ACS Catal.*, vol. 6, no. 9, pp. 5786–5796, Sep. 2016, doi: 10.1021/acscatal.6b00871.

[65] T. Taniike, P. Chammingkwan, V. Q. Thang, K. Goto, T. Fujitani, and M. Terano,

"Chemisorption-Induced Activation of $MgCl_2$ Film as Realistic Route for Heterogeneous Ziegler-Natta Surfaces under Ultrahigh Vacuum," *J. Phys. Chem. C*, vol. 121, no. 43, pp. 24085–24092, Nov. 2017, doi: 10.1021/acs.jpcc.7b08242.

[66] J. P. Perdew, K. Burke, and M. Ernzerhof, "Generalized Gradient Approximation Made Simple," *Phys. Rev. Lett.*, vol. 77, no. 18, pp. 3865–3868, Oct. 1996, doi: 10.1103/PhysRevLett.77.3865.

[67] B. Delley, "An all-electron numerical method for solving the local density functional for polyatomic molecules," *J. Chem. Phys.*, vol. 92, no. 1, pp. 508–517, Jan. 1990, doi: 10.1063/1.458452.

[68] M. Dolg, U. Wedig, H. Stoll, and H. Preuss, "Energy-adjusted ab initio pseudopotentials for the first row transition elements," *J. Chem. Phys.*, vol. 86, no. 2, pp. 866–872, Jan. 1987, doi: 10.1063/1.452288.

[69] A. Bergner, M. Dolg, W. Küchle, H. Stoll, and H. Preuß, "Ab initio energy-adjusted pseudopotentials for elements of groups 13-17," *Mol. Phys.*, vol. 80, no. 6, pp. 1431–1441, Dec. 1993, doi: 10.1080/00268979300103121.

[70] T. N. P. Luhtanen, M. Linnolahti, A. Laine, and T. A. Pakkanen, "Structural Characteristics of Small Magnesium Dichloride Clusters : A Systematic Theoretical Study," *J. Phys. Chem. B*, vol. 108, no. 13, pp. 3989–3995, 2004, doi: 10.1021/JP030464U.

[71] A. Marigo, C. Marega, R. Zannetti, G. Morini, and G. Ferrara, "Small- and wide-angle X-

ray scattering analysis of Ziegler-Natta catalysts: structural disorder, surface area and activity," *Eur. Polym. J.*, vol. 36, no. 9, pp. 1921–1926, Sep. 2000, doi: 10.1016/S0014-3057(99)00250-5.

[72] M. Chang, X. Liu, P. J. Nelson, G. R. Munzing, T. A. Gegan, and Y. V. Kissin, "Ziegler-Natta catalysts for propylene polymerization: Morphology and crystal structure of a fourth-generation catalyst," *J. Catal.*, vol. 239, no. 2, pp. 347–353, Apr. 2006, doi: 10.1016/j.jcat.2006.02.009.

[73] Y. Hiraoka, S. Y. Kim, A. Dashti, T. Taniike, and M. Terano, "Similarities and differences of the active sites in basic and advanced $MgCl_2$-supported ziegler-natta propylene polymerization catalysts," *Macromol. React. Eng.*, vol. 4, no. 8, pp. 510–515, Apr. 2010, doi: 10.1002/mren.200900070.

Chapter 3:
Insight into Multisite Nature of Heterogeneous Ziegler–Natta Catalyst from Non-Empirical Structure Determination

Abstract

A structural distribution is an intrinsic nature of $TiCl_4$-capped $MgCl_2$ nanoplates, and its comprehension would uncover the origin of distributions in the primary structure of polyolefins produced by Ziegler–Natta catalysts. Such fundamental understanding is one of the prerequisites of the systematic design of catalysts. In this chapter, a series of machine learning-aided structure determination was performed for $TiCl_4$-capped $MgCl_2$ nanoplates of different sizes and chemical compositions. Structural and electronic distributions of $TiCl_4$ were analyzed on the basis of 10^6 structures, which were obtained in the course of the structure determination. Such a systematic investigation revealed that i) $TiCl_4$ tends to adsorb on {110} surfaces as mononuclear species, while adsorption on {100} is not negligible, and that ii) even within the same mononuclear species on {110} surfaces, the steric environment and charge state of $TiCl_4$ are distributed. A preliminary examination on ethylene insertion suggested that the $TiCl_4$ distribution would generate the polymer primary structure distribution obtained by Ziegler–Natta catalysts.

Keywords: Ziegler–Natta catalyst, genetic algorithm, structure determination, density functional theory, surface reconstruction, active site distribution

3.1.Introduction

The reality of first-principle calculations is determined by the accuracy of the computational method and that of the employed molecular model in representing the structure of materials. However, for complex materials such as solid catalysts, the construction of molecular models is often an empirical process that relies on limited experimental knowledge and physicochemical inference. Furthermore, the structure of nanoparticles and surfaces is known to be sensitive to the surrounding physicochemical environment, where the adsorption plays a critical role in stabilizing coordinative unsaturation and this modulates the structure [1]–[6]. So far, most of simulations on solid catalysts assumed infinite ideal surfaces or clusters consisting of ideal surfaces that are cut out from the bulk, otherwise magic number clusters of bare particles [7], [8]. Thus, non-empirical structure determination of complex materials, especially in the presence of adsorbates, is highly demanded.

In Chapter 2, non-empirical structure determination of nanoparticles in the presence of adsorbates was realized by combining local search with DFT geometry optimization and global search with a genetic algorithm. Structure optimization using the genetic algorithm has been studied since 1990s [9]–[14]. However, reconstruction of the support surfaces upon adsorption has been scarcely accounted [15]. Structure determination was performed for $TiCl_4$-capped $MgCl_2$ nanoplates ($15MgCl_2/4TiCl_4$), which was regarded as the building block of the Ziegler–Natta catalyst for olefin polymerization. The majority of past DFT calculations on the same catalyst presumed ideal surfaces of $MgCl_2$ such as {110} and {104}, and adsorption of catalytic components was examined on the basis of non-reconstructable (i.e. static) surfaces [16]–[34]. The chapter 2 firstly incorporated the

dynamic aspect of $MgCl_2$ structures upon adsorption. It was revealed that the adsorption of $TiCl_4$ induces the reconstruction of $MgCl_2$ nanoplates in a way to expose small {110} terraces, and the resultant structure is not similar to that of ideal surfaces. Another important consequence of the $TiCl_4$ adsorption is the structural diversification: The $MgCl_2/TiCl_4$ system provided a dozen of metastable structures in a narrow energy span, while bare $MgCl_2$ of the same size offered only several. This observation suggests that the structure of the $MgCl_2/TiCl_4$ system is intrinsically distributed.

A distribution is an intrinsic nature of many supported catalysts of practical use, while its origin and roles in catalysis have not been sufficiently studied until recently [35]. This is an essential feature of classical olefin polymerization catalysts, in particular Ziegler-Natta and Phillips catalysts [36]–[38]. A distribution in the function of active sites, also known as the multisite nature, directly leads to a distribution in the primary structure of produced polymers, which helps these polymers to equip balanced physical properties as well as high tunability. The Phillips catalyst consists of oxochromium(VI) species covalently grafted on amorphous SiO_2. Its multisite nature is largely attributed to the amorphous structure of the support: Grafting sites are distributed in terms of the silanol reactivity and the siloxane ring strain [39], [40]. In recent publications, significant progress was made on computational prediction of the distribution in the Phillips and relevant catalysts [41], [42]. Reaction of metal halides with hydroxylated surfaces of a quenched disordered structure was simulated with the aid of microkinetics, and this afforded a practical representation of a distribution of metal species as well as site-averaged kinetics of ethylene polymerization. Because of the industrial importance, studies on mechanistic insights of Ziegler-Natta catalyst are still active [26], [43]. However, understanding and modeling of the multisite nature in the Ziegler-Natta catalyst are

largely behind. Lattice-matched adsorption of $TiCl_4$ on highly ionic $MgCl_2$ crystalline surfaces evokes a completely different mechanism to create a distribution.

In this chapter, non-empirical structure determination of $TiCl_4$-capped $MgCl_2$ nanoplates was performed for a wide range of sizes and compositions. The aim of such a systematic examination is to withdraw generalized features of the $MgCl_2/TiCl_4$ system and extend our understanding to the real catalyst. In particular, the non-empirical structure determination generates a numerous number of structures, and the analysis of these would provide a useful insight into the distribution in Ziegler-Natta catalysts.

3.2. Numerical methods

Non-empirical structure determination was performed for xMgCl$_2$/yTiCl$_4$ (x = 6–19, y = 0–4; [Ti] < 10 wt%). The size of 6–19$MgCl_2$ was chosen for computational feasibility, while 19$MgCl_2$ was expected to be not far from the experimentally observed primary particle of ca. 2.4–4.0 nm [44]–[47]. The number of $TiCl_4$ molecules was decided by referring to a typical Ti content of Ziegler–Natta catalysts, which is 1–3 wt% for propylene polymerization and up to 10 wt% for ethylene polymerization. The structure determination was performed on the basis of the program developed in Chapter 2. The program targets $MgCl_2/TiCl_4$ nanoplates, in particular a convex $MgCl_2$ monolayer whose lateral surfaces are capped with $TiCl_4$ molecules[48]. Initially, Mg^{2+} cations are placed on the basis of the self-avoiding random walk, and Cl^- anions are placed in the order of the coordination number of Mg^{2+} cations. Then, adsorption sites are defined on the lateral periphery of the $MgCl_2$ skeleton, and $TiCl_4$ molecules are randomly placed onto available sites. Thus, generated structures

are subjected to DFT geometry optimization, and their fitness is evaluated by the corresponding optimized energy. Next-generation structures are created through genetic operators on the basis of current-generation structures. The crossover operator inherits a common part of Mg^{2+} cations of two structures while randomly inheriting different parts from either of the two structures. The mutation operator randomly relocates a part of Mg^{2+} cations or adsorbates. The elite operator carries over a stable structure to the next generation. The parent structures in the crossover and mutation operation are chosen by fitness proportionate selection. The next-generation structures are similarly optimized, evaluated, and evolved. This cycle updates structures to lower the energy.

In the developed program, newly generated structures were cumulatively added to a database without allowing registration of mutually redundant structures, and repetitive calculations were thus avoided. To maintain the structure diversity in a generation, the crossover and elitism operators restricted structures having similar skeletons. The similarity of skeletons is defined as the proportion of a common part of Mg^{2+} cations, and structures having similarity higher than a predefined threshold are regarded as similar structures. The solution of the genetic algorithm was regarded as the optimal one, i.e. the most stable structure, when the solution satisfied the requirement that multiple runs independently converged to the same physicochemically reasonable structure after a sufficient number of generations. The energy of structures was expressed by the following equation:

$$E_{\text{cluster}} = E - N_{\text{MgCl}_2} \times E_{\text{MgCl}_2} - N_{\text{TiCl}_4} \times E_{\text{TiCl}_4} \quad (3.1)$$

where E is the energy of a structure after the geometry optimization, N_{MgCl_2} is the number of $MgCl_2$ units, E_{MgCl_2} is the energy of a $MgCl_2$ unit in bulk, N_{TiCl_4} is the number of $TiCl_4$ molecules, E_{TiCl_4} is the energy of a single $TiCl_4$ molecule in a vacuum. E_{cluster} expresses the formation energy

of a cluster on the basis of the sum of the exposure penalty of coordinatively unsaturated $MgCl_2$ surfaces and its stabilization by the $TiCl_4$ adsorption.

DFT geometry optimization was performed by DMol^3, using the same conditions as our recent works [48]: The GGA PBE functional [49] and the DNP basis set [50] with effective core potentials [51], [52]. These computational methods are feasible in terms of computational costs, while their validity was confirmed by the fact that the calculated results consistently reproduced a series of experimental results [33].

Parameters used in the genetic algorithm were appropriately tuned for each system because the configuration space largely depends on the cluster size and the number of $TiCl_4$ molecules. The population was basically increased with the increase of the complexity of the system to avoid being trapped in local minima. In the mutation, the maximum percentage of relocated cations and adsorbates was set to 20%. The number of relocated cations and adsorbates is stochastically chosen from positive integers in the range of 0–20%. The threshold of similarity was set to 90%, and the maximum number of similar structures in elites was set to 2.

3.3. Results and discussion

3.3.1 Most stable structures of xMgCl$_2$/yTiCl$_4$ clusters

Non-empirical structure determination was performed for xMgCl$_2$/yTiCl$_4$ clusters (x = 6–19, y = 0–4). The successful convergence of the evolution was verified for individual clusters on the basis of the fact that multiple independent searches reached the same structures. Figures 3.1-3.4 show evolutionary progress plots of the genetic algorithm for the structure determination of 12$MgCl_2$,

$12MgCl_2/3TiCl_4$, $19MgCl_2$, and $19MgCl_2/4TiCl_4$ as representative examples. The progress was monitored by the energy of the best-of-generation individual (i.e. the most stable structure in a generation).

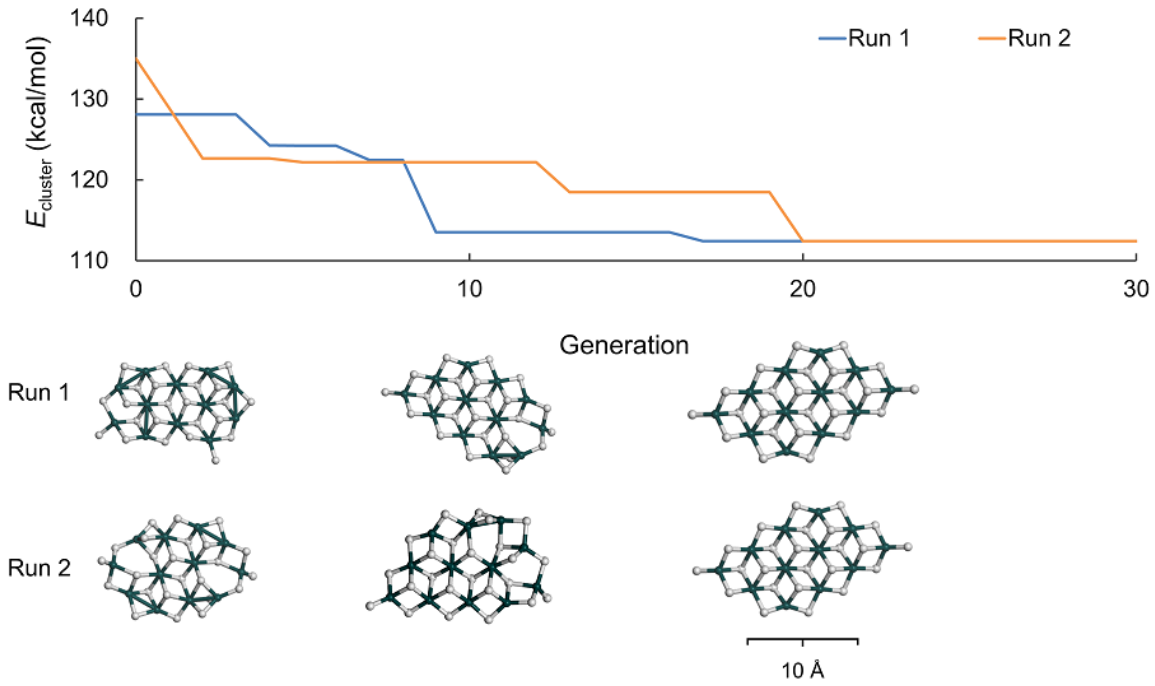

Figure 3.1. Evolutionary progress plot for the structure determination of $12MgCl_2$. The energy of the best-of-generation individual (i.e. the most stable structure in a generation) is plotted against the generation. The structure of the most stable individual is also shown for each 10 generations.

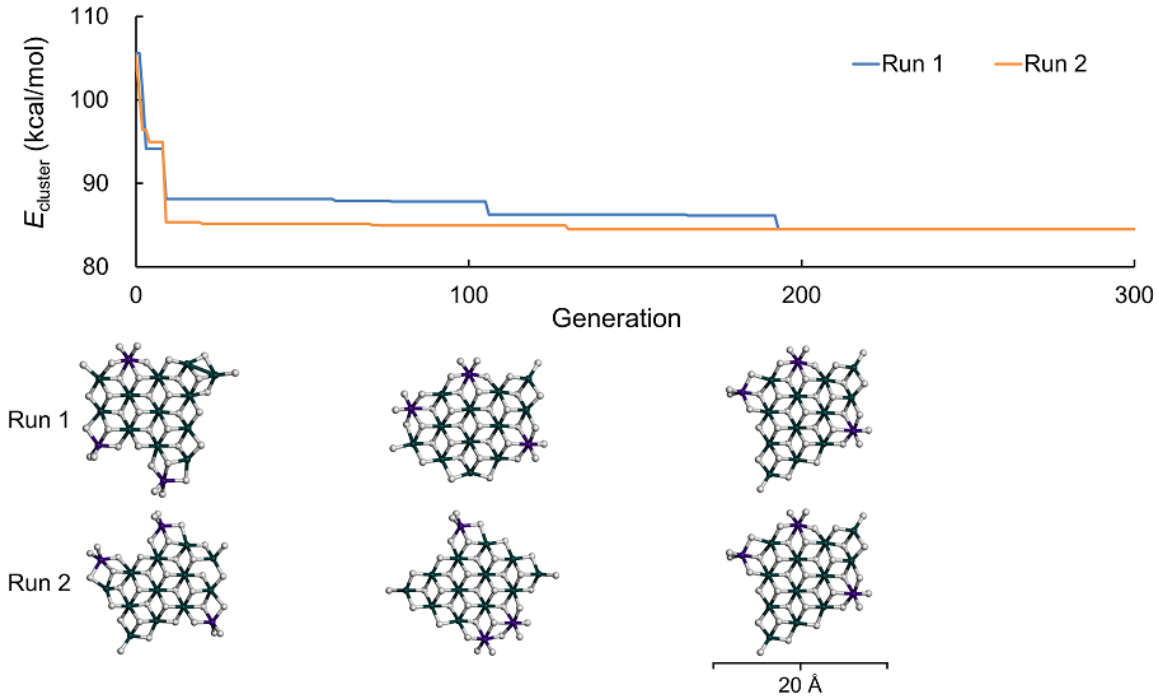

Figure 3.2. Evolutionary progress plot for the structure determination of $12MgCl_2/3TiCl_4$.

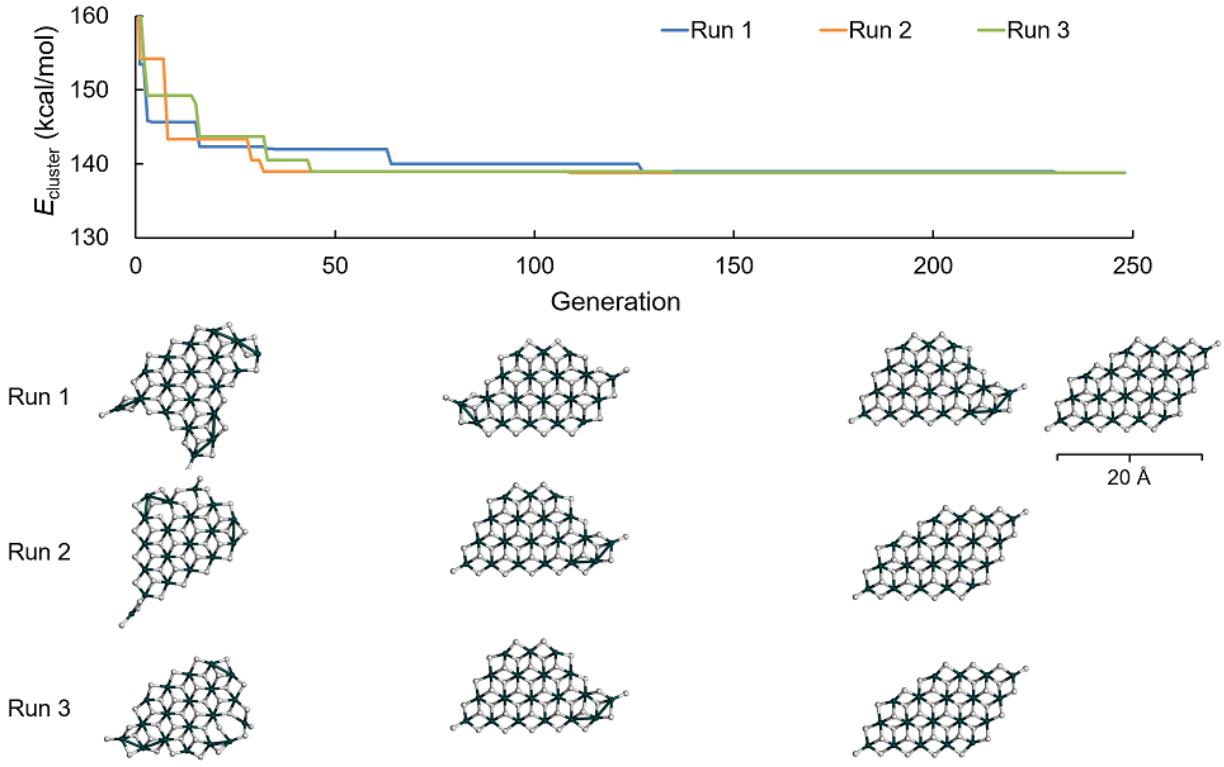

Figure 3.3. Evolutionary progress plot for the structure determination of $19MgCl_2$.

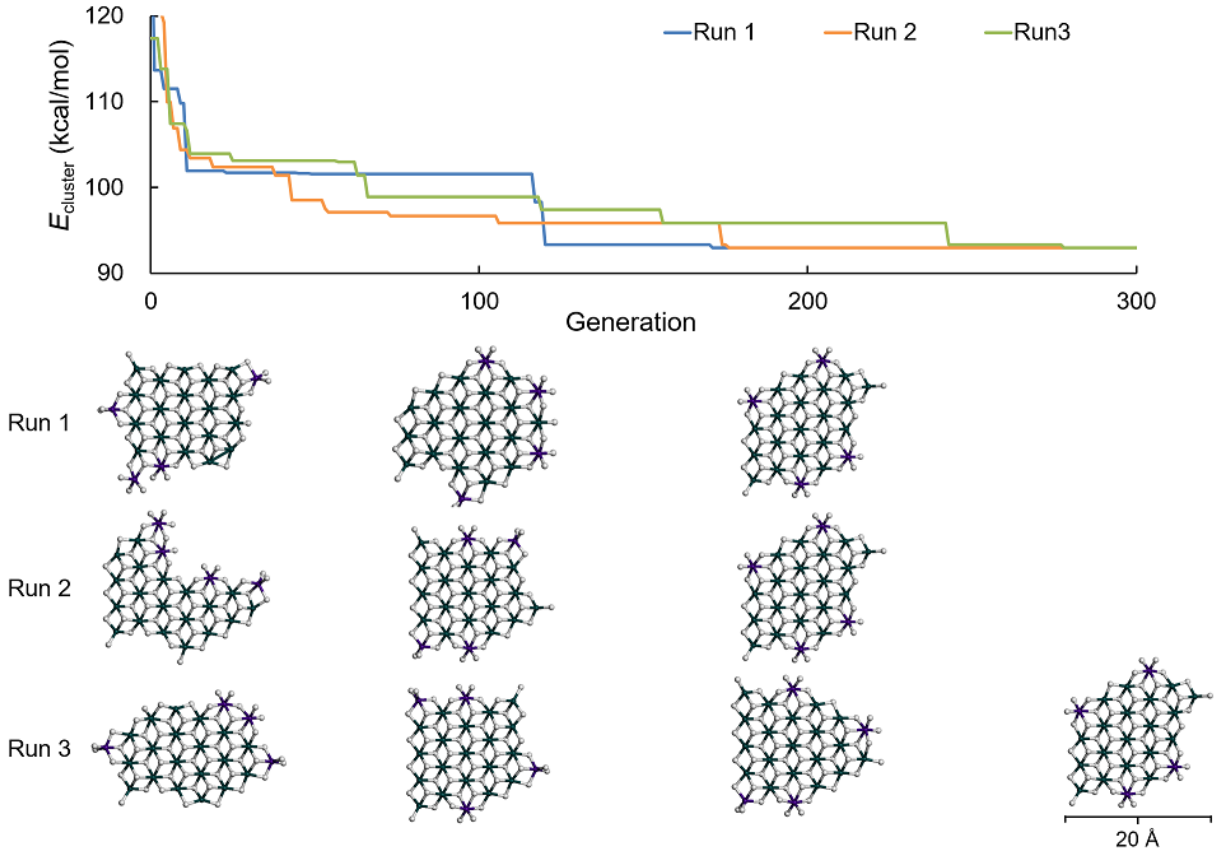

Figure 3.4. Evolutionary progress plot for the structure determination of $19MgCl_2/4TiCl_4$.

The evolution was continued until further evolution hardly introduced new metastable structures whose energies were not far from that of the most stable structure. The slower convergence in the presence of $TiCl_4$ was confirmed and it indicates that the adsorption significantly enlarges the diversity of energetically accessible structures. The cause of this diversity is that $TiCl_4$ allows the exposure of coordinatively less saturated {110} surfaces caused this diversity [48].

The most stable structures determined for bare $xMgCl_2$ clusters are summarized in Figure 3.5 together with the corresponding cluster energies ($E_{cluster}$). Comparison of these structures having different sizes dictates two important features that govern the energy of the structures. First, lateral

termination was almost exclusively made by the exposure of {100} surfaces to minimize coordinative unsaturation of surface Mg^{2+} cations. Second, the shape of the structures is mostly symmetric, especially in terms of the placement of two terminal Cl^- anions at the corners [21], [48]. This observation suggests that minimizing the polarization plays an important role in stabilizing $MgCl_2$ clusters. In Figure 3.6, $E_{cluster}$ of the most stable structures is plotted against the number of $MgCl_2$ units (N_{MgCl_2}, identical to x). The $E_{cluster}$ value basically increased along with N_{MgCl_2} as the length of lateral termination increased. On the other hand, when the $E_{cluster}$ value was normalized by the number of $MgCl_2$ units, it tended to decrease with N_{MgCl_2} due to the increasing contribution of the bulk. In an attempt to identify a descriptor for the cluster energies, it was found that the $E_{cluster}$ value linearly increased with the total number of coordinative vacancies (Figure 3.7), where a 5-fold coordinated Mg^{2+} cation affords one vacancy, 4-fold coordinated Mg^{2+} cation affords two vacancies, and so on. This result is consistent with a previous conclusion obtained by DFT calculations on symmetric $MgCl_2$ clusters with different sizes [21]. However, it must be also noted that the linear relationship with the number of coordination vacancies held only for the most stable structures, and the cluster energy of metastable structures was not solely described by it (Figure 3.8). This fact suggests the presence of other factors (such as polarization) that affect the energy of the structures.

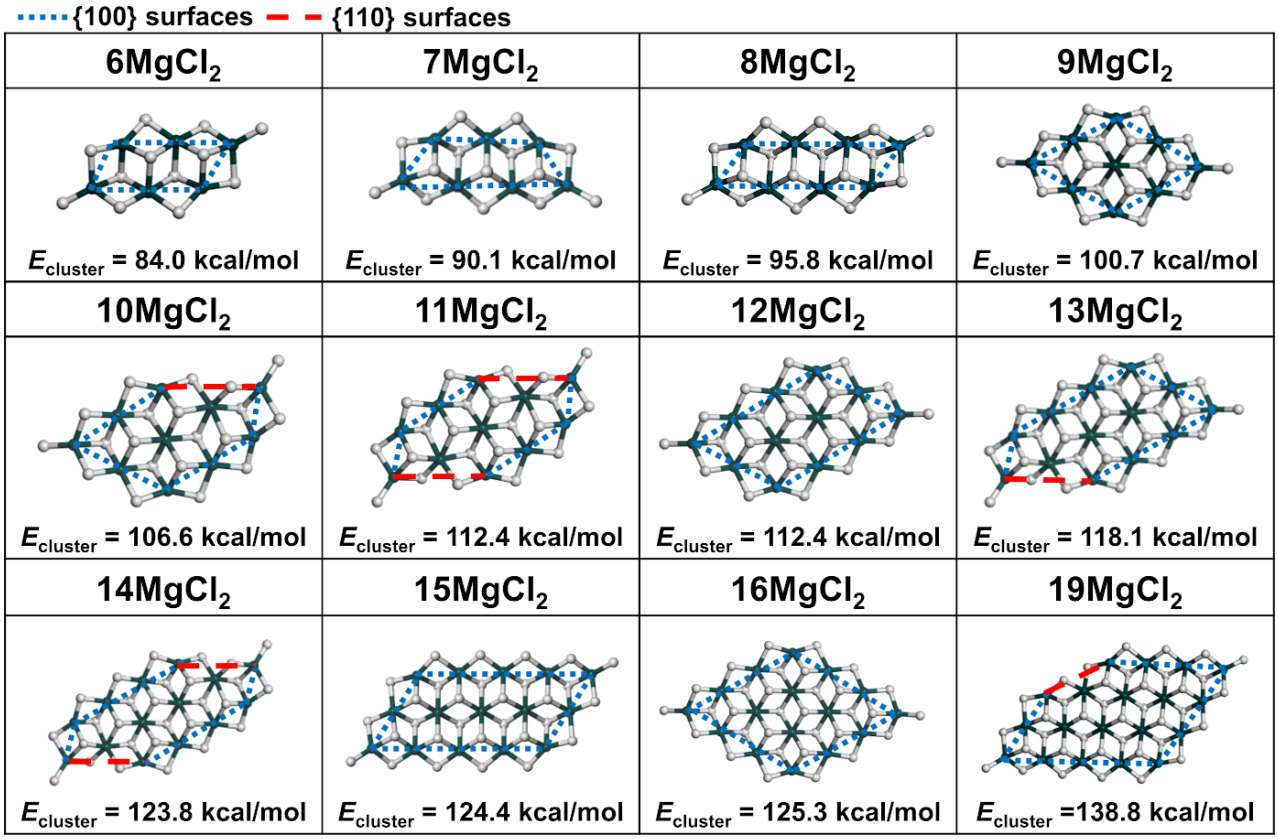

Figure 3.5. The most stable structures of bare xMgCl$_2$ clusters. The type of lateral termination is indicated by blue and red lines.

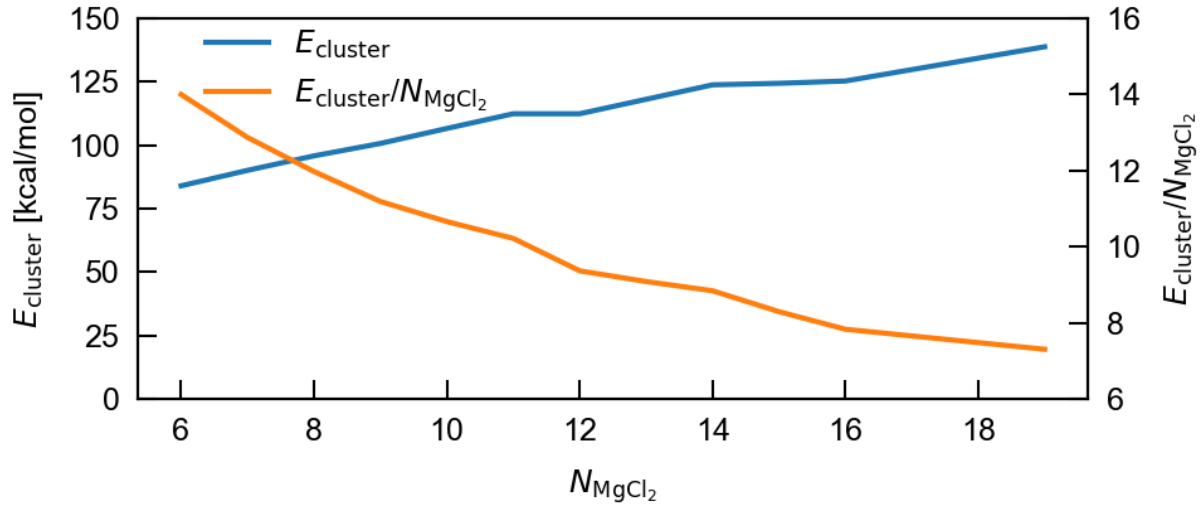

Figure 3.6. Cluster energy ($E_{cluster}$) of the most stable structures plotted against the number of $MgCl_2$ units (N_{MgCl_2}). The energy is also plotted after being normalized by N_{MgCl_2}.

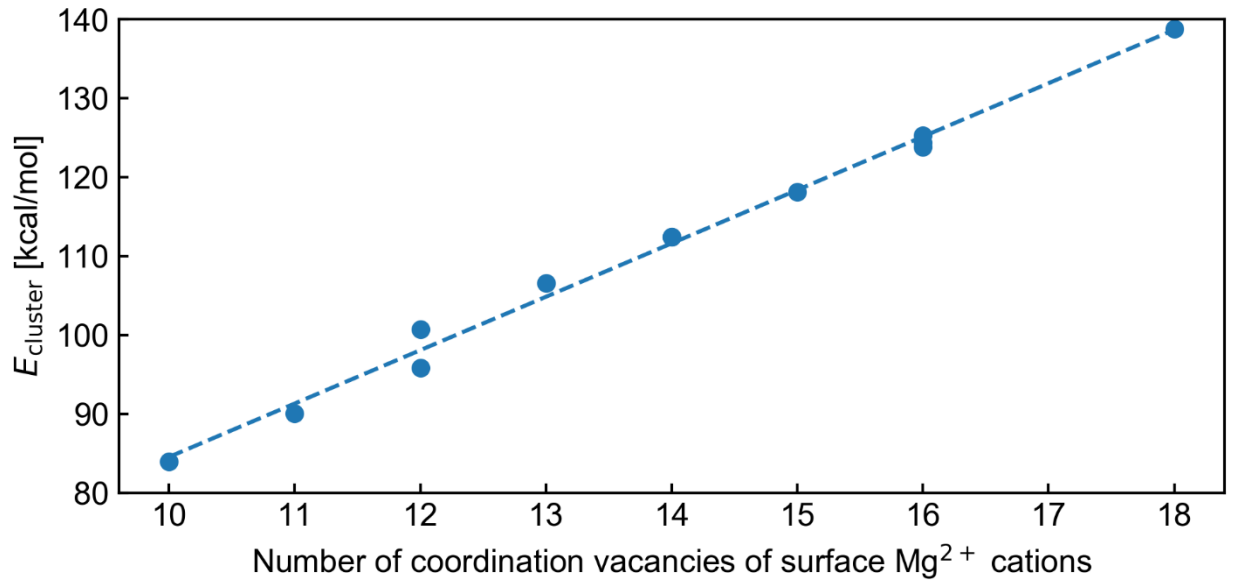

Figure 3.7. $E_{cluster}$ of the most stable structures plotted against the total number of coordination vacancies of surface Mg^{2+} cations. The number of coordination vacancies present in a structure is summed, where a 5-fold coordinated Mg^{2+} cation corresponds to one vacancy, a 4-fold coordinated Mg^{2+} cation to two vacancies, and so on.

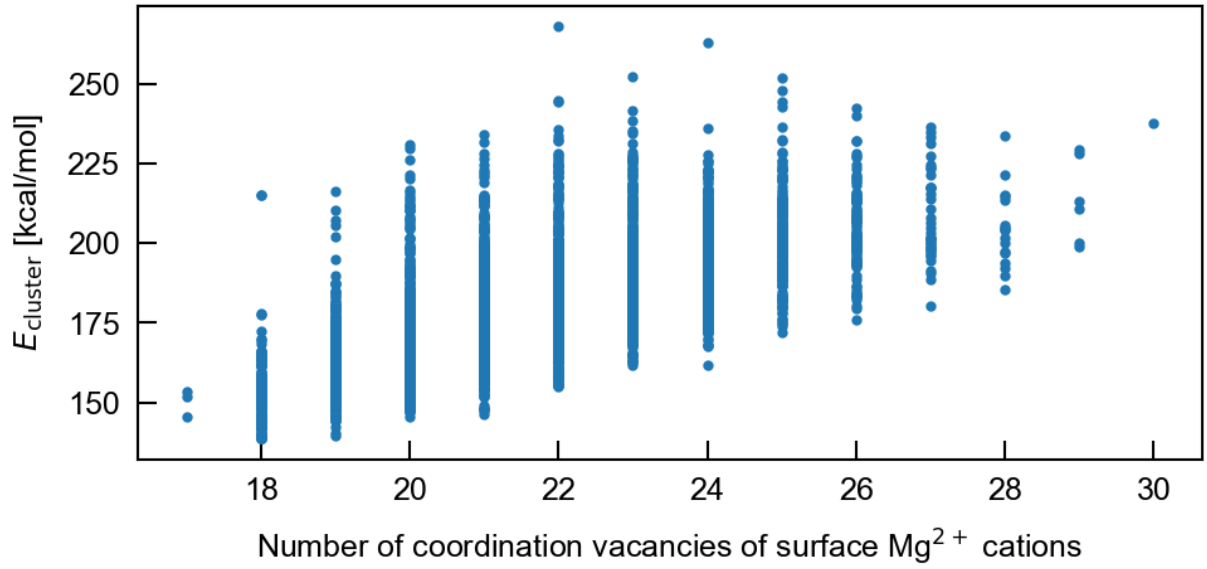

Figure 3.8. $E_{cluster}$ of metastable structures plotted against the total number of coordination vacancies of surface Mg^{2+} cations for $19MgCl_2$. The correlation was found to be largely inferior to that for the most stable structures in Figure 3.5.

Next, the most stable structures are shown for $x MgCl_2/y TiCl_4$ in Figures 3.9 and 3.10. Here, the columns correspond to the variation in the number of $MgCl_2$ units (x), while the rows correspond to that in the number of $TiCl_4$ molecules (y). Stepwise increasing the number of $TiCl_4$ molecules, the change in the structure of $MgCl_2$ was tracked. As can be seen in the figures, the occurrence of the reconstruction of $MgCl_2$ in the presence of one $TiCl_4$ molecule depended on the cluster size. In the case of 6, 7, 9, and $12MgCl_2$, the $TiCl_4$ adsorption occurred on the as-exposed {100} surfaces without reconstruction. On the other hand, 8 and $15MgCl_2$ transformed its morphology from a parallelogram to a diamond whose one corner was removed to expose a {110} terrace. Then, the terrace was capped by a $TiCl_4$ molecule to complete the diamond. In the case of $19MgCl_2$, the bare cluster originally

exposed a {110} terrace, and it was capped by $TiCl_4$. The addition of three $TiCl_4$ molecules induced reconstruction irrespective of the cluster size. The reconstruction accompanied relocation of $MgCl_2$ units to expose multiple {110} terraces, which were necessarily capped by $TiCl_4$ molecules. Likewise, a propensity for reconstruction increases for a larger number of $TiCl_4$ molecules per cluster, and a larger cluster has more chances for reconstruction simply because the number of $TiCl_4$ molecules per cluster increases at a fixed Ti content. The structure diversity also plays an important role: Reconstruction happens only when a metastable structure (of $MgCl_2$) that can better stabilize a given number of $TiCl_4$ molecules exists. In this sense, a larger cluster with increased diversity is more susceptible to reconstruction. Another important finding is that the reconstruction never occurred in a way to expose uncapped {110} terraces. This restriction resulted in the formation of short and segmented {110} terraces rather than long and connected {110} terraces, as shown in Figure 3.10. It is possible that ideal or flat {110} surfaces do not represent active surfaces of the real catalyst system, while short {110} terraces are introduced as defect sites on {100} terraces to bind $TiCl_4$ molecules. Indeed, a structure-performance relationship of alkoxysilane external donors was successfully simulated on the basis of a {110} edge structure introduced on {100} surfaces [53].

$E_{cluster}$ corresponds to the formation energy of a specific structure of $MgCl_2$. It reflected the energetic penalty for exposing coordination vacancies of Mg^{2+} cations in the absence of $TiCl_4$ (cf. Figure 3.7). Stabilization of such coordination vacancies by the adsorption of $TiCl_4$ led to a decline of $E_{cluster}$ along with the number of $TiCl_4$ molecules (Figures 3.9 and 3.10). The extent of the $E_{cluster}$ decline on the addition of one $TiCl_4$ molecule was compared among different cluster sizes. In the case of 6, 7, 9, and 12$MgCl_2$, the $E_{cluster}$ decline of 8–10 kcal/mol corresponded to the adsorption of

a $TiCl_4$ molecule on a {100} terrace without reconstruction. In the case of $19MgCl_2$, the adsorption of a $TiCl_4$ molecule on a {110} terrace caused an $E_{cluster}$ decline of 17 kcal/mol. These values were consistent with the adsorption energies of $TiCl_4$ calculated on ideal {100} and {110} surfaces [18], [20], [33]. For 8 and $15MgCl_2$, the addition of one $TiCl_4$ molecule induced reconstruction, and the $E_{cluster}$ decline respectively became 11 and 14 kcal/mol. These values were greater than those for 6, 7, 9, and $12MgCl_2$. Hence, stronger adsorption of $TiCl_4$ on a {110} terrace overcame the energetic penalty for reconstruction. Similar energy tendencies were obtained when the number of $TiCl_4$ molecule was increased, and therefore not described in detail.

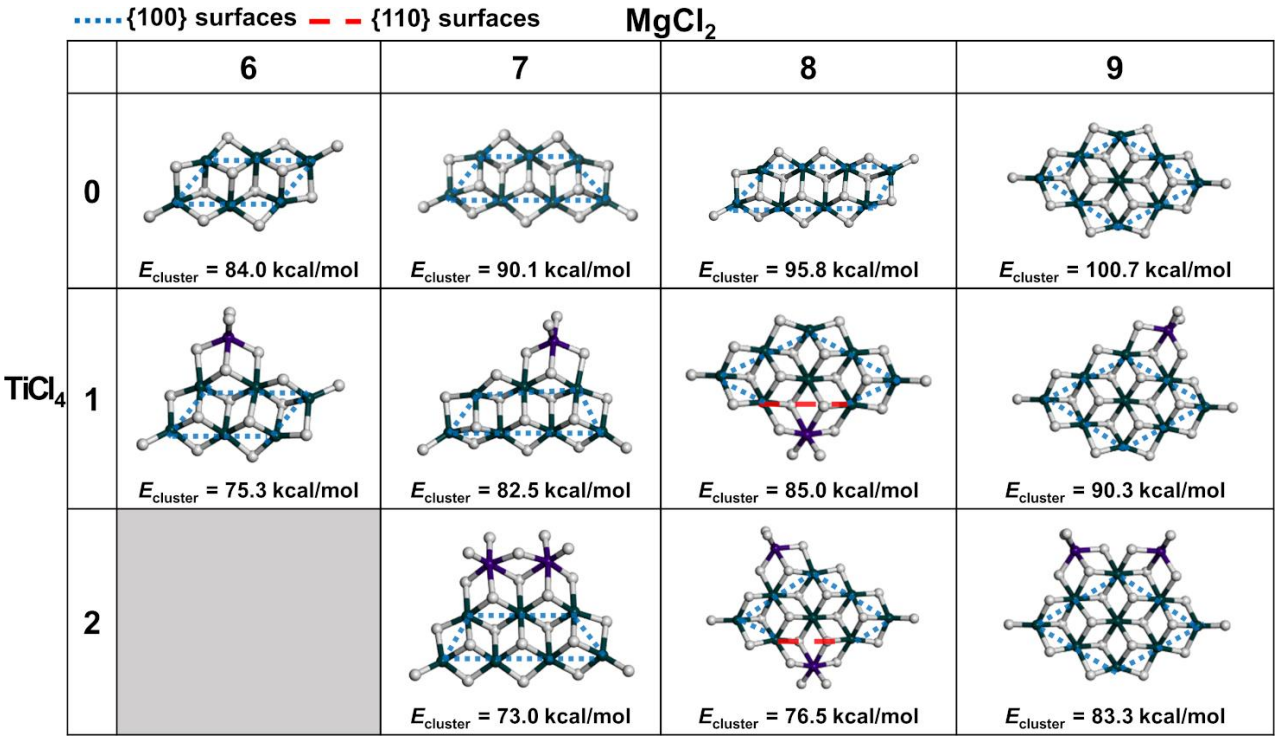

Figure 3.9. The most stable structures of $x MgCl_2/y TiCl_4$ (x = 6–9). Columns correspond to the number of $MgCl_2$ units, and rows correspond to the number of $TiCl_4$ molecules. The type of lateral termination is indicated by blue and red lines.

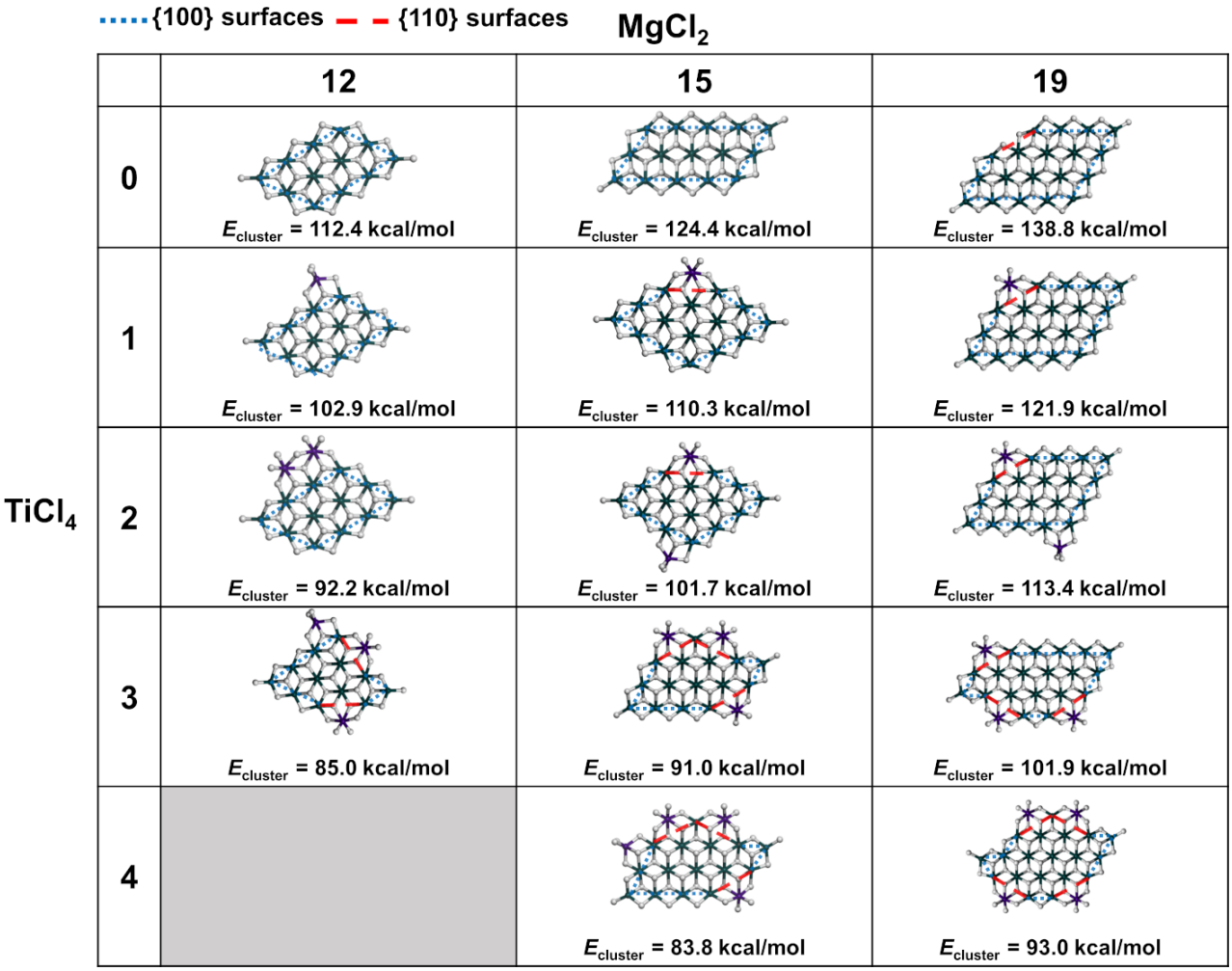

Figure 3.10. The most stable structures of xMgCl$_2$/yTiCl$_4$ (x = 12, 15, and 19).

3.3.2. Distribution of $TiCl_4$ on $MgCl_2$

In the course of structure determination, not only the most stable but also a huge number of metastable structures were obtained for each of xMgCl$_2$/yTiCl$_4$. A part of them had energies close to that of the most stable structure, i.e. energetically accessible. The number of energetically accessible structures increased for a larger cluster size and in particular when $TiCl_4$ was added, which was reflected by slower convergence in the genetic algorithm (cf. Figures 3.1–3.4). In Chapter 2, it was concluded that $TiCl_4$ on $MgCl_2$ is intrinsically distributed as combined consequences of the structure

diversity and non-ideal surfaces. Here, we analyzed the distribution of $TiCl_4$ in terms of steric and electronic environments for different cluster sizes and chemical compositions with an expectation to get insights into the distribution in the real catalyst system. To do so, the contribution of individual structures was estimated by the Boltzman factor,

$$p = e^{-\frac{\Delta E_{\text{cluster}}}{RT}} \quad (3.2),$$

where p is the relative population of a structure with respective to the most stable one, $\Delta E_{\text{cluster}}$ is its relative energy to that of the most stable one, and T was set to 350 K. It must be noted that the true distribution is not given without fully describing kinetics of catalyst formation, while relevant elementary reactions are hardly understood and expected to be extremely complicated. Hence, the distribution weighed by the Boltzman factor does not necessarily represent the true distribution, but it estimates relative availability of the structures at the given conditions. Besides, the structure database nearly completely collected all possible energetically accessible structures in a non-redundant manner. Such perfection is a prerequisite for evaluating a distribution. The modes of adsorption of $TiCl_4$ on $MgCl_2$ are classified into mononuclear species on {110} surfaces, and mononuclear and dinuclear species on {100} surfaces (Figure 3.11).

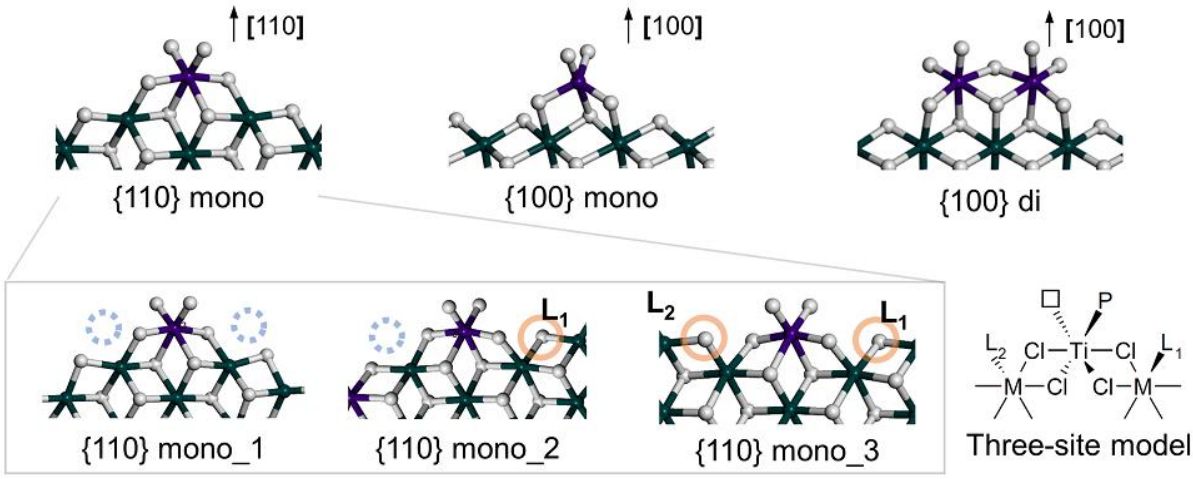

Figure 3.11. Classification of $TiCl_4$ molecules adsorbed on $MgCl_2$. The mononuclear species on {110} surfaces are further classified according to a three-site model [54].

Among these, the mononuclear species on {110} surfaces is believed to be catalytically most relevant [33], so that it was further classified into three different species (Types 1–3) according to the presence or absence of stereocontrolling ligands at two neighboring metal ions within the framework of a three-site model [54] (Figure 3.11). From the analysis of metastable structures with non-zero population at 350 K, the relative population of specific $TiCl_4$ species was derived for each of xMgCl$_2$/yTiCl$_4$, as demonstrated in Figure 3.12.

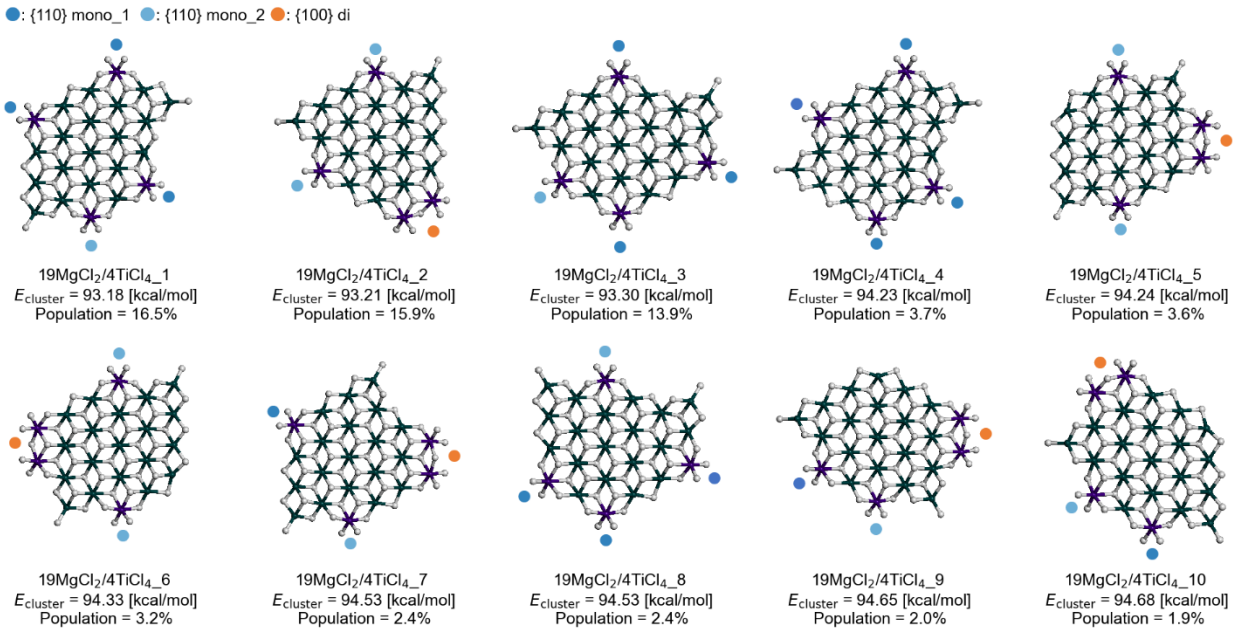

Figure 3.12. Top 10 structures of $19MgCl_2/4TiCl_4$. The relative population at 350 K and the classification of $TiCl_4$ species are given.

The results are shown in Figure 3.13. It can be seen that the distribution of $TiCl_4$ is sensitive to the cluster size and chemical composition. When the cluster size is small (x = 6, 9, and 12), the distribution is not present or small, and the mononuclear species on {100} surfaces is dominant in its population. This agrees with the earlier obtained conclusion that small clusters are not prone to the reconstruction, and $TiCl_4$ tends to adsorb on originally exposed {100} surfaces. The addition of two $TiCl_4$ molecules more or less induces the reconstruction of these small clusters, leading to the appearance of the mononuclear species on {110} surfaces. However, the dominant species are still those on {100} surfaces. The situation was found to be very different for larger clusters (x = 15 and 19). As larger clusters easily reconstruct by the addition of $TiCl_4$ molecules, the mononuclear species

on {110} surfaces is most popular regardless the chemical composition. On the other hand, the addition of $TiCl_4$ molecules also expands the structure diversity, which broadens the distribution, e.g. the two species on {100} surfaces occupy over 20% when more than one $TiCl_4$ molecule is added. The most interesting observation is that mononuclear species on {110} are not identical in terms of the surrounding steric environment. At the lowest coverage (= one $TiCl_4$ molecule per cluster), Type 1 without having stereocontrolling ligands dominates. However, in increasing the coverage, the population of Type 2 largely increases, and minor presence of Type 3 is also observed. This result suggests not only the distribution of stereospecificity of individual active sites but also the variation of average stereospecificity according to the surface coverage. It is experimentally known that the stereospecificity of a catalyst monotonously increases by immobilizing a larger amount of $TiCl_3$ on a $MgCl_2$ support of a fixed surface area [55], [56], which is likely consistent with the present results.

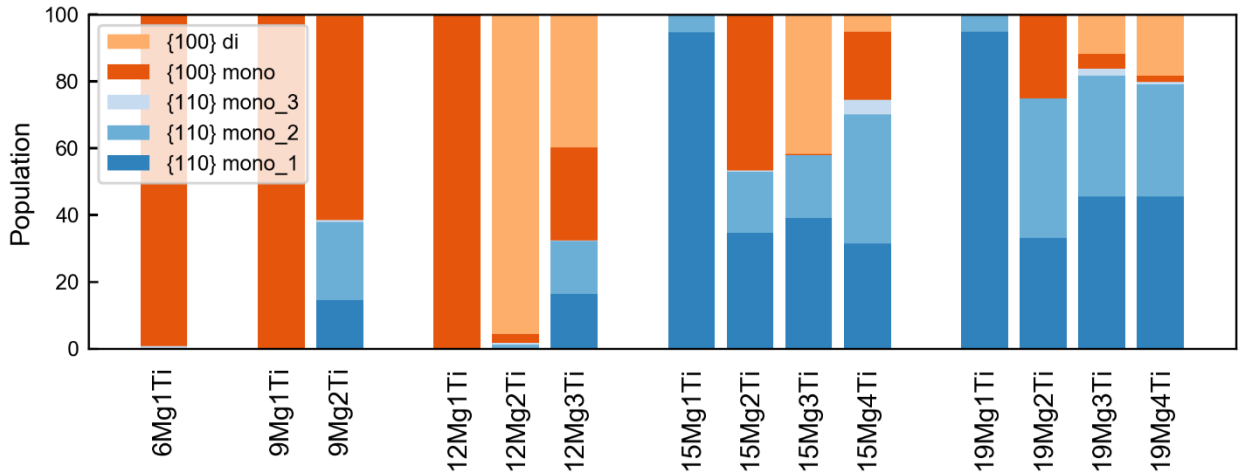

Figure 3.13. Distribution of different $TiCl_4$ species on $MgCl_2$. Adsorbed $TiCl_4$ molecules were classified into different species according to Figure 3.11. The distribution of individual species was derived for each of $x MgCl_2/y TiCl_4$ using Boltzman factor weights at 350 K.

Previous DFT calculations on a slab model reported that electron transfer between $MgCl_2$ and $TiCl_4$ largely depends on the adsorption mode of $TiCl_4$ species, which in turn affects the function of resultant active sites [18], [30]. Hence, the distribution of the charge state of $TiCl_4$ was derived, and it is exemplified in Figure 3.14 for $19MgCl_2/4TiCl_4$. The results for other clusters are summarized in Figures 3.15–3.17.

It was found that the mononuclear species on {110} surfaces are negatively charged as a result of an electronic donation from $MgCl_2$. The species on {100} surfaces are nearly neutral (dinuclear) or even positively charged (mononuclear). These findings are consistent with the previously reported results, while the distribution analysis gave an additional insight that the charge state of $TiCl_4$ is sensitive to the coordination environment. For example, species of Type 2 is less negatively charged than those of Type 1. The charge of Type 1 species is distributed due to the difference of coordination environments at positions farer than the ligand positions in the three-site model. As such, an ionic nature of the system allows $TiCl_4$ to electronically feel the surrounding environment in a remote fashion, which leads to the distribution in the charge state.

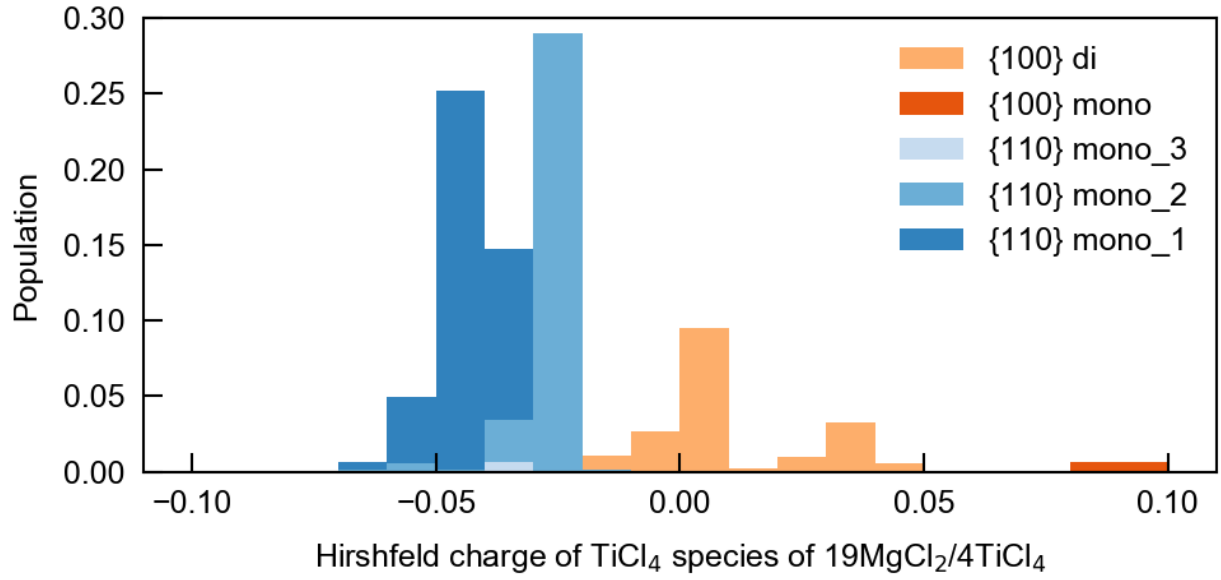

Figure 3.14. Charge-state distribution of $TiCl_4$ for $19MgCl_2/4TiCl_4$. The charge analysis was performed on the basis of the Hirshfeld method [57].

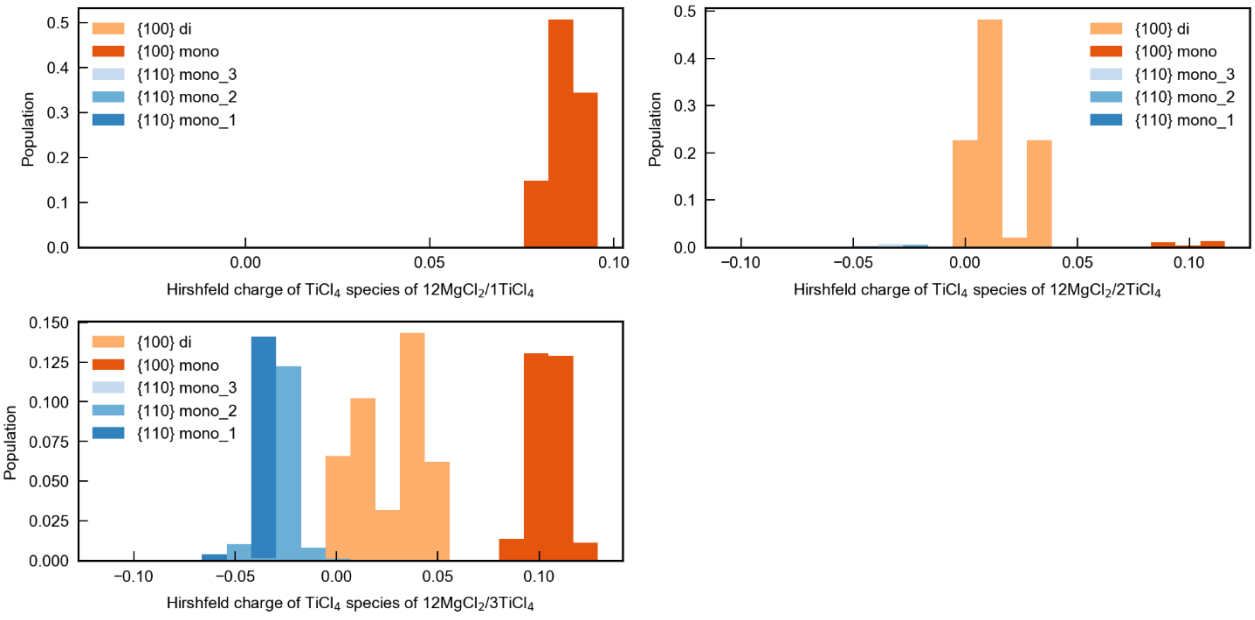

Figure 3.15. Charge-state distribution of $TiCl_4$ for $12MgCl_2/1–3TiCl_4$.

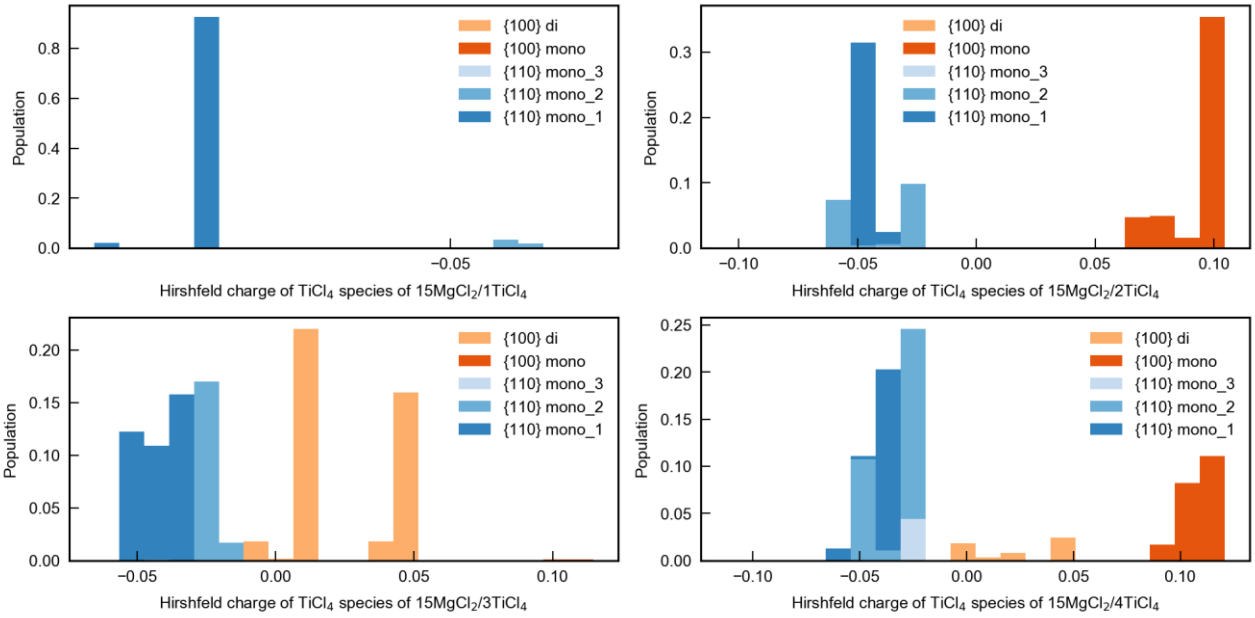

Figure 3.16. Charge-state distribution of $TiCl_4$ for $15MgCl_2$/1–4$TiCl_4$.

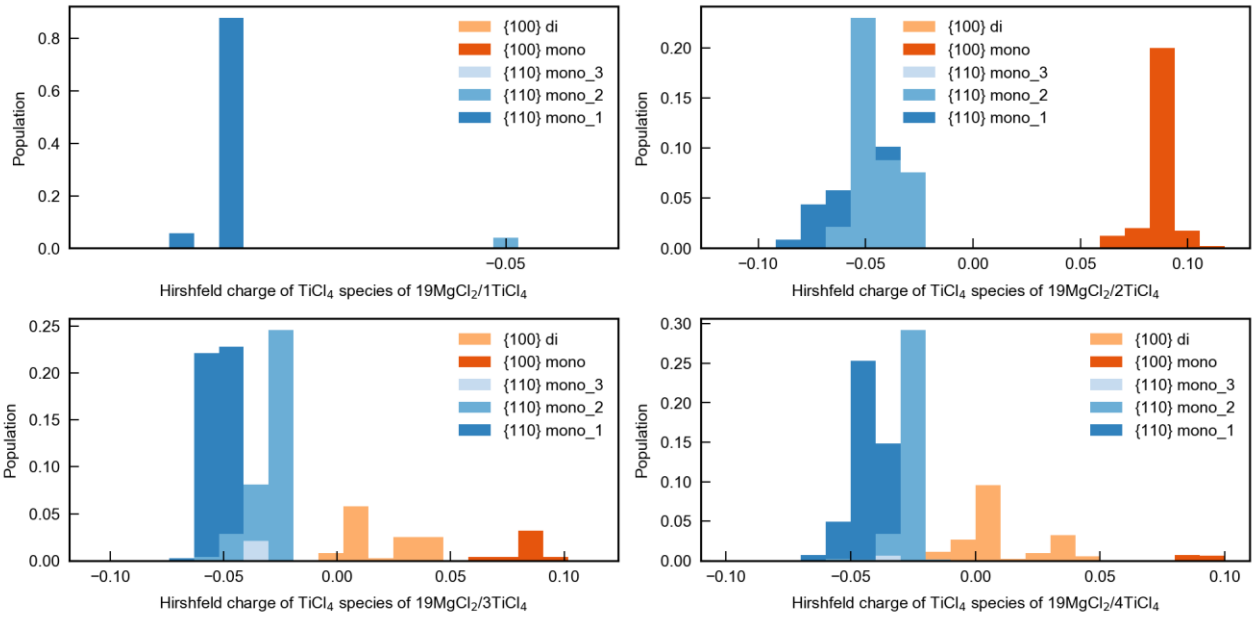

Figure 3.17. Charge-state distribution of $TiCl_4$ for $19MgCl_2$/1–4$TiCl_4$.

3.3.3. Influences of $TiCl_4$ distribution on the ethylene insertion

Lastly, a preliminary investigation was performed to infer whether the structural and electronic distributions of $TiCl_4$ can affect the polymerization performance when activated. For this, 12 structures of $19MgCl_2/4TiCl_4$ were chosen according to the energetic accessibility and the variation in the type of $TiCl_4$ species. The selected structures are listed in Figure 3.18.

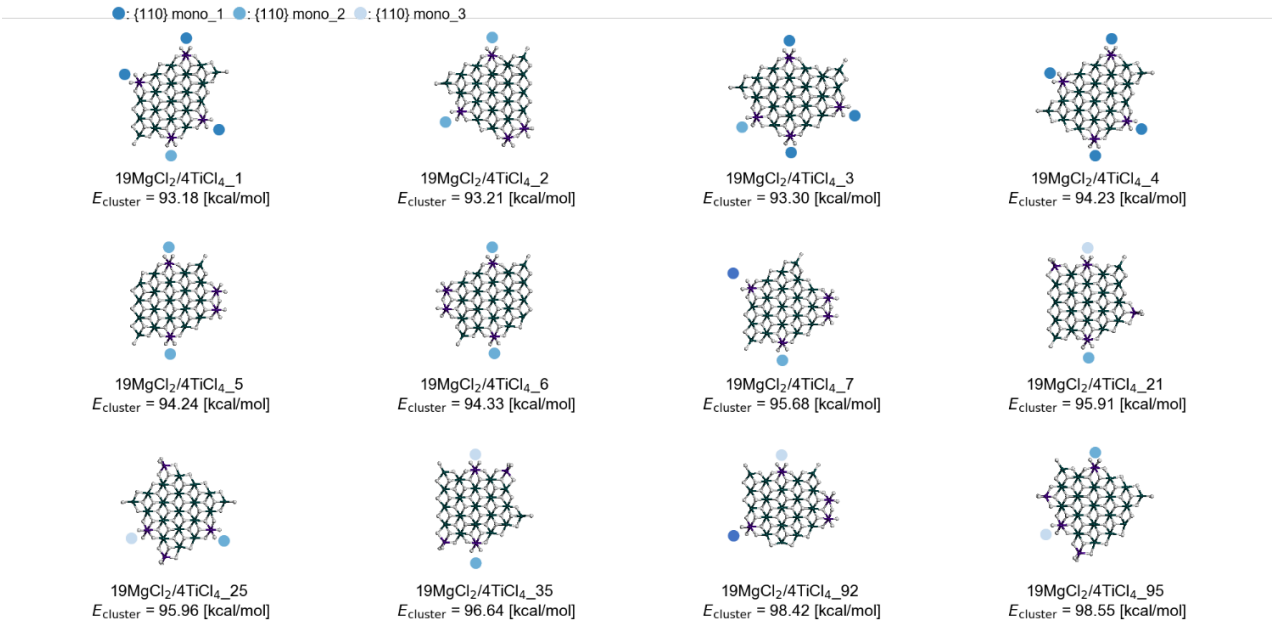

Figure 3.18. Selected structures for calculating the activation energy of ethylene insertion at mononuclear species of different types on {110} surfaces.

30 mononuclear species on {110} surfaces were identified in the 12 structures, and the activation energy of ethylene insertion was calculated for each of these species. In detail, $TiCl_4$ was converted to $TiCl_2Me$ [58], and then the apparent activation energy of ethylene insertion into Ti-Me was calculated. The transition state was approximated by the structure obtained at 2.2 Å of the distance between the carbon of the incoming ethylene and that of the methyl group. This approximation was

validated with the more accurate transition state determination. Further details are given in the literature [19,34,59]. Figure 3.19 shows the relationship between the calculated activation energy and the charge state of $TiCl_4$ (before its activation). It can be seen that the activation energy tends to decline as the Ti species becomes more electron-deficient [34]. This is because an electron-deficient active site enhances both of the π-complexation and the agostic interaction within the α-agostic-assisted Cosse–Arlman mechanism [59], [60]. Note that the calculations were performed for the sterically least demanding combination between ethylene and Ti-Me; thus, the difference of the steric environment affects the activation energy mainly through the charge state. Nonetheless, the obtained results strongly suggested that the distribution of $TiCl_4$ as an intrinsic nature of the $MgCl_2/TiCl_4$ system is impactful for the active-site performance. The distribution of the polymer primary structure in Ziegler–Natta olefin polymerization is well known and it has been explained as a result of the multisite nature of the catalysts. The present results correspond to the first non-empirical explanation of its origin.

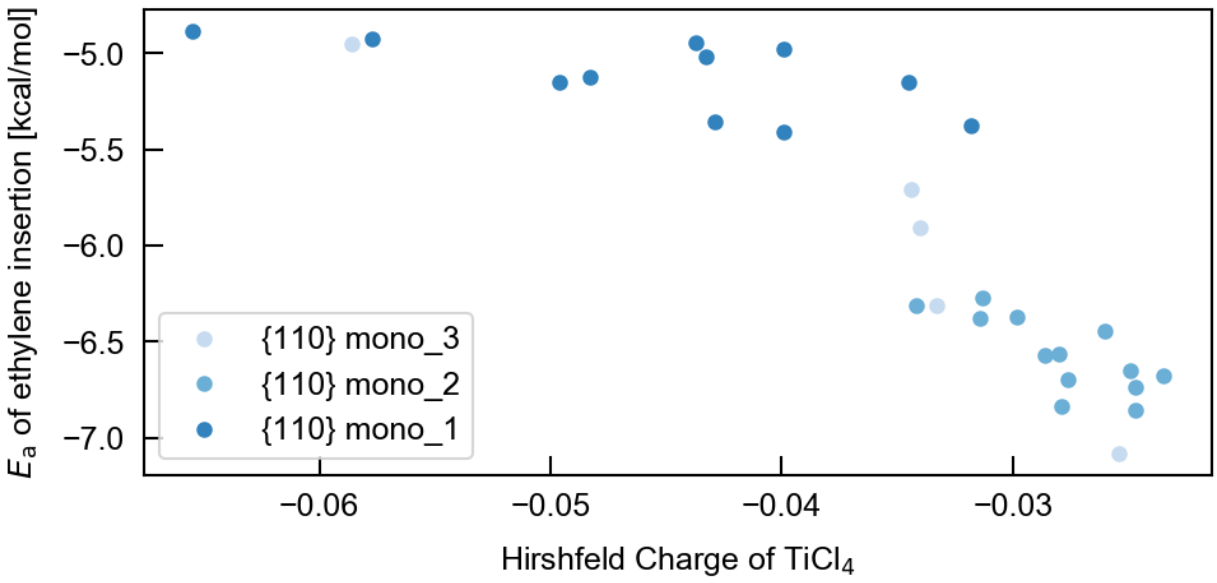

Figure 3.19. Distribution in the activation energy of ethylene insertion. 30 mononuclear species on {110} surfaces were selected from energetically accessible metastable structures for $19MgCl_2/4TiCl_4$. Converting $TiCl_4$ into $TiCl_2CH_3$, the apparent activation energy of ethylene insertion was calculated for individual species. The relationship among the Hirshfeld charge, the apparent activation energy, and the steric environment is represented.

3.4. Conclusion

$TiCl_4$-capped $MgCl_2$ nanoplates as a building block of heterogeneous Ziegler–Natta catalysts have a distribution in their structures. This distribution is expected to be relevant to the polydispersity in the produced polymer. In this work, we performed a series of non-empirical structure determination for $TiCl_4$-capped $MgCl_2$ nanoplates of different sizes and chemical compositions. The results of the structure determination suggested that most of $TiCl_4$ adsorb on {110} surfaces, although $TiCl_4$ adsorption on {100} surfaces is not negligible. Structural and electronic analysis on energetically accessible structures revealed that $TiCl_4$ has a distribution in the steric environment and the charge state. Preliminary calculations on the ethylene insertion activation energy suggested that such a

distribution is potentially important for the active-site performance. Thus, the present study proposes an important hypothesis that the multisite nature of heterogeneous Ziegler–Natta catalysts, hence, the polydispersity of the obtained polymer, is a general characteristic of the $MgCl_2/TiCl_4$ system. Understanding the multisite nature of the catalyst is expected to contribute to the systematic design of catalysts.

REFERENCES

[1] A. Andoni, J. C. Chadwick, H. J. W. Niemantsverdriet, and P. C. Thüne, "The role of electron donors on lateral surfaces of $MgCl_2$-supported Ziegler-Natta catalysts: Observation by AFM and SEM," *J. Catal.*, vol. 257, no. 1, pp. 81–86, Jul. 2008, doi: 10.1016/j.jcat.2008.04.020.

[2] H. Topsøe, "Developments in operando studies and in situ characterization of heterogeneous catalysts," *J. Catal.*, vol. 216, no. 1–2, pp. 155–164, May 2003, doi: 10.1016/S0021-9517(02)00133-1.

[3] M. D'Amore, K. S. Thushara, A. Piovano, M. Causà, S. Bordiga, and E. Groppo, "Surface Investigation and Morphological Analysis of Structurally Disordered $MgCl_2$ and $MgCl_2/TiCl_4$ Ziegler-Natta Catalysts," *ACS Catal.*, vol. 6, no. 9, pp. 5786–5796, Sep. 2016, doi: 10.1021/acscatal.6b00871.

[4] T. Taniike, P. Chammingkwan, V. Q. Thang, K. Goto, T. Fujitani, and M. Terano, "Chemisorption-Induced Activation of $MgCl_2$ Film as Realistic Route for Heterogeneous

Ziegler-Natta Surfaces under Ultrahigh Vacuum," *J. Phys. Chem. C*, vol. 121, no. 43, pp. 24085–24092, Nov. 2017, doi: 10.1021/acs.jpcc.7b08242.

[5] B. R. Goldsmith, E. D. Sanderson, R. Ouyang, and W. X. Li, "CO- and NO-induced disintegration and redispersion of three-way catalysts rhodium, palladium, and platinum: An ab initio thermodynamics study," *J. Phys. Chem. C*, vol. 118, no. 18, pp. 9588–9597, May 2014, doi: 10.1021/jp502201f.

[6] S. Linic and P. Christopher, "Overcoming Limitation in the Design of Selective Solid Catalysts by Manipulating Shape and Size of Catalytic Particles: Epoxidation Reactions on Silver," *ChemCatChem*, vol. 2, no. 9, pp. 1061–1063, Sep. 2010, doi: 10.1002/cctc.201000163.

[7] I. V. Yudanov, A. Genest, S. Schauermann, H. J. Freund, and N. Rösch, "Size Dependence of the adsorption energy of CO on metal nanoparticles: A DFT search for the minimum value," *Nano Lett.*, vol. 12, no. 4, pp. 2134–2139, Apr. 2012, doi: 10.1021/nl300515z.

[8] D. H. Lim and J. Wilcox, "DFT-based study on oxygen adsorption on defective graphene-supported Pt nanoparticles," *J. Phys. Chem. C*, vol. 115, no. 46, pp. 22742–22747, Nov. 2011, doi: 10.1021/jp205244m.

[9] D. J. Wales and H. A. Scheraga, "Global optimization of clusters, crystals, and biomolecules," *Science*, vol. 285, no. 5432. American Association for the Advancement of Science, pp. 1368–1372, Aug. 27, 1999, doi: 10.1126/science.285.5432.1368.

[10] D. M. Deaven and K. M. Ho, “Molecular geometry optimization with a genetic algorithm,” *Phys. Rev. Lett.*, vol. 75, no. 2, pp. 288–291, Jul. 1995, doi: 10.1103/PhysRevLett.75.288.

[11] M. D. Wolf and U. Landman, “Genetic Algorithms for Structural Cluster Optimization,” *J. Phys. Chem. A*, vol. 102, no. 30, pp. 6129–6137, Jul. 1998, doi: 10.1021/jp9814597.

[12] C. J. Heard, S. Heiles, S. Vajda, and R. L. Johnston, “$Pd_nAg_{(4-n)}$ and $Pd_nPt_{(4-n)}$ clusters on MgO (100): A density functional surface genetic algorithm investigation,” *Nanoscale*, vol. 6, no. 20, pp. 11777–11788, 2014, doi: 10.1039/c4nr03363a.

[13] H. A. Hussein, J. B. A. Davis, and R. L. Johnston, “DFT global optimisation of gas-phase and MgO-supported sub-nanometre AuPd clusters,” *Phys. Chem. Chem. Phys.*, vol. 18, no. 37, pp. 26133–26143, 2016, doi: 10.1039/c6cp03958h.

[14] J. A. Vargas, F. Buendía, and M. R. Beltrán, “New Au_N (N = 27-30) Lowest Energy Clusters Obtained by Means of an Improved DFT-Genetic Algorithm Methodology,” *J. Phys. Chem. C*, vol. 121, no. 20, pp. 10982–10991, May 2017, doi: 10.1021/acs.jpcc.6b12848.

[15] H. Xiang, S.-H. Wei, and X. Gong, “Structures of $[Ag_7(SR)_4]^-$ and $[Ag_7(DMSA)_4]^-$,” *J. Am. Chem. Soc.*, vol. 132, no. 21, pp. 7355–7360, Jun. 2010, doi: 10.1021/ja9108374.

[16] M. Boero, M. Parrinello, and K. Terakura, “First Principles Molecular Dynamics Study of Ziegler- Natta Heterogeneous Catalysis,” *J. Am. Chem. Soc*, vol. 120, no. 12, pp. 2746–2752, 1998, doi: 10.1021/ja972367i.

[17] M. Boero, M. Parrinello, and K. Terakura, “Ziegler-Natta heterogeneous catalysis by first principles computer experiments,” *Surf. Sci.*, vol. 438, no. 1–3, pp. 1–8, Sep. 1999, doi: 10.1016/S0039-6028(99)00537-3.

[18] T. Taniike and M. Terano, “High-precision Molecular Modelling for Ziegler-Natta Catalysts,” *J. Japan Pet. Inst.*, vol. 61, no. 3, pp. 182–190, 2018.

[19] V. Busico *et al.*, “Periodic DFT and High-Resolution Magic-Angle-Spinning (HR-MAS) ^{1}H NMR Investigation of the Active Surfaces of $MgCl_2$-Supported Ziegler−Natta Catalysts. The $MgCl_2$ Matrix,” *J. Phys. Chem. C*, vol. 112, no. 4, pp. 1081–1089, Jan. 2008, doi: 10.1021/jp076679b.

[20] M. D’Amore, R. Credendino, P. H. M. Budzelaar, M. Causá, and V. Busico, “A periodic hybrid DFT approach (including dispersion) to $MgCl_2$-supported Ziegler-Natta catalysts - 1: $TiCl_4$ adsorption on $MgCl_2$ crystal surfaces,” *J. Catal.*, vol. 286, pp. 103–110, Feb. 2012, doi: 10.1016/j.jcat.2011.10.018.

[21] R. Credendino, J. T. M. Pater, A. Correa, G. Morini, and L. Cavallo, “Thermodynamics of formation of uncovered and dimethyl ether-covered $MgCl_2$ crystallites. consequences in the structure of Ziegler-Natta heterogeneous catalysts,” *J. Phys. Chem. C*, vol. 115, no. 27, pp. 13322–13328, Jul. 2011, doi: 10.1021/jp201410n.

[22] R. Credendino, D. Liguori, G. Morini, and L. Cavallo, “Investigating phthalate and 1,3-diether coverage and dynamics on the (104) and (110) surfaces of $MgCl_2$-supported Ziegler-

Natta catalysts," *J. Phys. Chem. C*, vol. 118, no. 15, pp. 8050–8058, Apr. 2014, doi: 10.1021/jp501390e.

[23] D. V. Stukalov, I. L. Zilberberg, and V. A. Zakharov, "Surface species of titanium(IV) and titanium(III) in $MgCl_2$-Supported Ziegler-Natta catalysts. A periodic density functional theory study," *Macromolecules*, vol. 42, no. 21, pp. 8165–8171, Nov. 2009, doi: 10.1021/ma901413b.

[24] D. V. Stukalov and V. A. Zakharov, "Active site formation in $MgCl_2$-supported ziegler - Natta catalysts. A density functional theory study," *J. Phys. Chem. C*, vol. 113, no. 51, pp. 21376–21382, Dec. 2009, doi: 10.1021/jp907812k.

[25] D. V. Stukalov, V. A. Zakharov, and I. L. Zilberberg, "Adsorption species of ethyl benzoate in $MgCl_2$-supported ziegler-natta catalysts. A density functional theory study," *J. Phys. Chem. C*, vol. 114, no. 1, pp. 429–435, Jan. 2010, doi: 10.1021/jp908551k.

[26] N. Bahri-Laleh *et al.*, "Computational modeling of heterogeneous Ziegler-Natta catalysts for olefins polymerization," *Prog. Polym. Sci.*, vol. 84, pp. 89–114, Sep. 2018, doi: 10.1016/J.PROGPOLYMSCI.2018.06.005.

[27] M. Boero, M. Parrinello, S. Hüffer, and H. Weiss, "First principles study of propene polymerization in Ziegler-Natta heterogeneous catalysis," *J. Am. Chem. Soc.*, vol. 122, no. 3, pp. 501–509, 2000, doi: 10.1021/ja990913x.

[28] M. Boero, M. Parrinello, H. Weiss, and S. Hüffer, "A first principles exploration of a variety

of active surfaces and catalytic sites in Ziegler-Natta heterogeneous catalysis," *J. Phys. Chem. A*, vol. 105, no. 21, pp. 5096–5105, 2001, doi: 10.1021/jp010780d.

[29] M. Boero, M. Parrinello, K. Terakura, and H. Weiss, "Car-Parrinello study of Ziegler-Natta heterogeneous catalysis: Stability and destabilization problems of the active site models," *Mol. Phys.*, vol. 100, no. 18, pp. 2935–2940, Sep. 2002, doi: 10.1080/00268970110109899.

[30] T. Taniike and M. Terano, "Coadsorption and support-mediated interaction of Ti species with ethyl benzoate in $MgCl_2$-supported heterogeneous ziegler-natta catalysts studied by density functional calculations," *Macromol. Rapid Commun.*, vol. 28, no. 18–19, pp. 1918–1922, Sep. 2007, doi: 10.1002/marc.200700363.

[31] T. Taniike and M. Terano, "Reductive formation of isospecific Ti dinuclear species on a $MgCl_2$ (110) surface in heterogeneous ziegler-natta catalysts," *Macromol. Rapid Commun.*, vol. 29, no. 17, pp. 1472–1476, Sep. 2008, doi: 10.1002/marc.200800310.

[32] T. Taniike and M. Terano, "A Density Functional Study on the Influence of the Molecular Flexibility of Donors on the Insertion Barrier and Stereoselectivity of Ziegler-Natta Propylene Polymerization," *Macromol. Chem. Phys.*, vol. 210, no. 24, pp. 2188–2193, Dec. 2009, doi: 10.1002/macp.200900465.

[33] T. Taniike and M. Terano, "Coadsorption model for first-principle description of roles of donors in heterogeneous Ziegler-Natta propylene polymerization," *J. Catal.*, vol. 293, pp. 39–50, Sep. 2012, doi: 10.1016/j.jcat.2012.06.001.

[34] A. Matta, P. Chammingkwan, B. K. Singh, M. Terano, T. Kaneko, and T. Taniike, "Truxillic and truxinic acid-based, bio-derived diesters as potent internal donor in Ziegler-Natta catalyst for propylene polymerization," *Appl. Catal. A Gen.*, vol. 554, pp. 80–87, Mar. 2018, doi: 10.1016/J.APCATA.2018.01.030.

[35] B. R. Goldsmith, B. Peters, J. K. Johnson, B. C. Gates, and S. L. Scott, "Beyond Ordered Materials: Understanding Catalytic Sites on Amorphous Solids," *ACS Catal.*, vol. 7, no. 11, pp. 7543–7557, Nov. 2017, doi: 10.1021/acscatal.7b01767.

[36] A. Thakur, T. Wada, P. Chammingkwan, M. Terano, and T. Taniike, "Development of Large-Scale Stopped-Flow Technique and its Application in Elucidation of Initial Ziegler–Natta Olefin Polymerization Kinetics," *Polymers (Basel).*, vol. 11, no. 6, p. 1012, Jun. 2019, doi: 10.3390/polym11061012.

[37] N. Pasquini and A. Addeo, "Catalysts for Polymerization," in *Polypropylene Handbook*, 2nd ed., Boca Raton: Hanser Gardner Publications, 2005, pp. 11–112.

[38] M. P. McDaniel, "A Review of the Phillips Supported Chromium Catalyst and Its Commercial Use for Ethylene Polymerization," in *Advances in Catalysis*, vol. 53, no. C, Academic Press, 2010, pp. 123–606.

[39] C. A. Demmelmaier, R. E. White, J. A. van Bokhoven, and S. L. Scott, "Evidence for a chromasiloxane ring size effect in Phillips (Cr/SiO2) polymerization catalysts," *J. Catal.*, vol. 262, no. 1, pp. 44–56, Feb. 2009, doi: 10.1016/j.jcat.2008.11.024.

[40] U. Das *et al.*, “Effect of Siloxane Ring Strain and Cation Charge Density on the Formation of Coordinately Unsaturated Metal Sites on Silica: Insights from Density Functional Theory (DFT) Studies,” *ACS Catal.*, vol. 5, no. 12, pp. 7177–7185, Oct. 2015, doi: 10.1021/acscatal.5b01699.

[41] S. A. Khan, C. A. Vandervelden, S. L. Scott, and B. Peters, “Grafting metal complexes onto amorphous supports: From elementary steps to catalyst site populations: Via kernel regression,” *React. Chem. Eng.*, vol. 5, no. 1, pp. 66–76, Jan. 2020, doi: 10.1039/c9re00357f.

[42] C. A. Vandervelden, S. A. Khan, S. L. Scott, and B. Peters, “Site-averaged kinetics for catalysts on amorphous supports: An importance learning algorithm,” *React. Chem. Eng.*, vol. 5, no. 1, pp. 77–86, Jan. 2020, doi: 10.1039/c9re00356h.

[43] T. Pongchan, P. Praserthdam, and B. Jongsomjit, “Temperature effect on propylene polymerization behavior over Ziegler-Natta catalyst with different cocatalyst systems,” *Mater. Res. Express*, vol. 7, no. 2, p. 025309, Feb. 2020, doi: 10.1088/2053-1591/ab726d.

[44] R. Zannetti, C. Marega, A. Marigo, and A. Martorana, “Layer-lattices in Ziegler–Natta catalysts,” *J. Polym. Sci. Part B Polym. Phys.*, vol. 26, no. 12, pp. 2399–2412, Nov. 1988, doi: 10.1002/polb.1988.090261202.

[45] A. Marigo, C. Marega, R. Zannetti, G. Morini, and G. Ferrara, “Small- and wide-angle X-ray scattering analysis of Ziegler-Natta catalysts: structural disorder, surface area and

activity," *Eur. Polym. J.*, vol. 36, no. 9, pp. 1921–1926, Sep. 2000, doi: 10.1016/S0014-3057(99)00250-5.

[46] M. Chang, X. Liu, P. J. Nelson, G. R. Munzing, T. A. Gegan, and Y. V. Kissin, "Ziegler-Natta catalysts for propylene polymerization: Morphology and crystal structure of a fourth-generation catalyst," *J. Catal.*, vol. 239, no. 2, pp. 347–353, Apr. 2006, doi: 10.1016/j.jcat.2006.02.009.

[47] T. Wada *et al.*, "Revisiting the identity of δ-MgCl2: Part I. Structural disorder studied by synchrotron X-ray total scattering," *J. Catal.*, vol. 385, pp. 76–86, May 2020, doi: 10.1016/j.jcat.2020.03.002.

[48] G. Takasao, T. Wada, A. Thakur, P. Chammingkwan, M. Terano, and T. Taniike, "Machine Learning-Aided Structure Determination for $TiCl_4$–Capped $MgCl_2$ Nanoplate of Heterogeneous Ziegler–Natta Catalyst," *ACS Catal.*, vol. 9, no. 3, pp. 2599–2609, Mar. 2019, doi: 10.1021/acscatal.8b05080.

[49] J. P. Perdew, K. Burke, and M. Ernzerhof, "Generalized Gradient Approximation Made Simple," *Phys. Rev. Lett.*, vol. 77, no. 18, pp. 3865–3868, Oct. 1996, doi: 10.1103/PhysRevLett.77.3865.

[50] B. Delley, "An all-electron numerical method for solving the local density functional for polyatomic molecules," *J. Chem. Phys.*, vol. 92, no. 1, pp. 508–517, Jan. 1990, doi: 10.1063/1.458452.

[51] M. Dolg, U. Wedig, H. Stoll, and H. Preuss, “Energy-adjusted ab initio pseudopotentials for the first row transition elements,” *J. Chem. Phys.*, vol. 86, no. 2, pp. 866–872, Jan. 1987, doi: 10.1063/1.452288.

[52] A. Bergner, M. Dolg, W. Küchle, H. Stoll, and H. Preuß, “Ab initio energy-adjusted pseudopotentials for elements of groups 13-17,” *Mol. Phys.*, vol. 80, no. 6, pp. 1431–1441, Dec. 1993, doi: 10.1080/00268979300103121.

[53] S. Poonpong, S. Dwivedi, T. Taniike, and M. Terano, “Structure-Performance Relationship for Dialkyldimethoxysilane as an External Donor in Stopped-Flow Propylene Polymerization Using a Ziegler-Natta Catalyst,” *Macromol. Chem. Phys.*, vol. 215, no. 18, pp. 1721–1727, Sep. 2014, doi: 10.1002/macp.201400157.

[54] V. Busico *et al.*, “High-resolution 13C NMR configurational analysis of polypropylene made with $MgCl_2$-supported Ziegler-Natta catalysts. 1. The ‘model’ system $MgCl_2/TiCl_4$-2,6-dimethylpyridine/$Al(C_2H_5)_3$,” *Macromolecules*, vol. 32, no. 13, pp. 4173–4182, Jun. 1999, doi: 10.1021/ma981941n.

[55] T. Wada, T. Taniike, I. Kouzai, S. Takahashi, and M. Terano, “Propylene Polymerization Performance of Isolated and Aggregated Ti Species Studied Using a Well-Designed $TiCl_3$ /$MgCl_2$ Ziegler-Natta Model Catalyst,” *Macromol. Rapid Commun.*, vol. 30, no. 11, pp. 887–891, Jun. 2009, doi: 10.1002/marc.200900015.

[56] T. Taniike, S. Takahashi, T. Wada, K. Tonosaki, S. Dwivedi, and M. Terano, “Model

Catalysts for Clarification of Active Site-Polymer Relationship in Heterogeneous Olefin Polymerization," *Macromol. Symp.*, vol. 313–314, no. 1, pp. 1–7, Mar. 2012, doi: 10.1002/masy.201250301.

[57] F. L. Hirshfeld, "Bonded-atom fragments for describing molecular charge densities," *Theor. Chim. Acta*, vol. 44, no. 2, pp. 129–138, 1977, doi: 10.1007/BF00549096.

[58] N. Bahri-Laleh *et al.*, "Moving up and down the Titanium Oxidation State in Ziegler−Natta Catalysis," *Macromolecules*, vol. 44, no. 4, pp. 778–783, Feb. 2011, doi: 10.1021/ma1023582.

[59] E. J. Arlman and P. Cossee, "Ziegler-Natta catalysis III. Stereospecific polymerization of propene with the catalyst system $TiCl_3AlEt_3$," *J. Catal.*, vol. 3, no. 1, pp. 99–104, 1964, doi: 10.1016/0021-9517(64)90097-1.

[60] M. Brookhart and M. L. H. Green, "Carbon hydrogen-transition metal bonds," *J. Organomet. Chem.*, vol. 250, no. 1, pp. 395–408, Jul. 1983, doi: 10.1016/0022-328X(83)85065-7.

Chapter 4:
Origin of Stereospecificity in Donor-Free Ziegler–Natta Catalyst Studied Based on Machine Learning-Derived Catalyst Models

Abstract

Mononuclear $TiCl_4$ species adsorbed on the {110} surfaces have been considered to be a catalytic relevant species of heterogeneous Ziegler-Natta catalysts for propylene polymerization; however, a satisfactory explanation for the origin of stereospecificity in donor-free catalysts has not been given. Here, propylene polymerization simulations were performed based on $MgCl_2/TiCl_4$ nanoplates derived by machine-learning aided structure determination. The results addressed that the stereospecificity in absence of donor molecules originated from the presence of stereocontrolling ligand such as bridged Cl^- anions and terminal Cl^- anions of $TiCl_4$, which are provided by the defective surface and high coverage.

Keywords: Ziegler–Natta catalyst, genetic algorithm, structure determination, density functional theory, surface reconstruction, active site distribution

4.1. Introduction

Nowadays, global world production of polyolefins has exceeded 100 million tons. Polypropylene (PP) and high-density polyethylene (HDPE), the main constituents of polyolefins, are produced by Ziegler-Natta catalysts (ZNCs) [1]. This industrial significance has positioned the ZNCs as the subject of extensive research and development for almost 70 years since their discovery. Of the many variations, the most important form of the catalysts is $MgCl_2/TiCl_4$, where lateral surfaces of disorderedly stacked $MgCl_2$ nanoplates are capped by $TiCl_4$ as the active site precursor and can be modified with organic Lewis bases called donors [2].

The stereoregularity or the isotacticity of PP greatly affects its properties such as rigidity and toughness through crystallinity. In current industrial catalysts, internal and external donors are usually added to improve stereospecificity, but polymers obtained from donor-free catalysts are also known to be more or less isotactic [3]–[6]. The origin of the stereospecificity in donor-free catalysts has been a long-standing question, although it is essential for clarifying the fundamental mechanism of ZNCs.

The earliest hypothesis on the stereospecificity of $MgCl_2$-supported ZNCs was that dimeric $TiCl_4$ on {100} or analogous surfaces of $MgCl_2$ is isospecific, while monomeric $TiCl_4$ on {110} surfaces is aspecific [7], [8]. It was also presumed that donors improve the stereospecificity of the catalysts by poisoning the {110} surfaces [9]. However, this hypothesis is nowadays not believed plausible. The two main counter-evidences are that the latest DFT results reject the adsorption of $TiCl_4$ on the {100} surfaces in a thermodynamic condition, and that the polymer microstructure reflecting the active site structure is sensitive to the molecular structure of donors, suggesting that the donor

molecules are directly involved in the active site [10]. Accordingly, the {110} surfaces, which allow the adsorption of $TiCl_4$, are now believed as the catalytically relevant ones. Researchers believe that donor molecules adsorb on the {110} surfaces and interact non-bondedly with nearby Ti species, thus enhancing the stereospecificity of the Ti species. However, such an idea does not explain the origin of the stereospecificity of $MgCl_2/TiCl_4$ lacking donors, as the $TiCl_4$ mononuclear species on the {110} surfaces is regarded non-stereospecific.

In this chapter, I perform propylene polymerization simulation based on $MgCl_2/TiCl_4$ nanoplates derived in Chapter 3. These are considered to be the most realistic model for donor-free ZNCs. By comparing the propylene polymerization performance of Ti species situated in various environments, the origin of stereospecificity as well as the structure-performance relationship of the active sites is clarified.

4.2. Numerical methods

The DFT calculations were performed by $DMol^3$ of Materials Studio [11] with the following conditions: The GGA PBE [12] for the exchange-correlation functional, and the DNP [11] basis set with effective core potentials [13], [14]. For the optimization of the transition state, the convergence criteria for geometry optimization were set to 0.001255 kcal/mol in energy, 1.255 kcal/(mol Å) in force. Thermal smearing was used to improve the self-consistent field (SCF) convergence with a value of 0.005 Hartree. The orbital cutoff radius was set to 4.500 Å.

Two systems, $19MgCl_2/4TiCl_4$ and $19MgCl_2/9TiCl_4$, which are equal in size and have different surface coverage, were employed. The chosen size of 19MgCl2 is computationally feasible and

believed to be not far from the experimentally observed size. The chemical compositions referred the experimental observation that the $MgCl_2$ of ZNC catalysts is fully covered by $TiCl_4$ and donors. $19MgCl_2/4TiCl4$ is equivalent to the $TiCl_4$ coverage after removing donor. $19MgCl_2/9TiCl_4$ is equivalent to the coverage replacing donors by $TiCl_4$.

The $19MgCl_2/4TiCl_4$ system was obtained from Chapter 3, and the $19MgCl_2/9TiCl_4$ system was determined in this Chapter by the structure determination method described in Chapter 3. For energetically accessible and selected structures, the apparent activation energy of propylene insertion was calculated for each of Ti species.

It is widely accepted that the active sites of the ZNCs in propylene polymerization are alkylated and trivalent Ti species. Accordingly, $TiCl_4$ was converted to $TiCl_2$*i*Bu, and then the apparent activation energy of propylene insertion into Ti-*i*Bu was calculated. The insertion reaction for chain growth follows the Cosse-Arlman mechanism assisted with agostic interaction [15], [16] as shown in Figure 4.1. For the propylene insertion, four insertion pathways, namely, 1,2-*re*, 1,2-*si*, 2,1-*re*, and 2,1-*si* exist and the same number of pathways exists for insertion from the front and back sides of $MgCl_2$ layer corresponding to the position of growing chain. According to previous studies, the favorable orientation of the growing chain is α-agostic conformation with the anti-placement of the methyl group of propylene with respect to the C_α–C_β bond for the 1,2 insertion, and the syn-placement for the 2,1 insertion, respectively [17], [18]. Thus, the activation energies of eight different pathways were calculated for each Ti species as shown in Figure 4.2.

The transition state was approximated by the geometry-optimized structure obtained at 2.2 Å of the distance between the carbon of the incoming propylene and C_α of the *i*Bu group, i.e. the C_2–C_α

distance for the 1,2 insertion and the C_1–C_α distance for the 2,1 insertion. Such approximation is known to be accurate as the potential energy profile of ethylene/propylene insertion shows a gentle slope as a function of the reaction coordinate, i.e., the intercarbon distance [19], [20].

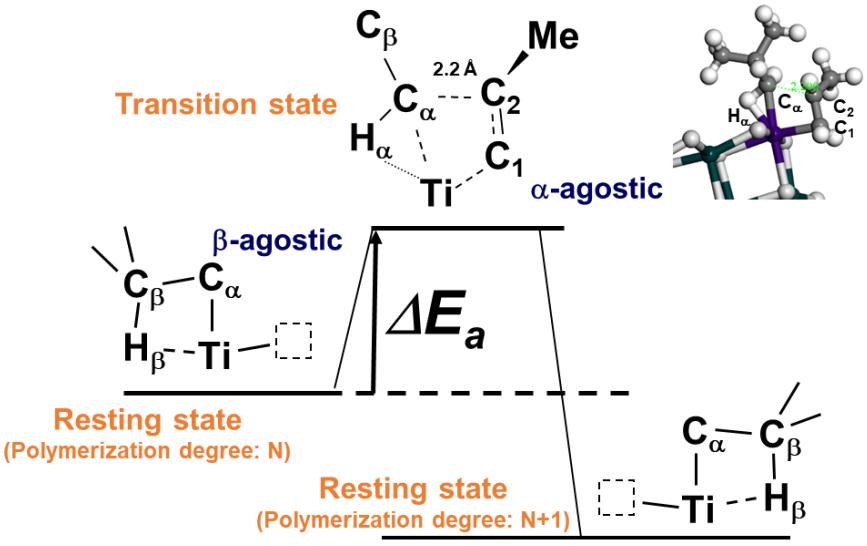

Figure 4.1. Energy diagram for propylene insertion reaction. 1,2-re insertion is chosen as example.

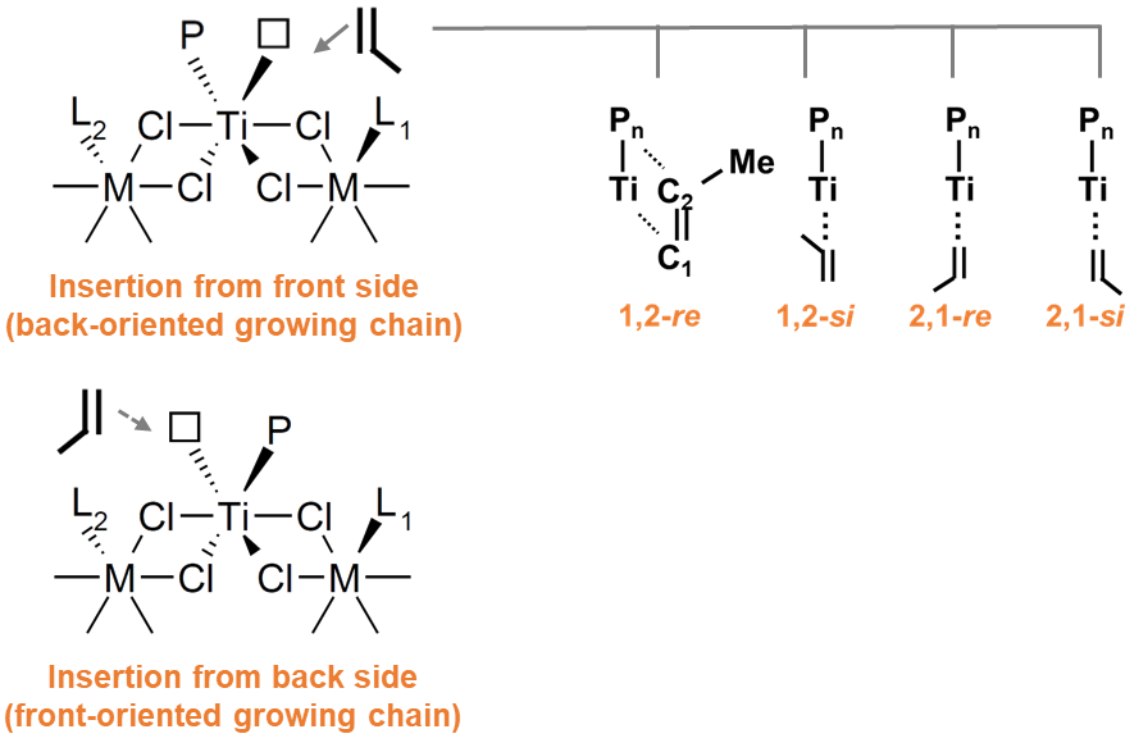

Figure 4.2. Eight different insertion pathways for propylene insertion reaction.

4.3. Results and discussion

For obtaining structures of a high-coverage system, non-empirical structure determination was performed for $19MgCl_2/9TiCl_4$. The successful convergence of the genetic algorithm was verified based on the fact that two independent searches reached the same energies and structures as shown in Figure 4.3. The convergence within 100 generations was much faster than that for $19MgCl_2$ and $19MgCl_2/4TiCl_4$ as shown in Chapter 3. The configuration space can be expressed by *the pattern of the* $MgCl_2$ *skeleton* × *the pattern of adsorption of* $TiCl_4$. In a system close to the full coverage such as $19MgCl_2/9TiCl_4$, the pattern of $TiCl_4$ adsorption was significantly reduced, resulting in the early convergence.

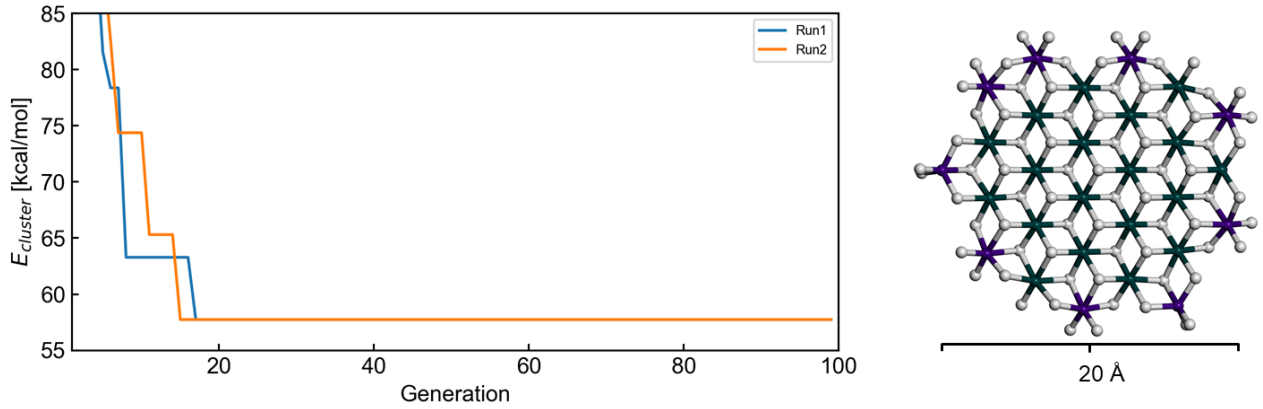

Figure 4.3. Evolutionary progress plot for the structure determination of $19MgCl_2/9TiCl_4$.

The obtained most stable structure dose not expose any coordinatively unsaturated Mg^{2+} ions. It is highly reconstructed in a way to expose {100} and {110} short terraces as well as many corners. Similar to low-coverage systems determined in Chapter 3, $19MgCl_2/9TiCl_4$ clusters have a distribution in the environment of Ti species, as shown in Figure 4.4. Ti species were classified into Type 1, 2 and 3 according to the presence or absence of stereocontrolling ligands. As a result of the high coverage, Type 2 and 3 with stereocontroling ligands became dominant among mononuclear species on {110}, and the fraction of {100} dinuclear species also increased.

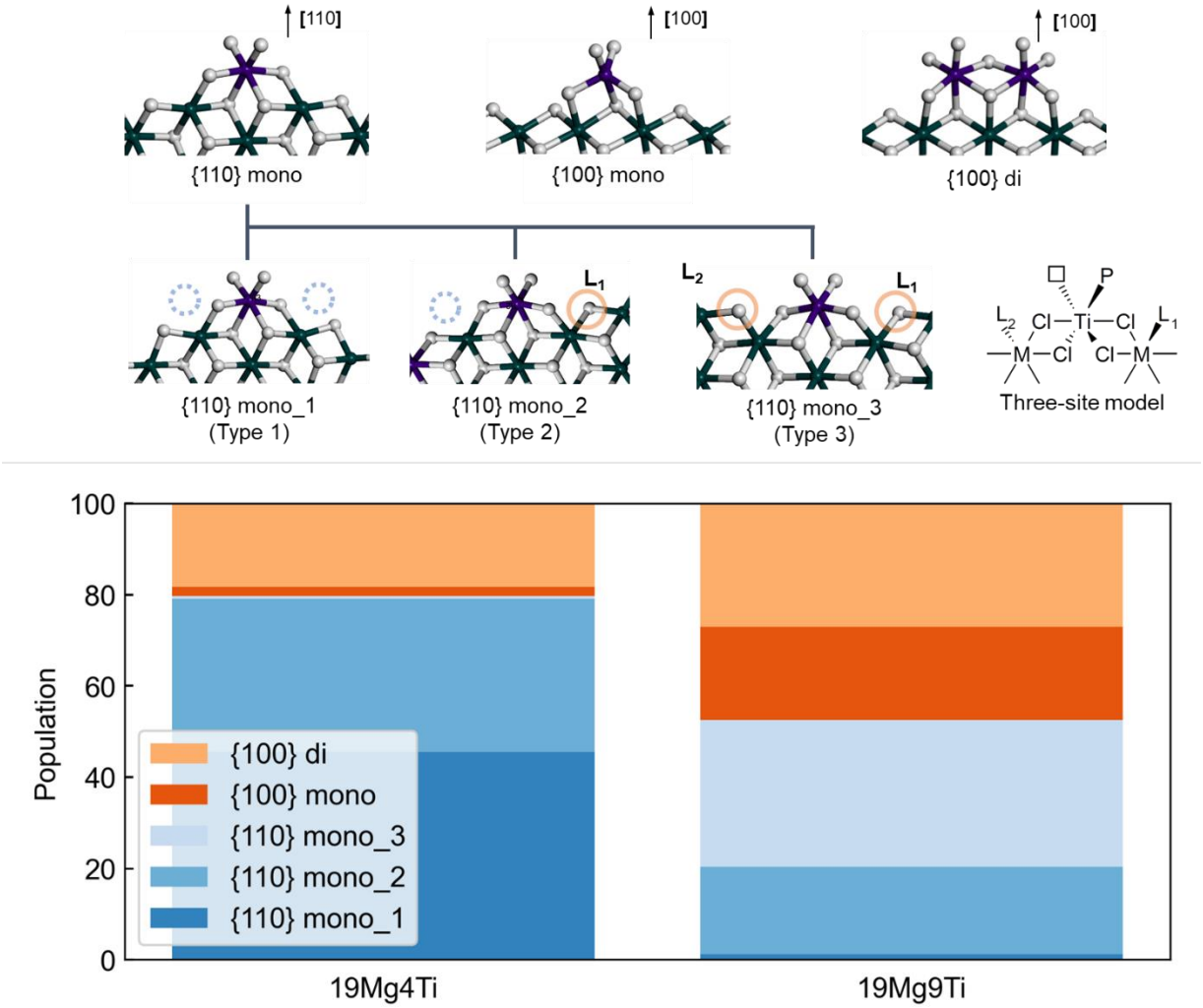

Figure 4.4. Distribution of different $TiCl_4$ species on $MgCl_2$. Adsorbed $TiCl_4$ molecules were classified into different species according to the three-site model.

The distribution of individual species was derived for each of $x MgCl_2/y TiCl_4$ using the Boltzman factor at 350 K.

In order to investigate the effect of the structural distribution of the active sites on the catalytic performance, propylene insertion simulations were performed. For this, six energetically accessible structures of $19MgCl_2/4TiCl_4$ and $19MgCl_2/9TiCl_4$ were selected in the order of stability,

respectively. These correspond to energetically accessible structures in the range of 2−3 kcal/mol from the most stable structure, and account for the majority of the Boltzmann factor-weighted distribution. In the selected structures, about 70 Ti species were identified, which belonged to either the mononuclear species on {110} surfaces or the dinuclear species on {100} surfaces. Note that the mononuclear species on {100} surfaces were excluded due to plausible irrelevance in catalysis. *i*Bu group was used as a model of the growing chain, and calculations for the dinuclear species on {100} were performed for each of the two Ti species. The activity of each Ti species was evaluated by the lowest activation energy ($\Delta E_{a,\,min}$) among 8 insertion pathways, i.e., stereo- and regiochemically different four insertion pathways from both of the front and back sides of a $MgCl_2$ plate.

The distribution of the lowest activation energy for each Type of Ti species is shown as a box-whisker plot in Figure 4.5 with further classification of Ti species. Note that when a terminal Cl^- anion was involved as a stereocontroling ligand, such Ti species were distinguished from those only having bridged Cl^- anions as the stereocontroling ligands. This leads to subclassification of Types 2 and 3 into 2b and 3b only with bridged Cl^- anions or Cl^- anions as a part of dinuclear species, and 2t and 3t with a terminal Cl^- anion. Also note that there are only two terminal Cl^- anions per cluster, so Type 2t and 3t become less and less important as the cluster size increases.

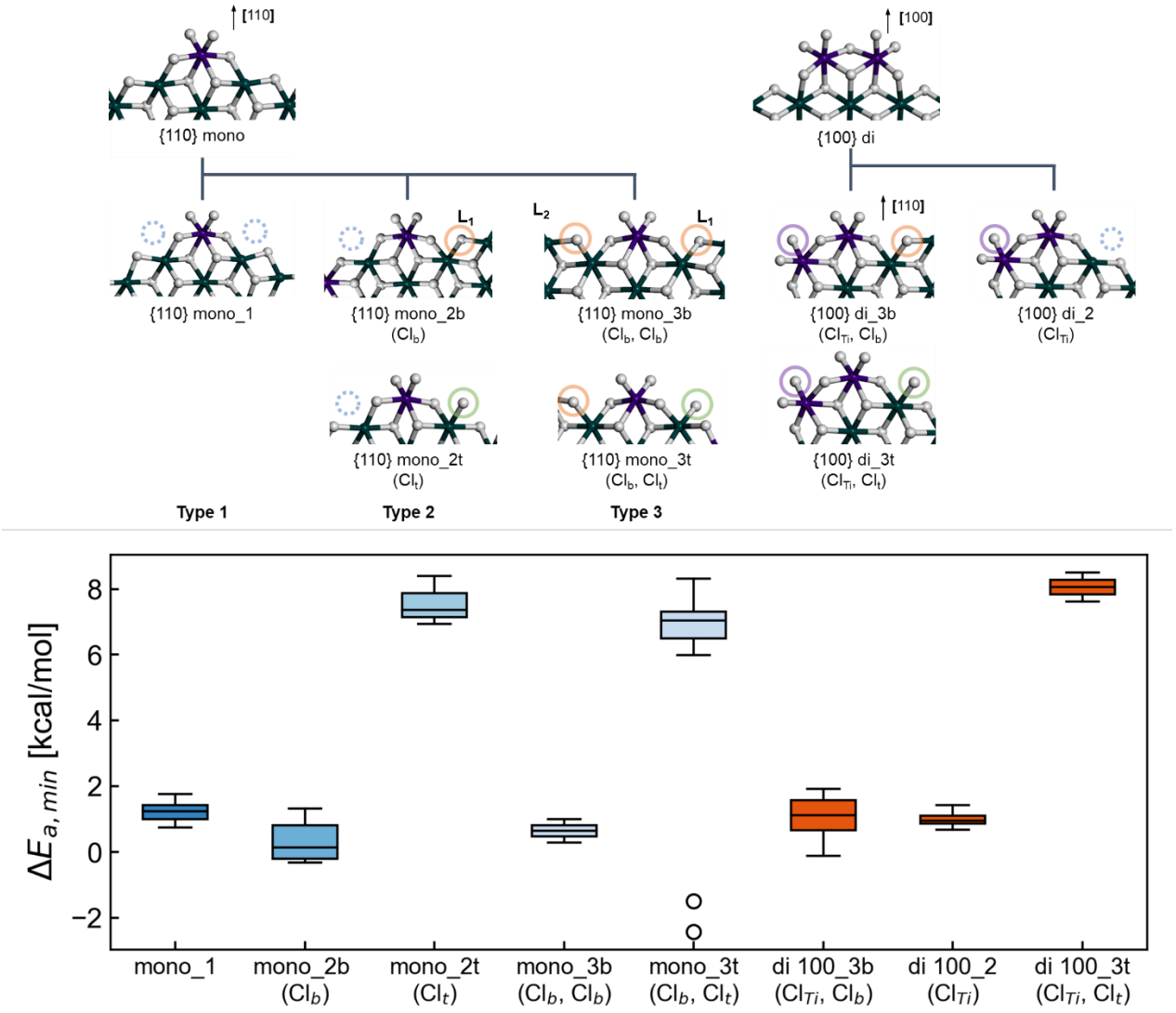

Figure 4.5. Distribution in the lowest activation energy of propylene insertion. About 70 Ti species, either of mononuclear species on {110} surfaces or dinuclear species on {100} surfaces, were selected from energetically accessible structures of $19MgCl_2/4TiCl_4$ and $19MgCl_2/9TiCl_4$. Converting $TiCl_4$ into $TiCl_2i$Bu, the apparent activation energy of propylene insertion was calculated for individual species. The letters b and t distinguish the non-involvement and involvement of a terminal Cl^- anion as a stereocontrolling ligand, respectively. Inside of brackets indicate the breakdown of the ligand, with Cl_b corresponding to bridged Cl^- anions, Cl_t to terminal Cl^- anion, and Cl_{Ti} to the terminal Cl^- anion of dinuclear species.

Compared to the ethylene insertion into Ti-Me shown in the previous chapter, the activation energy of the propylene insertion into Ti-*i*Bu was generally higher due to the steric congestion in the transition state. Besides, Ti species with a terminal Cl^- anion as a stereocontroling ligand showed about 5 to 6 kcal/mol higher activation energies than those without. This was due to that, in the resting state, a labile terminal Cl^- anion coordinated to the Ti species, which stabilized the resting state by about 13 kcal/mol. On the other hand, the stabilization of the transition state was smaller, about 7 kcal/mol, and this gap gave rise to the increase in the activation energy.

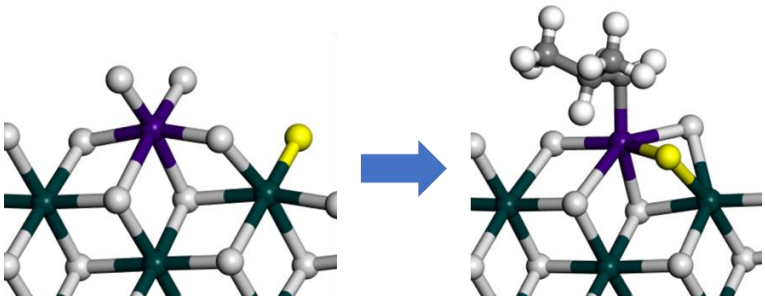

Figure 4.6. Stabilization of the resting state with a terminal Cl^- anion.

$\Delta E_{a,\,min}$ of Type 1, mononuclear species without stereocontrolling ligands, was centered at 1.6 kcal/mol. On the other hand, $\Delta E_{a,\,min}$ of mono_2b was about 1 kcal/mol lower than that of Type 1. This was explained by the asymmetry of the active site. For the same Ti species, there are two insertion directions corresponding to the front and back sides. When the carbon in the monomer is forming a σ-bond with the Ti center, the distance between Ti and Cl in the trans position of the monomer elongates. The asymmetry of the surrounding environment, especially in terms of the

stereocontroling ligands, causes the asymmetry of the insertion from different sides through the distance between Ti and Cl in the trans position. Specifically, in mono2_b, monomer insertion from the same direction as the ligand, i.e., growing chain orientation opposite to the ligand, was preferred. Thus, the asymmetric presence of the stereocontroling ligand lowers the activation energy for mono_2b as compared to mono_1.

Such asymmetry in the activation energy for the insertion position gives a suggestion for a chain-propagation mechanism of the Ziegler-Natta catalyst. Figure 4.7 plots the difference of the minimum activation energies between insertion from the front side and that from the back side, $\Delta\Delta E_{\text{front/back}}$. The Ti species of Type 2, which have only one stereocontroling ligand, and Types 2t and 3t, which have a particularly electron-withdrawing terminal Cl^- anion, showed an average $\Delta\Delta E_{\text{front/back}}$ value of about 1.5 kcal/mol. In this value, the probability of insertion from one side was estimated to be high at about 90% at 350 K. The mechanism of chain propagation has been classified into migratory insertion, in which the growing chain moves to the opposite side at each catalytic cycle, and back-skip insertion, in which the growing chain returns to the original position. At an active site where insertion from one side is dominant, chain-propagation is considered to proceed in the back-skip fashion. In addition, as seen in Type 2t, the coordination of the terminal Cl^- anion greatly enlarged the asymmetry of the active site and thus $\Delta\Delta E_{\text{front/back}}$. Such an electron-withdrawing ligand may enhance the insertion from the direction having the ligand, while the electron-donating ligand may enhance insertion from the opposite direction.

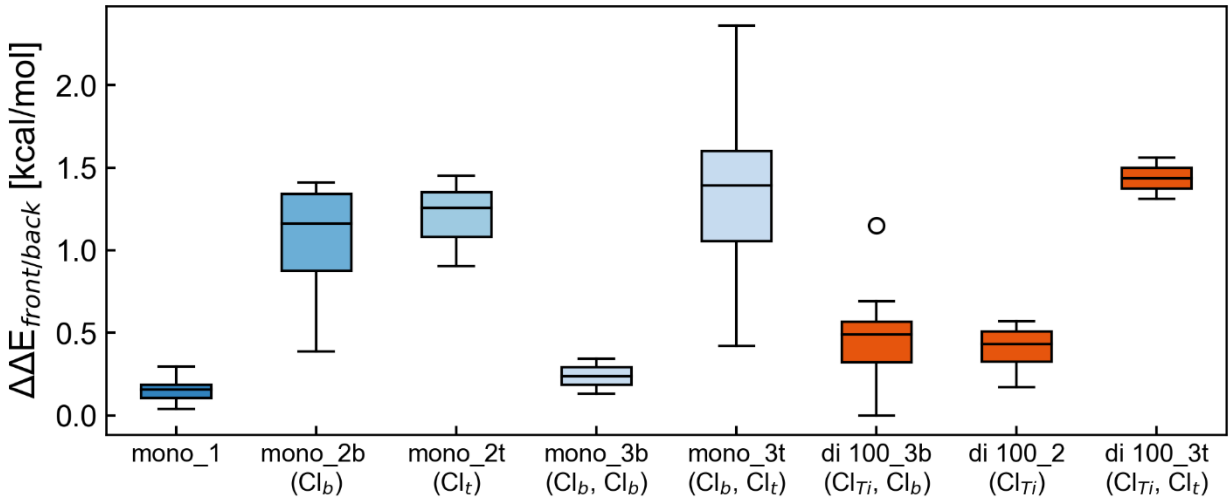

Figure 4.7. Distribution in the difference of minimum activation energies between insertion from the front side and that from the back side of a $MgCl_2$ layer.

The difference in the minimum activation energy between the 1,2-si and 1,2-re insertion, $\Delta\Delta E_{stereo}$, Type 1, dictates the stereospecificity of Ti species. The distribution in $\Delta\Delta E_{stereo}$ for each type of Ti species is summarized in Figure 4.8. As expected, Ti species of Type 1 without stereocontroling ligands did not show any stereospecificity. Type 2 Ti species with one stereocontroling ligand showed limited stereospecificity. This is because, in the light of the asymmetry, insertion from the ligand site, i.e., the case where the growing chain is on the opposite side of the ligand, is energetically favorable. In such orientations, the stereocontrolling ligand does not interfere with the growing chain for both 1,2-re insertion and 1,2-si insertion.1,2-re and 1,2-si insertions. When limiting the insertion direction to opposite side of the stereocontroling ligand, Type 2 species showed the stereoselectivity about 1.0 to 1.5 kcal/mol.

On the other hand, Ti species of Type 3 and dinuclear species with stereocontroling ligands on both sides show stereospecificity of about 0.75 kcal/mol to 1.5 kcal/mol. In addition, the increase of stereospecific Ti species of Type 3 and dinuclear species in $19MgCl_2/9TiCl_4$ shown in Figure 4.4 is in agreement with the experimentally observed enhancement of the stereoregularity of the produced polymer by donor-free catalyst with increasing Ti content [5]. Thus, it is suggested that the stereospecificity of the donor-free catalyst is originated from the Ti species having two stereocontrolling ligand on both sides, which are produced by high coverage.

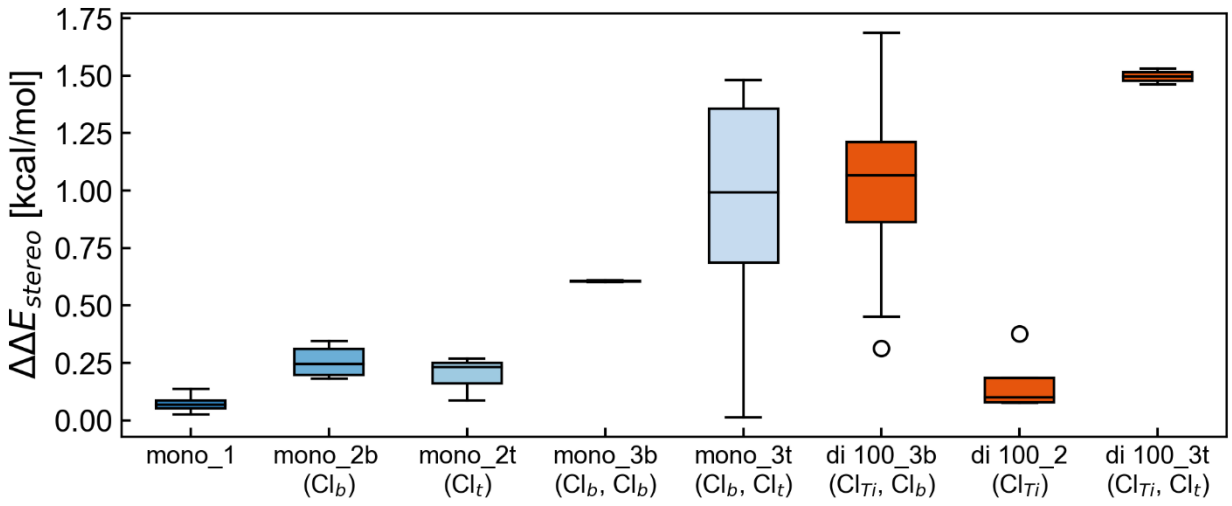

Figure 4.8. Distribution in the minimum activation energy between the 1,2-si and 1,2-re insertion of propylene.

4.4. Conclusion

In this Chapter, propylene insertion simulations were performed for Ti species present in machine learning-derived structures of $MgCl_2/TiCl_4$. The relationships between the structure of Ti active sites and their performance were extensively studied. Ti species having two stereocontrolling ligands,

such as mononuclear species of Type 3 on {110} surfaces and dinuclear species on {100} surfaces, were identified as the main species responsible for producing moderately isotactic PP in the absence of donors. The stereocontroling ligands in the $MgCl_2/TiCl_4$ system are mainly bridging Cl from $MgCl_2$ and $TiCl_4$ and terminal Cl^- anions on $TiCl_4$ for dinuclear species. Ligands with a stereocontrolling ability are bridging Cl^- anions and terminal Cl^- anions of $TiCl_4$ as a part of dinuclear species. Defective surfaces and high coverage are the way to afford such the ligands. In conclusion, this Chapter clarified, by using machine learning-derived realistic molecular models of $MgCl_2/TiCl_4$, the origin of the stereospecificity of the donor-free Ziegler-Natta catalysts.

REFERENCES

[1] V. Busico, "Ziegler-Natta catalysis: Forever young," *MRS Bull. 2013 383*, vol. 38, no. 3, pp. 224–228, Mar. 2013, doi: 10.1557/MRS.2013.50.

[2] N. Pasquini and A. Addeo, "Catalysts for Polymerization," in *Polypropylene Handbook*, 2nd ed., Boca Raton: Hanser Gardner Publications, 2005, pp. 11–112.

[3] K. Soga, T. Uozumi, and T. Shiono, "Highly isospecific catalyst for propene polymerization composed of $TiCl_4/MgCl_2$ and Cp_2TiMe_2 without donors," *Die Makromol. Chemie, Rapid Commun.*, vol. 10, no. 6, pp. 293–297, Jun. 1989, doi: 10.1002/MARC.1989.030100610.

[4] T. Taniike, P. Chammingkwan, and M. Terano, "Structure–performance relationship in Ziegler–Natta olefin polymerization with novel core–shell $MgO/MgCl_2/TiCl_4$ catalysts," *Catal. Commun.*, vol. 27, pp. 13–16, Oct. 2012, doi: 10.1016/J.CATCOM.2012.06.015.

[5] T. Wada, T. Taniike, I. Kouzai, S. Takahashi, and M. Terano, “Propylene Polymerization Performance of Isolated and Aggregated Ti Species Studied Using a Well-Designed $TiCl_3$ /$MgCl_2$ Ziegler-Natta Model Catalyst,” *Macromol. Rapid Commun.*, vol. 30, no. 11, pp. 887–891, Jun. 2009, doi: 10.1002/marc.200900015.

[6] T. Taniike and M. Terano, “Reductive formation of isospecific Ti dinuclear species on a $MgCl_2$ (110) surface in heterogeneous ziegler-natta catalysts,” *Macromol. Rapid Commun.*, vol. 29, no. 17, pp. 1472–1476, Sep. 2008, doi: 10.1002/marc.200800310.

[7] V. Busico, P. Corradini, L. De Martino, A. Proto, V. Savino, and E. Albizzati, “Polymerization of propene in the presence of MgCl,” *Die Makromol. Chemie*, vol. 186, no. 6, pp. 1279–1288, Jun. 1985, doi: 10.1002/macp.1985.021860617.

[8] P. Corradini, G. Guerra, R. Fusco, and V. Barone, “Analysis of models for the ziegler-natta stereospecific polymerization on the basis of non-bonded interactions at the catalytic site—II: Edges, steps and reliefs on the surface of layered modifications of TiCl3,” *Eur. Polym. J.*, vol. 16, no. 9, pp. 835–842, Jan. 1980, doi: 10.1016/0014-3057(80)90113-5.

[9] M. Toto, G. Morini, G. Guerra, P. Corradini, and L. Cavallo, “Influence of 1,3-diethers on the stereospecificity of propene polymerization by supported Ziegler-Natta catalysts. A theoretical their adsorption on (110) and (100) lateral cuts of $MgCl_2$ platelets,” *Macromolecules*, vol. 33, no. 4, pp. 1134–1140, 2000, doi: 10.1021/ma990959a.

[10] R. Credendino, D. Liguori, Z. Fan, G. Morini, and L. Cavallo, “Toward a Unified Model

Explaining Heterogeneous Ziegler-Natta Catalysis," *ACS Catal.*, vol. 5, no. 9, pp. 5431–5435, Sep. 2015, doi: 10.1021/acscatal.5b01076.

[11] B. Delley, "An all-electron numerical method for solving the local density functional for polyatomic molecules," *J. Chem. Phys.*, vol. 92, no. 1, pp. 508–517, Jan. 1990, doi: 10.1063/1.458452.

[12] J. P. Perdew, K. Burke, and M. Ernzerhof, "Generalized Gradient Approximation Made Simple," *Phys. Rev. Lett.*, vol. 77, no. 18, pp. 3865–3868, Oct. 1996, doi: 10.1103/PhysRevLett.77.3865.

[13] M. Dolg, U. Wedig, H. Stoll, and H. Preuss, "Energy-adjusted ab initio pseudopotentials for the first row transition elements," *J. Chem. Phys.*, vol. 86, no. 2, pp. 866–872, Jan. 1987, doi: 10.1063/1.452288.

[14] A. Bergner, M. Dolg, W. Küchle, H. Stoll, and H. Preuß, "Ab initio energy-adjusted pseudopotentials for elements of groups 13-17," *Mol. Phys.*, vol. 80, no. 6, pp. 1431–1441, Dec. 1993, doi: 10.1080/00268979300103121.

[15] E. J. Arlman and P. Cossee, "Ziegler-Natta catalysis III. Stereospecific polymerization of propene with the catalyst system $TiCl_3AlEt_3$," *J. Catal.*, vol. 3, no. 1, pp. 99–104, 1964, doi: 10.1016/0021-9517(64)90097-1.

[16] M. Brookhart and M. L. H. Green, "Carbon-hydrogen-transition metal bonds," *J. Organomet. Chem.*, vol. 250, no. 1, pp. 395–408, Jul. 1983, doi: 10.1016/0022-

328X(83)85065-7.

[17] T. Taniike and M. Terano, “Coadsorption model for first-principle description of roles of donors in heterogeneous Ziegler-Natta propylene polymerization,” *J. Catal.*, vol. 293, pp. 39–50, Sep. 2012, doi: 10.1016/j.jcat.2012.06.001.

[18] T. Taniike and M. Terano, “High-precision Molecular Modelling for Ziegler-Natta Catalysts,” *J. Japan Pet. Inst.*, vol. 61, no. 3, pp. 182–190, 2018.

[19] A. Correa, F. Piemontesi, G. Morini, and L. Cavallo, “Key elements in the structure and function relationship of the $MgCl_2$/$TiCl_4$/Lewis base Ziegler-Natta catalytic system,” *Macromolecules*, vol. 40, no. 25, pp. 9181–9189, Dec. 2007, doi: 10.1021/MA071294C/SUPPL_FILE/MA071294C-FILE001.PDF.

[20] M. Boero, M. Parrinello, and K. Terakura, “First Principles Molecular Dynamics Study of Ziegler−Natta Heterogeneous Catalysis,” *J. Am. Chem. Soc.*, vol. 120, no. 12, pp. 2746–2752, Apr. 1998, doi: 10.1021/JA972367I.

Chapter 5:
Preventing Premature Convergence in Evolutionary Structure Determination of Complex Molecular Systems: Demonstration in a Few-nm Sized $TiCl_4$-Capped $MgCl_2$ Nanoplate

Abstract

The combination of a genetic algorithm for global search and local geometry optimization enables non-empirical structure determination for complex materials such as practical solid catalysts. However, premature convergence in the genetic algorithm hinders the determination of the global minimum for complicated systems. Here, we implemented a distributed genetic algorithm based on the migration from a structure database for avoiding the premature convergence, and thus realized the structure determination for $TiCl_4$-capped $MgCl_2$ nanoplates with the size comparable to that of real Ziegler-Natta catalysts. The resulting molecular models are featured with a realistic size and non-ideal surfaces, and believed to be useful for decoding various spectroscopic observations.

Keywords: Structure determination, genetic algorithm, premature convergence, Ziegler-Natta catalyst

5.1. Introduction

In today's chemistry and materials science, computational science has become a powerful tool for understanding materials structures and properties at a molecular level. However, for complex materials such as practical solid catalysts, it is still hard to construct reliable molecular models due to limited experimental characterizations, which motivates the development of non-empirical structure determination methods. A combination of global search by a genetic algorithm (GA) and local geometry optimization has been attempted for such structure determination since the 1990s [1]–[7]. Only recently, the same method has been used to study practical materials such as catalysts at a level of DFT precision. I realized non-empirical structure determination for $TiCl_4$-capped $MgCl_2$ nanoplates, which correspond to primary particles of the heterogeneous Ziegler-Natta catalyst [8]–[10]. The structure determination was performed for 6–19$MgCl_2$/0–4$TiCl_4$, where the size of the nanoplates is smaller than the experimentally observed 2.4–7.6 nm [11]–[14]. The challenge of increasing the size of structures arises from the exponential expansion of a parametric space to be explored. In other words, the number of local minima in the potential energy surface increases exponentially with respect to the number of atoms, causing the local minima entrapment in GA, generally called the premature convergence problem.

Here implemented a distributed genetic algorithm (DGA) [15] for the non-empirical structure determination of large structures. The strategy is based on the migration from a structural database that collects the outputs of multiple GA runs. In usual DGA, subpopulations evolve in parallel and independently, and exchange individuals at a certain interval. My strategy is to collect the outputs of multiple GA runs into a single global database, and use this database as a pool of genes through

a migration operator (Scheme 5.1). The use of a global database maximizes the diversity of migrants, and enables asynchronous implementation of multiple GA runs, which allows the addition of subpopulations in the middle of structure determination. In the field of non-empirical structure determination, DGA was hardly implemented to avoid premature convergence.

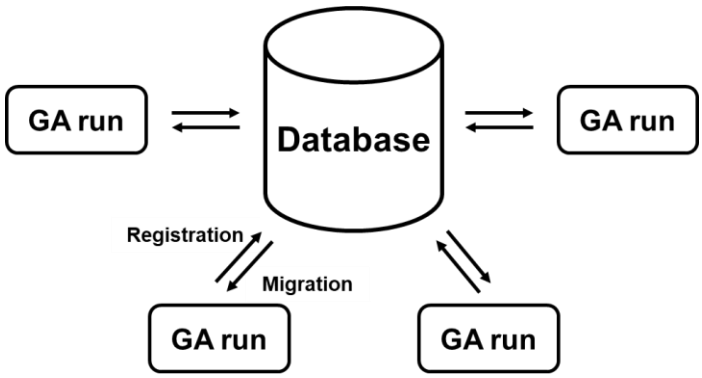

Scheme 5.1. Scheme of a distributed genetic algorithm in this Chapter. The database holds all structures and calculation results without allowing the registration of mutually redundant structures. In each GA run, a migration operator is executed at a certain generation interval to add structures from the global database to the population.

The developed DGA was demonstrated in the structure determination of $30MgCl_2$, $30MgCl_2/2TiCl_4$, $40MgCl_2$, $50MgCl_2$, and $50MgCl_2/3TiCl_4$. In particular, $50MgCl_2/3TiCl_4$ has a size of 3 nm and a Ti content of 2.7 wt%, both of which are consistent with experimental observations. By introducing the migration operator, premature convergence was successfully avoided; thus realistic models of Ziegler-Natta catalysts were successfully obtained.

5.2. Computational details

In Chapter 2, a structure determination program was developed for $MgCl_2/TiCl_4$ nanoplates combining the genetic algorithm for global search and DFT for local geometry optimization [8]. The

program generates the structure of the $MgCl_2$ monolayer whose lateral surfaces are capped by $TiCl_4$ on the basis of random numbers under physicochemical restrictions. These generated structures are subjected to geometry optimization by DFT, and the optimized structures are evaluated based on their energy and individually assigned a "fitness score." A structure with higher fitness has a higher opportunity to be selected for genetic operations such as crossover, mutation, and elitism operations, thus inheriting its feature to the next generation. The repetition of this cycle evolves the structures in a way to lowers the energy. For avoiding redundant calculations, the structure determination program registers newly created structures and their calculation results in a database to avoid redundant calculations. Different GA runs share the same structure database, which is referred to as the global database. The migration operator proposed herein utilizes this global structure database, where the migration operator refers to the global database and copy structures to the population of each GA run with certain intervals. The migrant structures are selected from the global database using the fitness-based roulette method, where structures with lower energy than the most stable structure within the destination GA run are excluded from the selection, i.e. the migration does not directly update the best-scored structure of the GA run. In the actual implementations, the population in a single GA run was set to 92, which consisted of 30 structures for crossover, 18 for skeleton mutation, 12 for adsorbate mutation, and the remaining 32 for elitism. The migration was typically applied by adding 8 migrants from the global database every 5 generations.

All DFT geometry optimizations were performed by DMol^3 [16] at the level of GGA PBE[17] using the DNP basis set [16] with effective core potentials [18], [19]. Further details are found in the previous Chapters or in literature [9], [10], [20].

5.3. Results and discussion

Figures 5.1a and 5.1b show evolutionary progress plots of three GA runs for the structure determination of $30MgCl_2$ with and without the migration operator, respectively. Without the migration operator, two of the three runs did not converge to the most stable structure, and could not escape from a metastable structure with an energy about 1 kcal/mol higher than the most stable one. The most stable structure and that metastable structure have similar structural features in terms of preferential exposure of the {100} lateral surfaces and symmetrical placement of the two terminal Cl^- anions (Figure 5.2). However, these two structures are located far apart in the parametric space spanned by the atomic coordinates, and metastable structures present in the intermediate area of the parametric space are not as stable. This is why the two runs failed to escape from the metastable structure once trapped.

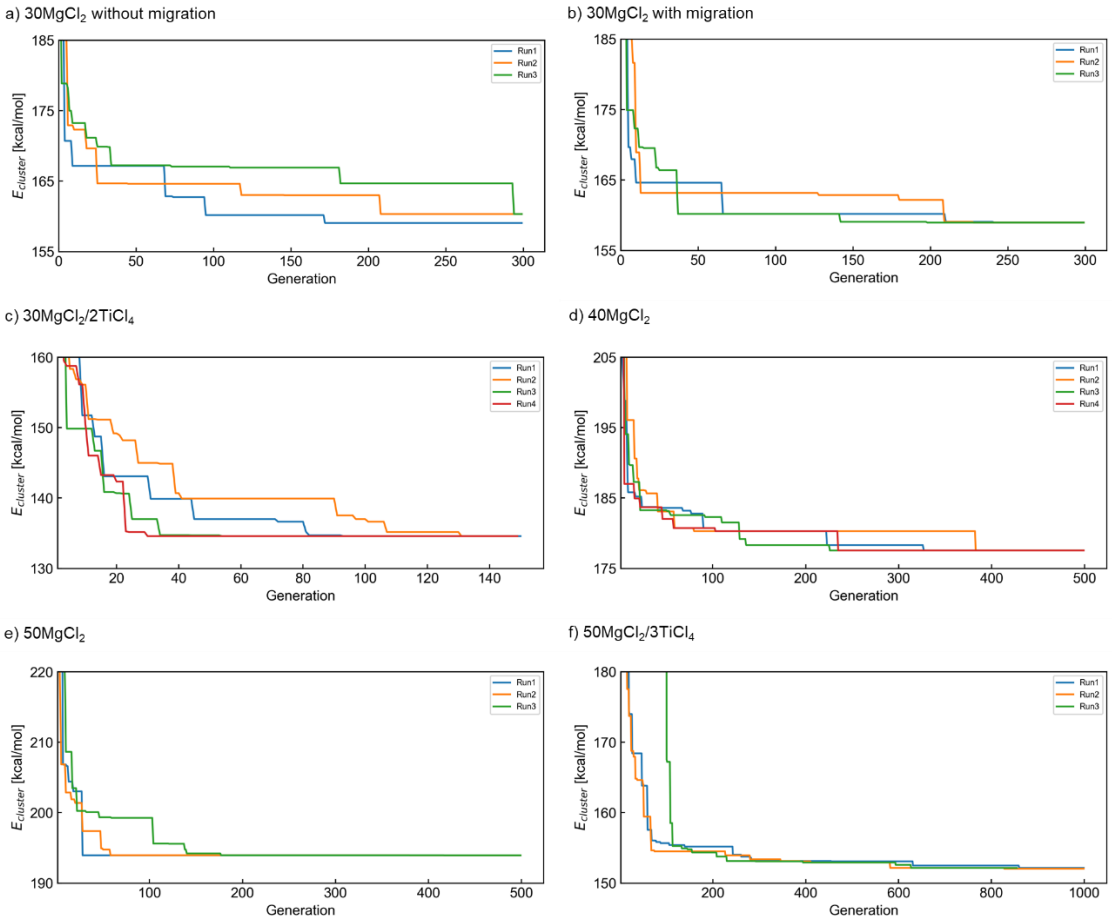

Figure 5.1. Evolutionary progress plots for the structure determination of (a,b) 30MgCl, (c) $30MgCl_2/2TiCl_4$, (d) $40MgCl_2$, (e) $50MgCl_2$ and (f) $50MgCl_2/3TiCl_4$. The energy of the best-of-generation individual (i.e. the most stable structure in a generation) is plotted against the generation. Structure determination of (b-f) is performed with the migration operator at an interval of 5 generations.

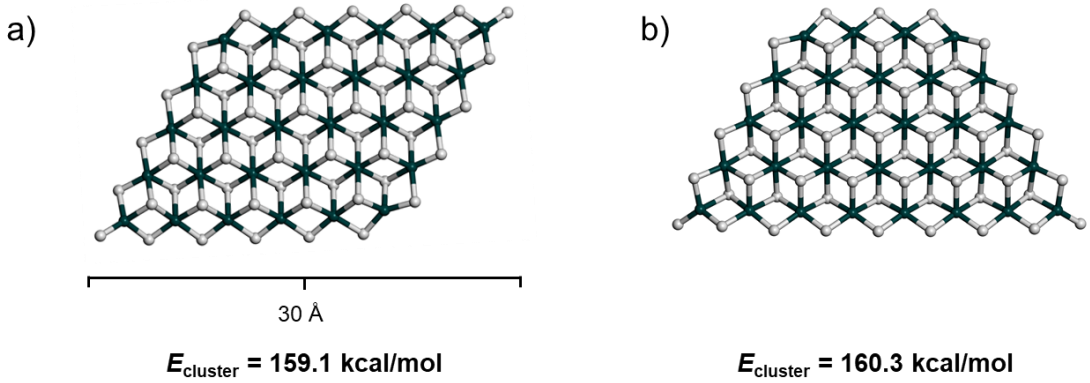

Figure 5.2. (a) The most stable structure of $30MgCl_2$. (b) The second stable structure of $30MgCl_2$ causing local minima entrapment in structure determination without the migration operator.

By introducing the migration operator, all three runs converged to the global minimum in Figure 5.2a. The impact of the migration on the genetic diversity is compared in Figure 5.3, where the structures of $30MgCl_2$ explored in the course of evolution in the absence and presence of the migration are respectively projected onto a two-dimensional space. The structures were fingerprinted in two steps: The molecular structures were converted to pair distribution functions (PDFs), and the PDFs were dimensionally reduced by principal component analysis (PCA). The obtained principal components were used as descriptors. As can be seen in Figure 5.3, where the distribution of the data expands in terms of quartile ranges and tails and quartile ranges, the introduction of the migration operator increased the diversity of structural features explored.

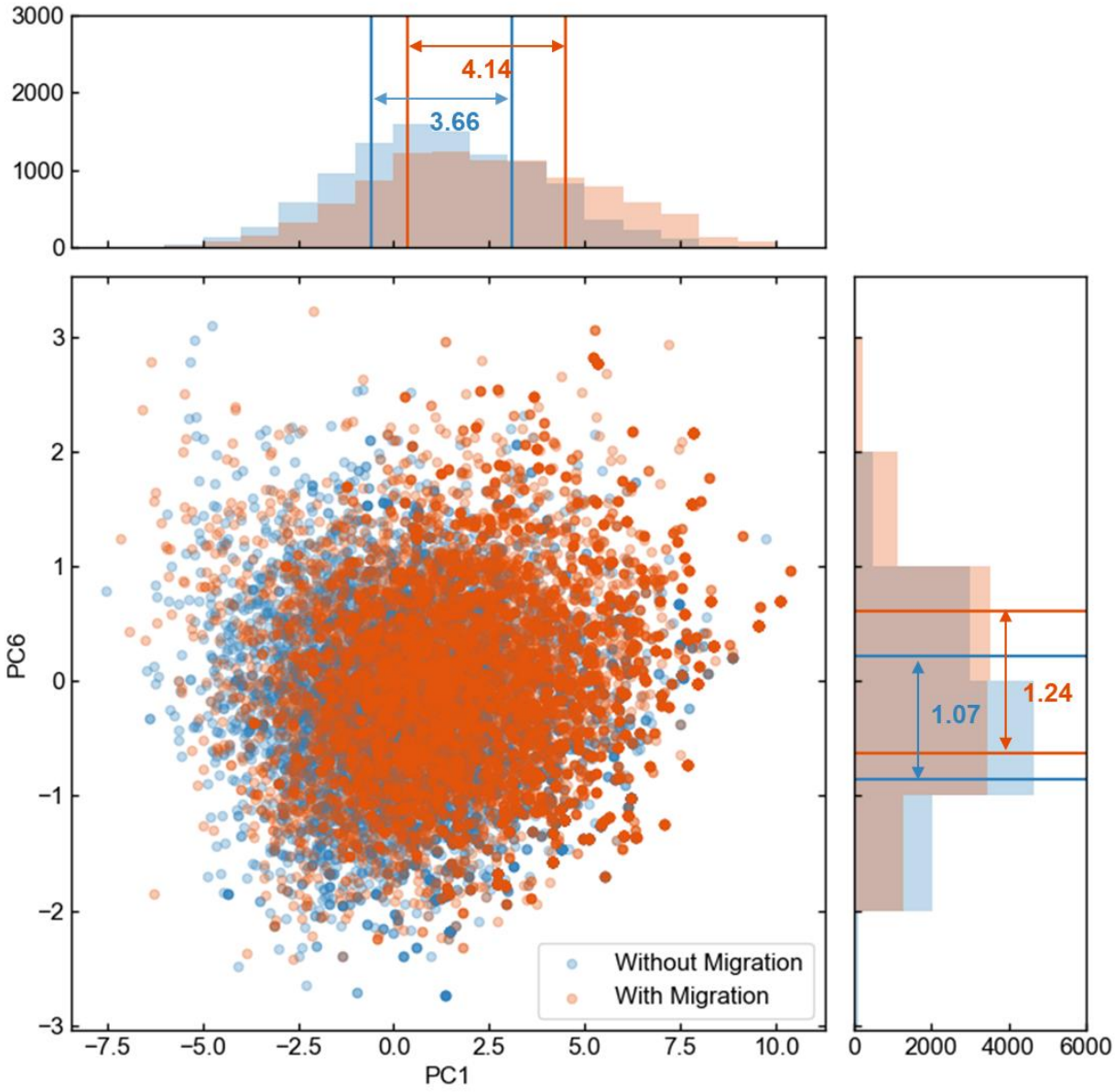

Figure 5.3. Representation of the diversity of structural features explored by GA in the absence and presence of the migration operator. The structural features created in the structure determination of $30MgCl_2$ are compared. Structural features were obtained by dimensional reduction of pair distribution functions of molecular structures by principal component analysis. The values written in the data distribution on each principal component correspond to the quartile range.

The developed DGA with the migration operator was employed for the structure determination of further larger systems, $30MgCl_2/2TiCl_4$, $40MgCl_2$, $50MgCl_2$ and $50MgCl_2/3TiCl_4$. In all the cases, DGA successfully converged into the same global minimum without premature convergence (Figures 5.1c to 5.1f).

The most stable structures of bare $30MgCl_2$, $40MgCl_2$, and $50MgCl_2$ are shown in Figures 5.4a–c, respectively. In general, when the size of the $MgCl_2$ cluster is small, the stable structure tends to possess a parallelogram or trapezoid morphology, which is necessary to make the lateral surfaces consist mainly of {100} terraces and to keep the two highly polarized terminal Cl^- anions away from each other. Indeed, the most stable structures of $30MgCl_2$ and $40MgCl_2$ possess a parallelogram shape with symmetrical placement of terminal Cl^- anions to eliminate the overall polarization. Contrary, the most stable structure of $50MgCl_2$ became hexagonal. As the cluster size increases, the distance between the two Cl^- anions becomes farther, and the morphology that can reduce the ratio of surface atoms to the bulk becomes more advantageous. The hexagon is the shape closest to the circle that can be created by combining the {100} terraces.

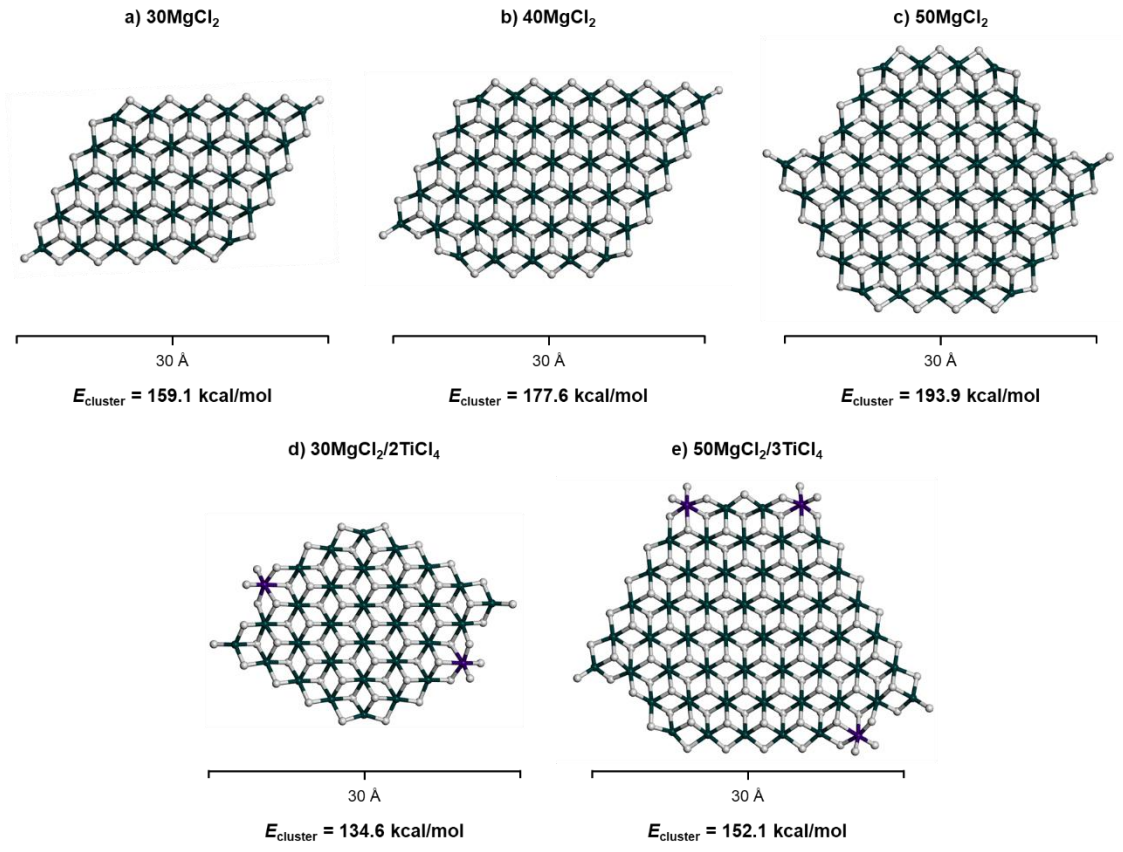

Figure 5.4. The most stable structures of $30MgCl_2$, $40MgCl_2$, $50MgCl_2$, $30MgCl_2/2TiCl_4$, and $50MgCl_2/3TiCl_4$.

Figures 5.4d and 5.4e show the most stable structures of $30MgCl_2/2TiCl_4$ and $50MgCl_2/3TiCl_4$. $30MgCl_2/2TiCl_4$ exhibited a symmetrical shape based on a rhombus consisting of 6×6 $MgCl_2$ units, with 3×2 Mg^{2+} cations removed to form {110} steps. $50MgCl_2/3TiCl_4$ had a shape that corners of a hexagon were removed to expose {110} terraces. In line with smaller systems [9], the addition of $TiCl_4$, which preferentially adsorbs to {110} surfaces, reconstructed $MgCl_2$ to expose {110} terraces, and, all the exposed {110} terraces were capped by $TiCl_4$. The decrease in $E_{cluster}$ by the addition of $TiCl_4$ molecules corresponds to the sum of the adsorption energy and the penalty of exposing coordinatively unsaturated surfaces by surface reconstruction. In the cases of $30MgCl_2$ and $50MgCl_2$,

the $E_{cluster}$ declined by 12.3 and 13.9 kcal/mol per $TiCl_4$, respectively. This indicates that the adsorption energy of $TiCl_4$ gradually increases as a larger $MgCl_2$ cluster facilitates the charge redistribution upon chemisorption.

5.4. Conclusion

In this Chapter, an asynchronous distributed GA was implemented for non-empirical structure determination, which is based on the migration from a global structure database. This enabled to solve the premature convergence problem, i.e., the local minima entrapment, and realized the structure determination for $30MgCl_2$, $30MgCl_2/2TiCl_4$, $40MgCl_2$, $50MgCl_2$, and $50MgCl_2/3TiCl_4$, which have realistic sizes compared to actual primary particles of Ziegler-Natta catalysts. The qualitative property of having a $TiCl_4$ distribution is invariant to size, but the size of $MgCl_2$ quantitatively affects the $TiCl_4$ distribution on $MgCl_2$ such as that $MgCl_2$ surfaces are easily reconstructed, and $TiCl_4$ on the {110} surface becomes dominant in larger sizes. This study provides the practical model of Ziegler-Natta catalyst which is applicable for the various applications such as spectroscopic simulations [21], [22].

REFERENCES

[1] D. M. Deaven and K. M. Ho, “Molecular geometry optimization with a genetic algorithm,” *Phys. Rev. Lett.*, vol. 75, no. 2, pp. 288–291, Jul. 1995, doi: 10.1103/PhysRevLett.75.288.

[2] D. J. Wales and H. A. Scheraga, “Global optimization of clusters, crystals, and

biomolecules," *Science*, vol. 285, no. 5432. American Association for the Advancement of Science, pp. 1368–1372, Aug. 27, 1999, doi: 10.1126/science.285.5432.1368.

[3] M. D. Wolf and U. Landman, "Genetic Algorithms for Structural Cluster Optimization," *J. Phys. Chem. A*, vol. 102, no. 30, pp. 6129–6137, Jul. 1998, doi: 10.1021/jp9814597.

[4] M. Chen and D. A. Dixon, "Tree Growth—Hybrid Genetic Algorithm for Predicting the Structure of Small $(TiO_2)n$, n = 2–13, Nanoclusters," *J. Chem. Theory Comput.*, vol. 9, no. 7, pp. 3189–3200, Jul. 2013, doi: 10.1021/CT400105C.

[5] H. A. Hussein, J. B. A. Davis, and R. L. Johnston, "DFT global optimisation of gas-phase and MgO-supported sub-nanometre AuPd clusters," *Phys. Chem. Chem. Phys.*, vol. 18, no. 37, pp. 26133–26143, 2016, doi: 10.1039/c6cp03958h.

[6] J. A. Vargas, F. Buendía, and M. R. Beltrán, "New Au_N (N = 27-30) Lowest Energy Clusters Obtained by Means of an Improved DFT-Genetic Algorithm Methodology," *J. Phys. Chem. C*, vol. 121, no. 20, pp. 10982–10991, May 2017, doi: 10.1021/acs.jpcc.6b12848.

[7] R. Huang, J.-X. Bi, L. Li, and Y.-H. Wen, "Basin Hopping Genetic Algorithm for Global Optimization of PtCo Clusters," *J. Chem. Inf. Model.*, vol. 60, no. 4, pp. 2219–2228, Apr. 2020, doi: 10.1021/ACS.JCIM.0C00130.

[8] G. Takasao, T. Wada, A. Thakur, P. Chammingkwan, M. Terano, and T. Taniike, "Machine Learning-Aided Structure Determination for $TiCl_4$–Capped $MgCl_2$ Nanoplate of

Heterogeneous Ziegler–Natta Catalyst," *ACS Catal.*, vol. 9, no. 3, pp. 2599–2609, Mar. 2019, doi: 10.1021/acscatal.8b05080.

[9] G. Takasao, T. Wada, A. Thakur, P. Chammingkwan, M. Terano, and T. Taniike, "Insight into structural distribution of heterogeneous Ziegler–Natta catalyst from non-empirical structure determination," *J. Catal.*, vol. 394, pp. 299–306, Feb. 2021, doi: 10.1016/j.jcat.2020.11.005.

[10] G. Takasao, T. Wada, A. Thakur, P. Chammingkwan, M. Terano, and T. Taniike, "Dataset of energetically accessible structures of $MgCl_2$/$TiCl_4$ clusters for Ziegler-Natta catalysts," *Data Br.*, vol. 34, p. 106654, Feb. 2021, doi: 10.1016/j.dib.2020.106654.

[11] R. Zannetti, C. Marega, A. Marigo, and A. Martorana, "Layer-lattices in Ziegler–Natta catalysts," *J. Polym. Sci. Part B Polym. Phys.*, vol. 26, no. 12, pp. 2399–2412, Nov. 1988, doi: 10.1002/polb.1988.090261202.

[12] A. Marigo, C. Marega, R. Zannetti, G. Morini, and G. Ferrara, "Small- and wide-angle X-ray scattering analysis of Ziegler-Natta catalysts: structural disorder, surface area and activity," *Eur. Polym. J.*, vol. 36, no. 9, pp. 1921–1926, Sep. 2000, doi: 10.1016/S0014-3057(99)00250-5.

[13] M. Chang, X. Liu, P. J. Nelson, G. R. Munzing, T. A. Gegan, and Y. V. Kissin, "Ziegler-Natta catalysts for propylene polymerization: Morphology and crystal structure of a fourth-generation catalyst," *J. Catal.*, vol. 239, no. 2, pp. 347–353, Apr. 2006, doi:

10.1016/j.jcat.2006.02.009.

[14] T. Wada *et al.*, “Revisiting the identity of δ-MgCl2: Part I. Structural disorder studied by synchrotron X-ray total scattering,” *J. Catal.*, vol. 385, pp. 76–86, May 2020, doi: 10.1016/j.jcat.2020.03.002.

[15] T. Starkweather, D. Whitley, and K. Mathias, “Optimization using distributed genetic algorithms,” *Lect. Notes Comput. Sci. (including Subser. Lect. Notes Artif. Intell. Lect. Notes Bioinformatics)*, vol. 496 LNCS, pp. 176–185, 1990, doi: 10.1007/BFB0029750.

[16] B. Delley, “An all-electron numerical method for solving the local density functional for polyatomic molecules,” *J. Chem. Phys.*, vol. 92, no. 1, pp. 508–517, Jan. 1990, doi: 10.1063/1.458452.

[17] J. P. Perdew, K. Burke, and M. Ernzerhof, “Generalized Gradient Approximation Made Simple,” *Phys. Rev. Lett.*, vol. 77, no. 18, pp. 3865–3868, Oct. 1996, doi: 10.1103/PhysRevLett.77.3865.

[18] M. Dolg, U. Wedig, H. Stoll, and H. Preuss, “Energy-adjusted ab initio pseudopotentials for the first row transition elements,” *J. Chem. Phys.*, vol. 86, no. 2, pp. 866–872, Jan. 1987, doi: 10.1063/1.452288.

[19] A. Bergner, M. Dolg, W. Küchle, H. Stoll, and H. Preuß, “Ab initio energy-adjusted pseudopotentials for elements of groups 13-17,” *Mol. Phys.*, vol. 80, no. 6, pp. 1431–1441, Dec. 1993, doi: 10.1080/00268979300103121.

[20] T. Taniike and M. Terano, “Coadsorption model for first-principle description of roles of donors in heterogeneous Ziegler-Natta propylene polymerization,” *J. Catal.*, vol. 293, pp. 39–50, Sep. 2012, doi: 10.1016/j.jcat.2012.06.001.

[21] A. Piovano *et al.*, “Electronic Properties of Ti Sites in Ziegler–Natta Catalysts,” *ACS Catal.*, pp. 9949–9961, 2021, doi: 10.1021/ACSCATAL.1C01735.

[22] M. D’Amore *et al.*, “Spectroscopic Fingerprints of $MgCl_2$/$TiCl_4$ Nanoclusters Determined by Machine Learning and DFT,” *J. Phys. Chem. C*, vol. 125, no. 36, pp. 20048–20058, Sep. 2021, doi: 10.1021/ACS.JPCC.1C05712.

Chapter 6:
General Conclusion

Heterogeneous Ziegler-Natta catalysts are the main catalysts for the industrial production of polyolefins. The detailed morphology and surface exposure of their primary particles are still unclear despite its importance for understanding of the adsorption of catalytic components and catalytic performance. Computational studies on this catalyst assumed slab and cluster models that represented by predefined surfaces, but such assumption did not give an explanation of the origin of multisite nature, which is important properties of this catalyst, i.e., the distribution of produced polymers. In this thesis, I realized non-empirical structure determination for primary particles of heterogeneous Ziegler-Natta catalysts by means of combining the genetic algorithm and DFT calculation for modeling the real nanocluster of Ziegler-Natta catalysts, and I clarified the origin of the multisite nature and the stereospecificity in the donor-free catalyst, which are the long-standing question in this field thorough simulations on derived models.

In Chapter 2, I developed a non-empirical structure determination program for $TiCl_4$-capped $MgCl_2$ nanoplates of Ziegler-Natta catalysts by a combination of a genetic algorithm for global search and DFT geometry optimization for local optimization. The program was demonstrated for $7MgCl_2$, $15MgCl_2$ and $15MgCl_2/4TiCl_4$ and their most stable structures were successfully obtained without pre-knowledge. The stable structure of bare $MgCl_2$ was terminated by the {100} surface with the lowest coordinative unsaturation, which limits the variety of energetically accessible structures. In contrast, in $TiCl_4$-capped $MgCl_2$, the preferential adsorption of $TiCl_4$ on the {110} surface reconstructed $MgCl_2$ to expose small {110} terraces. Furthermore, the adsorption of $TiCl_4$ greatly increased the variety of energetically accessible structures. In this chapter, I concluded that

$TiCl_4$ reconstructs the $MgCl_2$ skeletons and that $TiCl_4$ is intrinsically distributed as a combined consequence of non-ideal surfaces and structural diversity.

In Chapter 3, I attempted to determine the structure of $TiCl_4$-terminated $MgCl_2$ nanoplates of various sizes and compositions to derive catalytic chemical knowledge. The system of interest is $xMgCl_2/yTiCl_4$ (x = 6-19, y = 0-4; [Ti] < 10 wt%). The structure and charge distributions were analyzed for a million structures obtained in the process of structure determination. These systematic investigations revealed that $TiCl_4$ prefer the monomeric adsorption on the {110} surface, but adsorption on the {100} surface cannot be ignored, and that there is a distribution of the steric environment and charge state of $TiCl_4$ among the same mononuclear species on the {110} surface. Furthermore, I calculated the activation energy for the ethylene insertion reaction and showed that the distribution of $TiCl_4$ could cause the performance distribution, i.e., the primary structure distribution of the synthesized polymer. This is the first hypothesis for the origin of the multi-site nature of the Ziegler-Natta catalysts derived from computational chemistry.

In Chapter 4, I performed propylene polymerization simulations based on $MgCl_2/TiCl_4$ nanoplates derived in Chapter 3. The relationships between the structure of Ti active sites and their performance were investigated. As suggested in Chapter 3, the distribution of structure also produced a distribution of catalyst performance in propylene polymerization. Ti species having two stereocontrolling ligands, such as mononuclear species of Type 3 on {110} surfaces and dinuclear species on {100} surfaces showed isospecificity. The ligands with steric control ability are bridging Cl^- anions and terminal Cl^- anions on $TiCl_4$, which are part of the dinuclear species, and the defective

surface and high coverage produce such ligands. This chapter clarified the origin of stereospecificity in the donor-free catalyst, which is a long-standing question for Ziegler-Natta catalysts.

In Chapter 5, I improved the search efficiency of the structure determination program by implementing an asynchronous distributed genetic algorithm with migration operators from the structure database. A structure database holds all the structures and calculation results generated in different GA runs, and each GA adds structures from the database to the population every certain generations as migrants. This implementation solved the premature convergence problem by preserving genetic diversity in the population of GAs and significantly improved convergence to the global solution. This resulted in structure determination for $30MgCl_2$, $50MgCl_2$, and $50MgCl_2/3TiCl_4$, systems with sizes comparable to those of real catalysts.

In conclusion, this thesis has achieved non-empirical structure determination by incorporating adsorbate adsorption and dynamic surface reconstruction and established a highly accurate and non-empirical modeling method for complex solid materials with sizes comparable to real catalyst nanoparticles. On the basis of the non-empirical structure determination, I proposed an important hypothesis that the multisite nature of heterogeneous Ziegler–Natta catalysts, hence, the polydispersity of the obtained polymer, is a general characteristic of the $MgCl_2/TiCl_4$ system. The origin of the stereospecificity, which is one of the important properties in Ziegler-Natta catalyst was also clarified.

I believe that the research in this thesis brings essential contributions for the systematic design of catalysts for Ziegler-Natta catalysts and important advances in establishing a methodology for

modeling complicated supported catalysts and elucidation of their structure-performance relationship.

Acknowledgments

First of all, I would like to express my deepest gratitude to my supervisor Prof. Toshiaki Taniike for his continuous support in my Ph. D course and excellent guidance, encouragement and constructive criticism. This work would never have been achieved without his kind helps. I would like to thank Senior Lecturer Patchanee Chammingkwan, Asst. Professor Toru Wada, and Asst. Prof. Ashutosh Thakur for their many helpful discussions and advice. I would like to thank Prof. Elena Groppo and Dr. Alessandro Piovano in University of Turin for their helpful discussions and great collaboration. I am also thankful to the staff of RCACI, especially for Ms. Kanae Miyashita for their cooperation in the use of parallel computing servers. I deeply appreciate Prof. Shinya Maenosono, Prof. Yoshifumi Oshima, Assoc. Prof. Kenta Hongo and Prof. Takeshi Shiono for their review and valuable suggestions. Finally, I wish to express my gratitude to all the laboratory members for their kind encouragements.

Gentoku Takasao

List of Publications and Other Achievements

Publications

[1] G. Takasao, T. Wada, A. Thakur, P. Chammingkwan, M. Terano, and T. Taniike, "Machine Learning-Aided Structure Determination for $TiCl_4$–Capped $MgCl_2$ Nanoplate of Heterogeneous Ziegler–Natta Catalyst," *ACS Catalysis*, vol. 9, no. 3, pp. 2599–2609, Mar. 2019, doi: 10.1021/acscatal.8b05080.

[2] G. Takasao, T. Wada, A. Thakur, P. Chammingkwan, M. Terano, and T. Taniike, "Insight into structural distribution of heterogeneous Ziegler–Natta catalyst from non-empirical structure determination," *Journal of Catalysis*, vol. 394, pp. 299–306, Feb. 2020, doi: 10.1016/j.jcat.2020.11.005.

[3] G. Takasao, T. Wada, A. Thakur, P. Chammingkwan, M. Terano, and T. Taniike, "Dataset of energetically accessible structures of $MgCl_2$/$TiCl_4$ clusters for Ziegler-Natta catalysts," *Data in Brief*, vol. 34, p. 106654, Feb. 2021, doi: 10.1016/j.dib.2020.106654.

[4] T. Wada *et al.*, "Revisiting the identity of δ-$MgCl_2$: Part I. Structural disorder studied by synchrotron X-ray total scattering," *Journal of Catalysis*, vol. 385, pp. 76–86, May 2020, doi: 10.1016/j.jcat.2020.03.002.

[5] A. Piovano *et al.*, "Revisiting the identity of δ-$MgCl_2$: Part II. Morphology and exposed surfaces studied by vibrational spectroscopies and DFT calculation," *Journal of Catalysis*, vol. 387, pp. 1–11, Jul. 2020, doi: 10.1016/j.jcat.2020.04.017.

[6] A. Piovano *et al.*, “Electronic Properties of Ti Sites in Ziegler–Natta Catalysts,” *ACS Catalysis*, pp. 9949–9961, 2021, doi: 10.1021/ACSCATAL.1C01735.

International Conferences

Oral

"Features of $TiCl_4$ on Primary Particles of Ziegler-Natta Catalysts Studied by Machine Learning-Aided DFT Calculations",

Gentoku Takasao, Toru Wada, Patchanee Chammingkwan, Minoru Terano, Toshiaki Taniike, Asian Polyolefin Workshop 2019, Hiroshima University, 2019, December 5, Hiroshima, Japan

“Non-empirical structure determination for heterogeneous Ziegler-Natta catalyst based on machine learning-aided DFT calculation”,

Gentoku Takasao, Toru Wada, Patchanee Chammingkwan, Minoru Terano, Toshiaki Taniike, First international symposium on High-Throughput Catalysts Design (HTCD 2021), Lille (France) / Online, 2021 June 14-15, France / Online

"Origin of multisite nature of Ziegler-Natta Catalysts Studied by Machine Learning-Aided DFT Calculations",

Gentoku Takasao, Toru Wada, Patchanee Chammingkwan, Minoru Terano, Toshiaki Taniike, Asian Polyolefin Workshop 2021, Online, 2021 December 20-21, Online / Thailand

Poster

"Modeling primary particles of Ziegler-Natta catalysts based on machine learning-aided DFT calculations",

Gentoku Takasao, Toru Wada, Ashutosh Thakur, Patchanee Chammingkwan, Minoru Terano, Toshiaki Taniike, 5th Blue Sky Conference, Federico II University of Naples, Dutch Polymer Institute, 2019, June 25-27, Sorrento, Italy

Domestic Conferences

"Structures of $TiCl_4$-Capped $MgCl_2$ Nanoparticles Determined by Machine Learning-Aided DFT Calculations",

Gentoku Takasao, Toru Wada, Patchanee Chammingkwan, Minoru Terano, Toshiaki Taniike,

第 49 回石油・石油化学討論会(国内学会), 公益社団法人石油学, 2019 年 10 月 31 日.